



THE UNIVERSITY OF
WAIKATO
Te Whare Wānanga o Waikato

Research Commons

<http://waikato.researchgateway.ac.nz/>

Research Commons at the University of Waikato

Copyright Statement:

The digital copy of this thesis is protected by the Copyright Act 1994 (New Zealand).

The thesis may be consulted by you, provided you comply with the provisions of the Act and the following conditions of use:

- Any use you make of these documents or images must be for research or private study purposes only, and you may not make them available to any other person.
- Authors control the copyright of their thesis. You will recognise the author's right to be identified as the author of the thesis, and due acknowledgement will be made to the author where appropriate.
- You will obtain the author's permission before publishing any material from the thesis.

A Portable Generator Incorporating Mini-Tubular Solid Oxide Fuel Cells

A thesis submitted in partial fulfilment
of the requirements for the degree of

Doctor of Philosophy
in Engineering

at the
University of Waikato

by
Andrew Justin Hyde



THE UNIVERSITY OF
WAIKATO
Te Whare Wānanga o Waikato

University of Waikato

2008

ABSTRACT

Modern society has become reliant on battery powered electronic devices such as cell phones and laptop computers. The standard way of recharging these devices is by connecting to a reticulated electricity supply. In situations with no electricity supply some other recharging method is required. Such a possibility is a small, portable, generator based on fuel cell technology, specifically mini-tubular solid oxide fuel cells (MT-SOFC). MT-SOFCs have been developed since the 1990s but there is limited analysis, discussion or research on developing and constructing a portable generator based on MT-SOFC technology. Such a generator, running on a portable gas supply, requires combining the key aspects of cell performance, a heating and fuel reforming system, and cell manifolds.

Cell design, fuel type, fuel flow rate, current-collection method and operating temperature all greatly affected MT-SOFCs performance. Segmenting the cathode significantly increased the power output. Maximum power density from an electrolyte supported MT-SOFC was 140 mW/cm^2 .

The partial oxidation reactor (POR) developed provided the required heat to maintain the MT-SOFCs at an operating temperature suitable for generating electricity. The exhaust gas from the POR was a suitable fuel for MT-SOFCs, having sufficient carbon monoxide and hydrogen to generate electricity.

Various manifold materials were evaluated including solid metal blocks and folded sheet metal. It was found that manifolds made from easily worked alumina fibre board decreased the thermal stresses and therefore the fracture rate of the MT-SOFCs.

The final prototype developed comprised a partial oxidation reactor and MT-SOFCs mounted in alumina fibre board manifolds within a well-insulated enclosure, which could be run on LPG.

Calculated efficiency of the final prototype was 4%. If all the carbon monoxide and hydrogen produced by the partial oxidation reactor were converted to electrical energy, efficiency would increase to 39%. Under ideal conditions, efficiency would be 78%. Efficiency of the prototype can be improved by increasing the fuel and oxygen utilisation ratios, ensuring heat from the exhaust gases is transferred to the incoming gases, and improving the methods for collecting current at both the anode and cathode.

ACKNOWLEDGEMENTS

I am and always will be extremely grateful to Professor Janis Swan who encouraged me to continue my research career, supported me in many ways throughout my doctoral work and who has always expressed confidence in my abilities. Special thanks to Dr Rob Torrens for his steadfast support of my research, for his valuable advice and technical expertise, and for his principled camaraderie.

I would like to convey my appreciation and love to my family, especially my parents. Thank you for your support and patience, for this has taken so long.

I am fortunate to have many, many friends in New Zealand and other countries that have supported me, kept in contact, and encouraged me to finish my thesis. They are too numerous to name individually but my heartfelt thanks to you all.

I would also like to praise the University of Waikato staff that supported me and my research: Professor Deliang Zhang, Professor Cam Nelson, Dr Michael Walmsley, Mary Dalbeth, the technicians in the Department of Engineering, and many others. I would not have completed my thesis without your support.

I also extend my appreciation to Professor Nigel Sammes and Dr Geoff Tompsett who introduced me to the mini-tubular solid oxide fuel cell field. Thanks are also due to Professor Kevin Kendall and Dr Caine Finnerty who helped extend my knowledge and skills during my time in the United Kingdom.

TABLE OF CONTENTS

Abstract.....	i
Acknowledgements.....	iii
Table of Contents.....	v
List of Figures.....	x
List of Tables.....	xiii
Nomenclature.....	xiv
1 Introduction.....	1
1.1 Requirement and demand for electricity.....	1
1.2 Portable energy generation / storage.....	1
1.3 Fuel cells.....	2
1.4 Portable fuel cells.....	2
1.5 Research aims.....	3
1.6 Thesis outline.....	3
2 Literature Review.....	5
2.1 Fuel Cells.....	5
2.1.1 History.....	5
2.1.2 Types of fuel cells.....	5
2.2 SOFC Technologies.....	7
2.2.1 Introduction.....	7
2.2.2 Planar SOFC.....	7
2.2.3 Tubular SOFC.....	9
2.2.4 MT-SOFC.....	10
2.2.5 Technology overview.....	11
2.3 SOFC Fuels.....	11
2.3.1 Reforming.....	12
2.4 SOFC Operating Principles.....	13
2.4.1 Electrochemical reactions.....	14
2.4.2 Electromotive force (EMF) of a hydrogen fuel cell.....	14
2.4.3 EMF of a fuel cell using carbon monoxide.....	15
2.4.4 Operational fuel cell voltages.....	15
2.4.5 Current.....	17
2.4.6 Fuel utilisation.....	17
2.4.7 Reversible power output.....	18
2.4.8 Actual power output.....	18

2.4.9	Thermodynamic efficiency	18
2.4.10	Thermal efficiency	18
2.4.11	Published data	19
2.5	Mini-Tubular SOFC	19
2.5.1	Heating	21
2.5.2	Manifolds and sealing	24
2.5.3	Electrical connections	24
2.5.4	Fuel and reforming	25
2.5.5	Balance of plant	25
2.5.6	MT-SOFC system design	28
2.6	MT-SOFC Components	28
2.6.1	Electrolyte	28
2.6.2	Anodes	29
2.6.3	Anode current collection	29
2.6.4	Cathodes	29
2.6.5	Cathode current collection	30
2.6.6	Interconnects	30
2.7	MT-SOFC Generator Concept	30
2.7.1	Integrated heating and fuel reforming	30
2.7.2	Development	31
2.7.3	Modelling	31
2.8	Summary	31
2.8.1	MT-SOFC knowledge	31
2.8.2	Knowledge gaps	32
2.8.3	Scope	35
2.8.4	Research questions	35
2.8.5	Hypothesis	36
3	Experimental Set-up & Trials	37
3.1	Gas analysis	37
3.1.1	Equipment	38
3.1.2	Overview of GC operation	39
3.1.3	GC method	40
3.1.4	Constant quantity	40
3.1.5	Calibration	40
3.1.6	Analysis method	41
3.1.7	Calculating gas concentrations	41
3.1.8	SG1 - Standard gas #19792	42
3.1.9	SG2 - Standard gas #M7014	43
3.1.10	SG3 - Standard gas #MA84047	44
3.1.11	Ethane	45
3.1.12	Nitrogen	46

3.1.13	Dry air composition	47
3.1.14	Carbon dioxide	48
3.1.15	Linearity of TCD response.....	48
3.1.16	Experimental set-up	49
3.1.17	Sampling technique.....	49
3.2	Electrochemical analysis	49
3.2.1	Objective	49
3.2.2	Fuel cells	50
3.2.3	Anode ink compositions and preparations	52
3.2.4	Anode coating technique.....	53
3.2.5	Cathode ink compositions and preparations	53
3.2.6	Cathode coating technique	54
3.2.7	Firing.....	54
3.2.8	Anode reduction.....	55
3.2.9	Open circuit voltage measurement.....	55
3.2.10	Under-load voltage and current measurements.....	55
3.2.11	Operational parameters	56
3.2.12	Equipment	56
3.2.13	Test conditions	57
3.2.14	Data and results.....	57
3.3	Manifold design.....	57
3.3.1	Objectives	58
3.3.2	Machined-metal manifolds	59
3.3.3	Sheet-metal manifolds.....	59
3.3.4	Alumina fibre-board manifolds.....	59
3.4	Thermal profiles	59
3.4.1	Objectives	60
3.4.2	Equipment.....	60
3.4.3	Data and results.....	61
3.4.4	Construction and operation	61
3.4.5	Operational parameters	62
3.5	Summary	62
4	Electrochemical Analysis	63
4.1	Introduction	63
4.2	Batch variations.....	63
4.3	Fuel flow rate.....	66
4.3.1	Reynolds Number	66
4.3.2	Experimental	67
4.4	Hydrocarbon fuels	70
4.4.1	Methane.....	71
4.4.2	Propane	73

4.5	Operating temperature	74
4.6	Fuel cell active length.....	75
4.7	Cathode segmentation.....	76
4.8	Cathode current collection wires	78
4.9	Silver conductive ink.....	79
4.10	Silver nitrate wash coat.....	81
4.11	Anode current collector	82
4.12	Pinned anode current collectors.....	84
4.13	Platinum wash coat.....	85
4.14	Combined improvements.....	86
4.15	Summary.....	88
5	Prototype Development	91
5.1	Manifolds.....	91
5.1.1	Machined-metal manifolds (P1, P2 & P3)	91
5.1.2	Sheet-metal manifolds (P4 & P5).....	93
5.1.3	Alumina fibre-board manifolds (P6 & P7).....	95
5.1.4	Summary	96
5.2	Fuel system.....	96
5.2.1	Anode-gas-recycling	96
5.2.2	Summary	100
5.3	Heating system	100
5.3.1	Electrical heating.....	100
5.3.2	Partial oxidation reactors.....	103
5.3.3	Summary.....	106
5.4	Final prototype (P7).....	107
5.4.1	Design	107
5.4.2	Performance	107
5.5	Summary.....	108
6	Gas Analysis	109
6.1	Fuel Evaluation.....	109
6.1.1	Natural gas	109
6.1.2	Kovea gas.....	110
6.1.3	Liquid petroleum gas (LPG)	111
6.2	Air:fuel ratios.....	112
6.2.1	Rotameter verification.....	112
6.2.2	Oxygen:propane, oxygen:butane and oxygen:LPG ratios.....	113
6.3	Partial oxidation reactor exhaust gas	114
6.3.1	Reactor A	115
6.3.2	Reactor B.....	117
6.4	Summary.....	119

7	Prototype Analysis.....	121
7.1	System processes.....	121
7.2	System boundary.....	122
7.3	Analysis logic.....	123
7.4	Heat loss to the surroundings.....	123
7.4.1	Radial heat loss.....	124
7.4.2	Axial heat loss.....	125
7.4.3	Total heat loss.....	125
7.5	Fuel for partial oxidation reactor.....	125
7.6	Air for partial oxidation reactor.....	126
7.7	Partial oxidation reactor exhaust.....	126
7.8	Fuel for fuel cells.....	127
7.9	Electrical energy generated.....	128
7.9.1	Predicted potential.....	128
7.9.2	Predicted current.....	128
7.9.3	Power output.....	129
7.10	Air for fuel cells.....	129
7.11	Fuel exhaust from fuel cells.....	129
7.12	Air exhaust from fuel cells.....	130
7.13	Efficiency.....	130
7.14	Strategies to improve efficiency.....	131
7.14.1	Fuel cells.....	131
7.14.2	Thermal management.....	132
7.14.3	System design.....	132
7.15	Analysis limitations.....	133
7.16	Summary.....	134
8	Conclusions and Recommendations.....	135
8.1	MT-SOFC Performance.....	135
8.2	Prototype.....	136
8.3	Gas analysis.....	137
8.4	Prototype analysis.....	138
8.5	Recommendations for future research.....	138
9	References.....	139
	Appendix I – Certificates of Analysis.....	145
	Appendix II – Analysis Worksheets.....	147

LIST OF FIGURES

Figure 2 1 Planar cell configurations	8
Figure 2 2 Planar SOFC design.....	8
Figure 2 3 Planar SOFC with external manifolds	9
Figure 2 4 End view of tubular SOFC produced by Siemens Westinghouse [22]	9
Figure 2 5 Tubular SOFC constructed with (almost) no seals	10
Figure 2 6 A single MT-SOFC.....	10
Figure 2 7 Transport processes within a SOFC.....	14
Figure 2 8 MT-SOFC encapsulated by quartz tubing	21
Figure 2 9 Schematic of MT-SOFC test rig [14].....	22
Figure 2 10 MT-SOFC module [14]	23
Figure 2 11 Schematic of the burner components of a modified MT-SOFC [47].....	23
Figure 2 12 Schematic of SOFC stack and extra balance of plant [23]	26
Figure 3 1 Loop sampling with two column sequence reversal.	38
Figure 3 2 Chromatogram of SG1	42
Figure 3 3 Chromatogram of SG2.....	43
Figure 3 4 Chromatogram of SG3.....	44
Figure 3 5 Chromatogram of ethane standard gas.....	45
Figure 3 6 Chromatogram of nitrogen standard gas.....	46
Figure 3 7 Chromatogram of dry air standard gas.....	46
Figure 3 8 Chromatogram of carbon dioxide standard gas	47
Figure 3 9 Linearity of TCD response	48
Figure 3 10 Schematic of gas sampling points for MT-SOFC generator.....	49
Figure 3 11 MT-SOFC fabrication processes.....	50
Figure 3 12 Lemming design MT-SOFC	51
Figure 3 13 GT2 design MT-SOFC, two wire (a) and four wire (b).....	51
Figure 3 14 HS2 design MT-SOFC.....	52
Figure 3 15 MT-SOFC co-firing regime	55
Figure 3 16 Plan view of thermocouple locations.....	62
Figure 4 1 IV performance at 900°C. Cells AJH3, AJH6, AJH11 and AJH12 are presented in the order given in the legend.	65
Figure 4 2 IP performance at 900°C. Cells AJH3, AJH6, AJH11 and AJH12 are presented in the order given in the legend.	65
Figure 4 3 Effect of fuel flow rate on current density	67
Figure 4 4 Effect of fuel flow rate on power density	67
Figure 4 5 Effect of fuel flow rate and temperature on power density.....	68
Figure 4 6 Effect of fuel flow rate on current density [15]	69
Figure 4 7 Effect of fuel flow rate on power density [15].....	69
Figure 4 8 Effect of air-to-methane ratios on power density.....	71

Figure 4 9 Effect of using hydrogen or methane on current densities	72
Figure 4 10 Effect of using hydrogen or methane on power densities.....	72
Figure 4 11 Effect of hydrogen and propane on current densities	73
Figure 4 12 Effect of hydrogen and propane on power densities	73
Figure 4 13 Effect of operating temperature on current density	74
Figure 4 14 Effect of operating temperature on power density	74
Figure 4 15 Effect of fuel cell active length on current density	75
Figure 4 16 Effect of fuel cell active length on power density	75
Figure 4 17 Effect of cathode segmentation on current density.....	76
Figure 4 18 Effect of cathode segmentation on power density	77
Figure 4 19 Effect of cathode segmentation on current density.....	77
Figure 4 20 Effect of cathode segmentation on power density	78
Figure 4 21 Effect of number of wires on current density	79
Figure 4 22 Effect of number of wires on power density	79
Figure 4 23 Effect of silver conductive ink on current density	80
Figure 4 24 Effect of silver conductive ink on power density	80
Figure 4 25 Effect of silver nitrate on current density	81
Figure 4 26 Effect of silver nitrate on power density.....	82
Figure 4 27 Effect of anode current collection method on current density	83
Figure 4 28 Effect of anode current collection method on power density	83
Figure 4 29 Effect of pinned anode current collection on current density	84
Figure 4 30 Effect of current collection methods on power density	85
Figure 4 31 Effect of platinum wash coat on current density	86
Figure 4 32 Effect of platinum wash coat on power density.....	86
Figure 4 33 Effect of combined improvements on current density.....	87
Figure 4 34 Effect of combined improvements on power density	87
Figure 5 1 Machined metal manifolds (P1 & P2)	91
Figure 5 2 Multi-cell metal manifolds (P3)	92
Figure 5 3 Folded sheet-metal manifold system (P5)	94
Figure 5 4 Alumina fibre manifolds (P7).....	95
Figure 5 5 System design showing anode recycling	97
Figure 5 6 System design showing valve to turn off the bubbler.....	97
Figure 5 7 Effect of applied potential and polarity to pump throughput.....	98
Figure 5 8 Effect of fuel addition to fuel cell performance.....	99
Figure 5 9 Effect of controller on furnace temperature profile	101
Figure 5 10 Thermal profile using electrical heating	102
Figure 5 11 Effect of temperature fluctuations on fuel cell performance	102
Figure 5 12 System design using partial oxidation reactor and liquid fuels	103
Figure 5 13 Effect of temperature on vapour pressure.....	104

Figure 5 14 System design using partial oxidation reactor using LPG fuel.....	105
Figure 5 15 Thermal profile using partial oxidation reactor	105
Figure 5 16 Start-up profile of partial oxidation reactor	106
Figure 6 1 Effect of air:LPG ratio on temperature and exhaust gas composition (Reactor A)	116
Figure 6 2 Effect of air:LPG ratio on temperature and exhaust gas composition (Reactor B).....	117
Figure 6 3 Effect of air:LPG ratio on carbon monoxide and hydrogen yield.....	118
Figure 7 1 Conceptual MT-SOFC generator showing system boundary	122

LIST OF TABLES

Table 2 1 Fuel cell characteristics [21]	7
Table 2 2 Fuel cell reaction electrochemistry [21].....	7
Table 2 3 Organisations developing SOFC technology.....	11
Table 2 4 Effect of temperature on for [22].....	15
Table 2 5 Published data for SOFC systems.....	20
Table 2 6 Molecules and compounds removed by molecular sieves	27
Table 3 1 Thermal conductivities of gases [66].....	39
Table 3 2 Peak areas and composition of SG1.....	42
Table 3 3 Peak areas and composition of SG2.....	43
Table 3 4 Peak areas and composition of SG3.....	44
Table 3 5 Peak areas and concentrations for ethane standard gas.....	45
Table 3 6 Peak area and composition of nitrogen standard gas	45
Table 3 7 Peak areas and composition for dry air.....	47
Table 3 8 Peak area and concentration for carbon dioxide standard gas	47
Table 3 9 A1 ingredients and suppliers (60:40 weight% Ni/YSZ)	52
Table 3 10 A2 ingredients and suppliers (90:10 weight% Ni/YSZ)	53
Table 3 11 C1 ingredients and suppliers.....	54
Table 3 12 C2 ingredients and suppliers.....	54
Table 3 13 Materials for manifold development.....	58
Table 5 1 Design features of prototypes	108
Table 6 1 Composition [mol•%] of reticulated natural gas.....	110
Table 6 2 Composition [mol•%] of Kovea gas canisters K1-K4	111
Table 6 3 Composition [mol•%] of LPG cylinders LPG1 and LPG2.....	111
Table 6 4 Set and measured air:fuel ratios using rotameters and GC analysis	113
Table 6 5 Set, measured and calculated combustion ratios for full and partial oxidation of LPG samples	114
Table 6 6 Composition [mol•%] of near stoichiometric air:LPG mixture	114
Table 6 7 Mean carbon dioxide and hydrogen concentrations in exhaust gas [mol•%] with respect to air:LPG ratios	118
Table 7 1 Flow rates of product gases.....	127
Table 7 2 Theoretical concentration [mol•%] of product gas, dry basis.....	127
Table 7 3 Species concentration [mol•%] of fuel cell exhaust gas	130

NOMENCLATURE

Symbol	Description	Unit
e	Electron charge	C
F	Faraday's constant	C/mol
R	Universal gas constant	J/K·mol
N_A	Avogadro number	1/mol
EMF	Electromotive force (potential)	V
V_{rev}°	Reversible EMF	V
I	Current	A
P	Power	kJ/s
E	Energy	kJ
G	Gibb's free energy	kJ/kg
$\Delta_r G^\circ$	Reversible Gibb's free energy	kJ/mol
H	Enthalpy	kJ/kg
Q	Heat energy	kJ
\dot{Q}	Heat energy flux	kJ/s
A	Area	m ²
K	Equilibrium constant	
m	Mass	kg
\dot{m}	Mass flow rate	kg/s
M	Molecular weight (molar mass)	g/mol
n	Number of moles	mol
\dot{n}	Molar flow rate	mol/s
T	Temperature	K or °C
P	Partial pressure	Pa
V	Volume	m ³
R_T	Total resistance due to polarisation losses	Ω
U_f	Fuel utilisation ratio	
η	Efficiency	
Re	Reynolds number	
ρ	Density	kg/m ³
v	Mean velocity	m/s

d	Internal diameter	m
μ	Dynamic viscosity	kg/m·s
AFC	Alkaline fuel cell	
ASTM	American Society for Testing and Materials	
HHV	Higher heating value	kJ/kg
LHV	Lower heating value	kJ/kg
LSM	Lanthanum strontium manganate	
MCFC	Molten carbonate fuel cell	
MT-SOFC	Mini-tubular solid oxide fuel cell	
PAFC	Phosphoric acid fuel cell	
PEMFC	Polymer electrolyte membrane fuel cell	
SOFC	Solid oxide fuel cell	
TCD	Thermal conductivity detector	
YSZ	Yttria stabilised zirconia	

1 INTRODUCTION

1.1 REQUIREMENT AND DEMAND FOR ELECTRICITY

Humans have integrated electrical energy into everyday life because it increases productivity. As more and more of the world's population develops and gains access to electrical energy, demand for generation capacity will increase. Increased immigration and commercial and industrial activity also increases demand leading to new generation plants that use conventional techniques are being constructed, and research and development into new technologies for future needs is being undertaken.

1.2 PORTABLE ENERGY GENERATION / STORAGE

Technological developments in the late 20th century have increased the demand for portable power generation. Humans are encouraged to possess portable devices and gadgets, which require electricity to operate. Depending on power requirements, these devices are normally powered by batteries, although alternative energy sources are available. For example, desktop calculators are commonly powered by solar panels. Larger and more complex portable devices, such as mobile telephones, laptop computers and handheld computers, require larger power sources.

The batteries used in portable devices and gadgets typically are rechargeable using power from the national grid. Battery technologies are well developed, and end users consider them cheap, easy to use, and capable. Battery efficiency may not be the most important characteristic to the end user and is rarely discussed (although it can be a driver in developing other energy conversion technologies). Instead, the end user is more interested in battery's ability to perform its function for a set period or to supply power in a location where it is not possible or practical to connect to electricity.

1.3 FUEL CELLS

Fuel price increases and increased concern for environmental issues have increased the emphasis on having more efficient and lesser polluting generators. One option is fuel cells. A fuel cell is an electrochemical device that directly converts the chemical energy of a fuel into electrical energy. Batteries and fuel cells both convert chemical energy into electrical energy, but there are inherent differences. A battery stores the chemical reactants and products within the device whereas a fuel cell stores the reactants and products externally. The reactants in a battery can run out and need to be replaced or recharged but a fuel cell will continue operating as long as reactants are provided and products are removed.

1.4 PORTABLE FUEL CELLS

Portable fuel cell development has concentrated on the polymer electrolyte membrane fuel cell, but recent developments in solid oxide fuel cell designs have opened up new opportunities [1-5]. In particular, the mini-tubular solid oxide fuel cell (MT-SOFC) design has the potential to increase the power density of a portable generator to a useful level and can be fuelled by a readily available primary fuel resource. Researchers have investigated using MT-SOFCs since the mid-1990s [6]. Simple demonstrations of single MT-SOFCs generating electricity in a laboratory are commonplace [6-10]. Single MT-SOFCs can be operated on various liquid and gaseous fuels such as methanol and propane as well as hydrogen. A MT-SOFC has operated on landfill gas [11]. Butane has also been identified as a practical gas for portable MT-SOFC generators [12].

To demonstrate larger generating capacity, many groups have attempted to group many fuel cells together to form a stack [13]. The technical issues of operating a stack of cells are different to operating a single fuel cell in the laboratory [14-16]. A key issue in developing a portable MT-SOFC generator is to design a heating system to maintain the fuel cells at an optimum generating condition. Other issues such as the electrical connections between the fuel cells and the fuel reforming capabilities of the heating device are also worthy of research.

1.5 RESEARCH AIMS

Designing a portable generator that uses MT-SOFC technology requires new research to bridge the knowledge gap between operating a controlled laboratory experiment to presenting a functional prototype generator. This research aims to develop a portable generator using MT-SOFC technology. To maintain the fuel cells in optimum operating condition requires an integrated heating and fuel reforming system to be developed. The primary function of this system is to generate heat to maintain the fuel cells at the design temperature. The secondary function is to partially reform the fuel to minimise the potentially harmful effects to the fuel cells, such as carbon deposition on the anode of operating MT-SOFCs on hydrocarbon fuels.

1.6 THESIS OUTLINE

The literature related to the research aims are discussed in Chapter 2, which concludes with the research hypothesis. Chapter 3 describes the materials, analytical techniques and experimental set-up and methodology used. Chapter 4 presents and discusses the electrochemical data when the MT-SOFCs prototypes are operating under various conditions and Chapter 5 describes developing the prototypes. Chapter 6 presents and discusses the gas analysis data specific to the partial oxidation reactor and Chapter 7 develops a mathematical model for heat and mass transfer in a MT-SOFC generator. Chapter 8 summarises the conclusions and presents some ideas for further research.

2 LITERATURE REVIEW

2.1 FUEL CELLS

2.1.1 History

The discovery of fuel cells in 1839 is credited to Sir William Grove [17]. However, major effort into research and developing fuel cells has only occurred since the start of the space race in the 1950s. A contributing factor for the delayed development cells was the invention of internal combustion engines in the late 1800s.

Fuel cells offer an alternative energy conversion technique for generating electricity on a small, medium or large scale. Theoretically, fuel cells can convert the chemical energy of a fuel into electricity more efficiently than conventional technologies such as thermal power stations because fuel is directly converted into electrical energy. Emissions (particularly carbon dioxide) from a fuel cell will be lower than from existing generators producing the same electrical output.

2.1.2 Types of fuel cells

There are five major types of hydrogen fuel cells [9]:

- Alkaline fuel cell (AFC)
- Molten carbonate fuel cell (MCFC)
- Phosphoric acid fuel cell (PAFC)
- Polymer electrolyte membrane fuel cell (PEMFC)
- Solid oxide fuel cell (SOFC)

Alkaline fuel cells use hydrogen and oxygen, with potassium hydroxide as the electrolyte to conduct hydroxyl ions. Hydrogen molecules are oxidised at the anode by reaction with hydroxyl ions to produce water and free electrons. The electrons flow, through an externally applied load, to the cathode, where they react with oxygen and water to produce hydroxyl ions. The main drawback of the AFC is that it requires both pure hydrogen and pure oxygen. Alkaline fuel cells have been used by NASA in the Space Shuttles since the 1960s because they have high power generation efficiencies and produce water [18].

The PEMFC has an electrolyte made from a thin impermeable organic membrane that conducts hydrogen ions (essentially protons, hence its alternative name proton exchange membrane fuel cell). Hydrogen is oxidised at the anode to produce protons, which flow through the electrolyte, and free electrons, which flow through the externally-applied load and react with oxygen at the cathode to produce water. PEMFCs have been trialled in hybrid electric cars [19].

The electrolyte in a PAFC is phosphoric acid. It has the same electrochemistry as the PEMFC, but operates at a higher temperature (up to 200°C) whereas the PEMFC operates at temperatures up to 80°C. Due to its higher operating temperature, the PAFC can be used in cogeneration applications. One disadvantage of the PAFC is its long start-up time; therefore, the PAFC is being developed primarily for grid applications and industrial generation.

The conducting ion in a MCFC is a carbonate ion and the electrolyte is made from lithium, sodium or potassium carbonates. It operates at temperatures above 600°C (the melting point of carbonate salts), which allows ions to flow. Carbonate ions form at the cathode when oxygen reacts with carbon dioxide and free electrons from the anode reaction. Carbonate ions flow through the electrolyte to combine with hydrogen at the anode to produce water, carbon dioxide and electrons. MCFCs are being developed for grid applications and industrial generation [20].

The SOFC uses a non-porous ceramic that conducts oxygen ions at high temperatures (between 600°C and 1000°C). Oxygen disassociates at the cathode and oxygen ions flow through the electrolyte to combine with hydrogen at the anode. SOFCs are suitable for potentially many applications, from large power stations down to small portable generators. They also present the greatest opportunity for overall system efficiency in fuel cells.

The electrolyte material and operating temperature of the different types of fuel cells and the conducting ions and the electrochemical reactions occurring at the anode and cathodes are also summarised (Table 2-1 and Table 2-2). Of the fuel cells described, only PEMFCs and SOFCs are seriously being considered for

portable generation. This literature review now focuses solely on SOFCs. The various SOFC technologies are described in the next section.

Table 2-1 Fuel cell characteristics [21]

Type	Electrolyte	Operating temperature [°C]
AFC	KOH	90
PEMFC	$CF_3(CF_2)_nOCF_2SO_3^-$	80
PAFC	H_3PO_4	200
MCFC	$Li_2CO_3 - K_2CO_3$	650
SOFC	$Zr_{0.92}Y_{0.08}O_{1.96}$	1000

Table 2-2 Fuel cell reaction electrochemistry [21]

Type	Ion	Anode reaction	Cathode reaction
AFC	OH^-	$H_2 + 2OH^- \rightarrow 2H_2O + 2e^-$	$\frac{1}{2}O_2 + H_2O + 2e^- \rightarrow 2OH^-$
PEMFC	H^+	$H_2 \rightarrow 2H^+ + 2e^-$	$\frac{1}{2}O_2 + 2H^+ + 2e^- \rightarrow H_2O$
PAFC	H^+	$H_2 \rightarrow 2H^+ + 2e^-$	$\frac{1}{2}O_2 + 2H^+ + 2e^- \rightarrow H_2O$
MCFC	CO_3^{2-}	$H_2 + CO_3^{2-} \rightarrow H_2O + CO_2 + 2e^-$	$\frac{1}{2}O_2 + CO_2 + 2e^- \rightarrow CO_3^{2-}$
SOFC	O^{2-}	$H_2 + O^{2-} \rightarrow H_2O + 2e^-$	$\frac{1}{2}O_2 + 2e^- \rightarrow O^{2-}$

2.2 SOFC TECHNOLOGIES

2.2.1 Introduction

The two dominant cell geometries are planar and tubular. Under normal operating conditions, a single SOFC typically produces less than one volt of direct current so many cells are required to produce useful voltage and power. Cells can be arranged into a stack but the engineering issues involved in grouping cells into a stack can be complex including maintenance of high temperature seals, ensuring good electrical connections between components and managing the thermal flows within the stack.

2.2.2 Planar SOFC

The standard simple planar SOFC has a thin plate tape cast from the electrolyte material with the electrodes coated on each side. Other configurations such as anode or cathode supported cells are also possible (Figure 2-1).

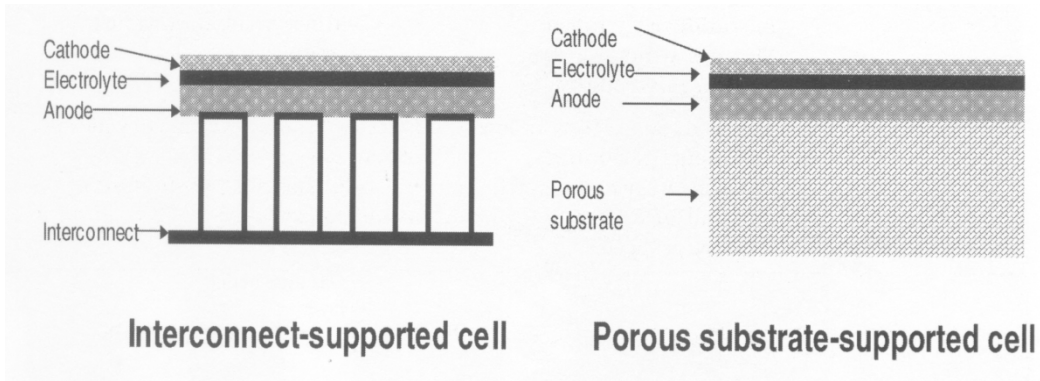


Figure 2-1 Planar cell configurations

Planar systems require many gas tight seals; gas leaks decrease potential and thus efficiency. Cells are connected in series using interconnects placed between the cells to separate fuel and oxidant gases and to provide electrical connection (Figure 2-2).

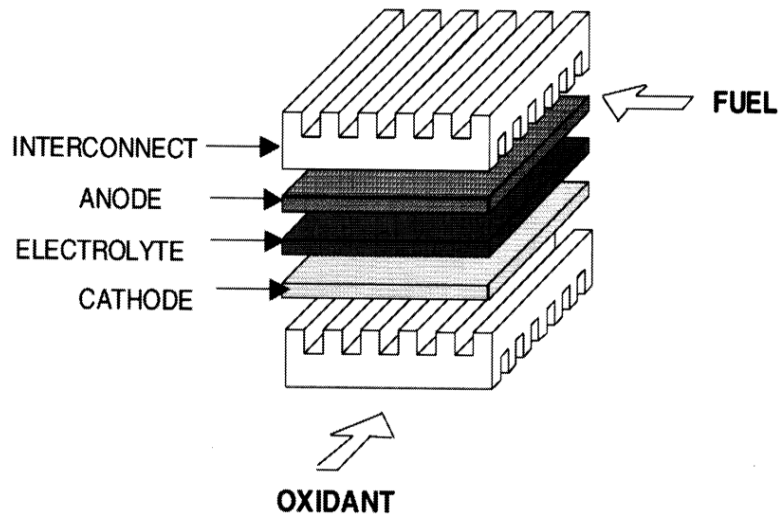


Figure 2-2 Planar SOFC design

Fuel and oxidant gas flows are further controlled with external manifolds (Figure 2-3).

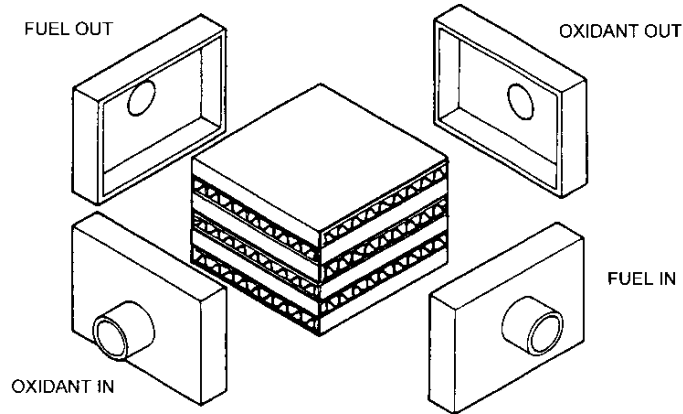


Figure 2-3 Planar SOFC with external manifolds

2.2.3 Tubular SOFC

Fuel in tubular SOFC systems with large diameter cells (>15 mm) is outside the cells and air is injected down the centre of the cell. The interconnect provides only an electrical connection between cells (Figure 2-4) rather than its dual role in planar systems separating fuel and oxidant gases.

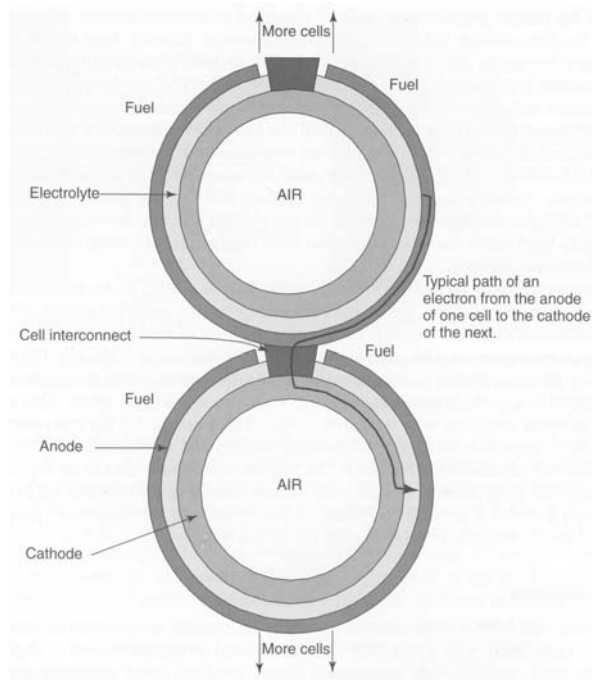


Figure 2-4 End view of tubular SOFC produced by Siemens Westinghouse [22]

As the tubular design inherently separates the fuel and oxidant gases, sealing is much easier and in some cases unnecessary (Figure 2-5).

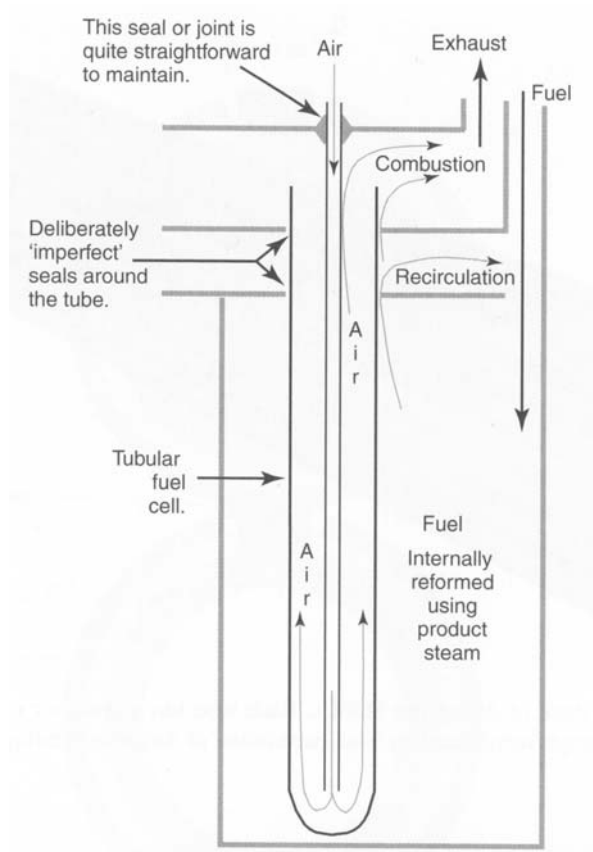


Figure 2-5 Tubular SOFC constructed with (almost) no seals

2.2.4 MT-SOFC

The mini-tubular SOFC (also called micro-tubular SOFC) or MT-SOFC is a subcategory of tubular SOFCs. These cells are between one and five millimetres in diameter [23]. The small size (Figure 2-6) means they can be used in portable electrical generation. A more detailed description of MT-SOFCs and their systems is in Section 2.5.

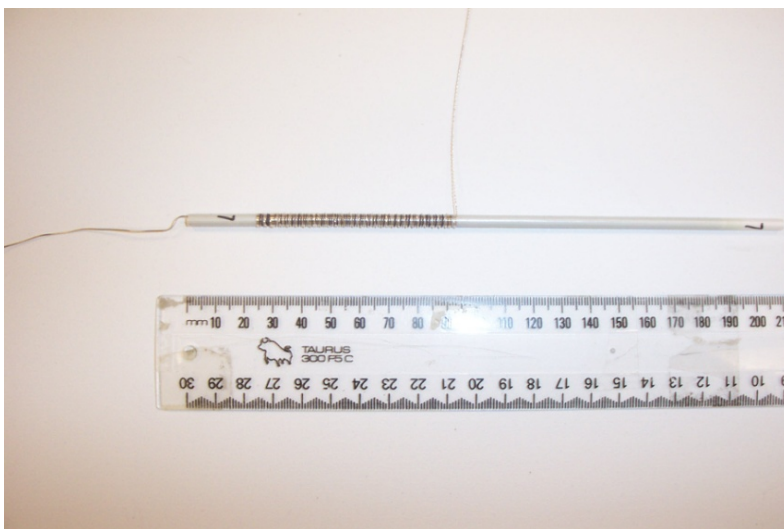


Figure 2-6 A single MT-SOFC

2.2.5 Technology overview

Many organisations around the world have developed SOFC technologies and systems, using different fuels and producing various electrical outputs (Table 2-3). There is a trend to use mini tubular systems for low power generation and tubular and planar systems for larger power generation.

Table 2-3 Organisations developing SOFC technology.

Organisation	Technology	Fuel	Output [W_e]	Reference
Tohoku University, JP	MT-SOFC	Butane	0.0165	[24]
Keele University, UK	MT-SOFC	Butane	0.1 – 1	[8]
Birmingham University, UK	MT-SOFC	Hydrogen	-	[14]
Gifu, JP	MT-SOFC	Butane	0.14	[12]
Keele University, UK	MT-SOFC	Butane	8	[4]
Nanodynamics, US	MT-SOFC	Butane	50	[25]
Alberta Research Council, CA	MT-SOFC	-	50 – 500	[26]
Connecticut University, US	MT-SOFC	Hydrogen	100	[15]
Keele University, UK	MT-SOFC	Diesel	100	[27]
Keele University, UK	MT-SOFC	Methane	200	[23]
Ceramic Fuel Cells Ltd, AU	Planar	LPG	1,000	[28]
Sulzer Hexis, CH	Planar	Methane	1,100	[29]
Acumentrics, US	MT-SOFC	Methane	5,000	[30]
Ceramic Fuel Cells Ltd, AU	Planar	LPG	5,000	[28]
Siemens Westinghouse, US	Tubular	Methane	123,000	[23]
Siemens Westinghouse, US	Tubular	Methane	172,000	[23]
Julich Research Centre, DE	Planar	Methane	200,000	[31]

2.3 SOFC FUELS

One key feature of fuel cells is their ability to use hydrogen as a fuel. This an ideal gas because theoretically water will be the only exhaust gas. Unfortunately, there is no naturally-occurring source of hydrogen on Earth so it must be manufactured. Hydrogen and oxygen can be produced by splitting water molecules electrolytically but the advantage of using electricity to make hydrogen only occurs when it is feasible and economic to store hydrogen and oxygen gases

for reaction at a later stage. Biological methods of producing hydrogen such as photosynthetic and anaerobic fermentation are *bona fide* renewable sources of sustainable energy along with solar, hydro and wind energy [32].

Gasification of coal produces hydrogen and carbon monoxide rich gas, which can fuel SOFCs. The endothermic coal gasification reaction can be coupled with the exothermic reaction in SOFCs to achieve more effective thermal management. Anodes have been proposed that can potentially oxidise carbon directly [33].

Currently, the main method for producing hydrogen is by reforming hydrocarbon fuels such as natural gas. Reforming produces carbon monoxide as well as hydrogen but SOFCs do not require high purity hydrogen and can even use carbon monoxide. Fuel cells allow consumers to generate electricity from primary energy resources. Although they will not greatly reduce human demand for hydrocarbon fuels, there is potential to use the hydrocarbon fuels more efficiently than with current technologies.

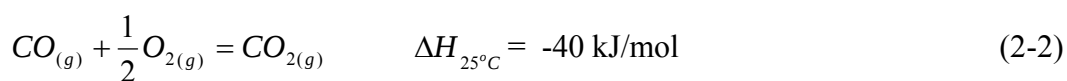
It is more practical to use a conventional fuel supply that is readily available, easily accessible and with much greater energy density than hydrogen. A small portable generator requires a compact, but dense fuel source. Liquid fuels are dense but using a liquid fuel in a portable SOFC generator requires extra balance of plant, which may make the generator impractical to carry and operate. Gaseous fuels such as propane and butane are dense and commercially available in portable storage containers.

2.3.1 Reforming

There are two methods of reforming hydrocarbon fuels in a SOFC - steam reforming or partial oxidation. Solid oxide fuel cells can also either steam reform or partial oxidise the fuel over the anode, a feature termed “internal reforming”. Asano *et al.* [1] investigated a platinum electrode that catalyses methane premixed with air to hydrogen and carbon monoxide. Proprietary catalysts in specially-designed fuel processors can achieve conversion efficiencies greater than 90% [2, 28]. Steam reforming has the advantage that it avoids carbon deposition but this can also be achieved by partial oxidation reforming [34], a process that requires

the fuel to be mixed with oxygen or air before passing over a catalyst. Propane can be cracked into carbon and hydrogen and has been investigated as a fuel for a portable polymer electrolyte fuel cell [35]. Partial oxidation reforming occurs when hydrocarbon fuels are premixed with oxygen or air in a range of ratios over a suitable catalyst. Research on reforming reactions for SOFCs has focused on minimising the chance of carbon deposition on the anode [7, 10, 36, 37]. Steam reforming reactions reduce carbon deposition more effectively than partial oxidation reactions, so research has focused on steam reforming. However, steam reforming in a portable SOFC generator is a disadvantage because water is required.

Recent publications acknowledge the advantages of using partial oxidation reactions to also heat fuel cells to their operating temperature, particularly for small portable systems, with the added benefit of avoiding carbon deposition [38-40]. Heat released from the partial oxidation reaction can be used to maintain fuel cells at their operating temperature, removing the need for an external heater. Partial oxidation of propane can sustain the temperature at 500-600°C [38], and with appropriate design considerations could be sufficient for traditional electrolyte-supported MT-SOFC. Partial oxidation of propane to carbon monoxide and hydrogen produces 207 kJ/mol of energy (Equation 2-1), and the oxidation of carbon monoxide gives an additional 40 kJ/mol (Equation 2-2).



2.4 SOFC OPERATING PRINCIPLES

Fuel cells generate electricity via an electrochemical process. This section discusses performance criteria associated with SOFCs, initially using hydrogen but also looking at hydrocarbon fuels. Consideration of these reactions highlights the factors that affect fuel cell performance.

2.4.1 Electrochemical reactions

A SOFC has three main components, two electrodes separated by an electrolyte (Figure 2-7). Hydrogen is the fuel in this example but the analysis can be modified for other fuels. Fuel and oxidant gases are able to diffuse into the porous electrodes, but the electrolyte is dense enough to keep the fuel and oxidant gases separated.

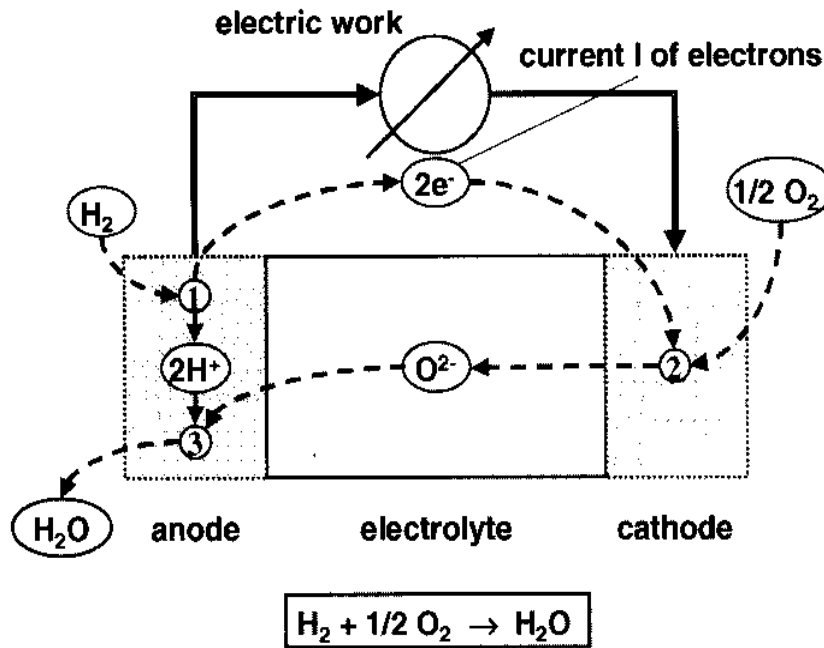


Figure 2-7 Transport processes within a SOFC

Half cell reactions for the anode (Equation 2-3) and cathode (Equation 2-4) are:



The overall reaction is:



2.4.2 Electromotive force (EMF) of a hydrogen fuel cell

The reversible EMF is derived from the first and second laws of thermodynamics.

$$V_{rev} = \frac{-\Delta^r G}{n^{el} \cdot F} \quad (2-6)$$

Where: $\Delta^r G^\circ = -237.2 \text{ kJ/mol}$ for hydrogen (Table 2-4)

$F = 96485 \text{ C/mol}$ (Faraday's constant)

$n^{el} = 2$ for ionisation of hydrogen

Substituting into Equation 2-6, the reversible EMF using hydrogen at 25°C is 1.229 V. The reversible EMF decreases with increasing temperature and will subsequently affect the potential system efficiency (Equation 2-10).

Table 2-4 Effect of temperature on $\Delta^r G^\circ$ for $H_2 + \frac{1}{2}O_2 \rightarrow H_2O$ [22]

Temperature (°C)	$\Delta^r G^\circ$ (kJ/mol)	Water Phase
25	-237.2	Liquid
80	-228.2	Liquid
80	-226.1	Gas
100	-225.2	Gas
200	-220.4	Gas
400	-210.3	Gas
600	-199.6	Gas
800	-188.6	Gas
1000	-177.4	Gas

2.4.3 EMF of a fuel cell using carbon monoxide

Equation 2-6 can also be used to calculate the reversible EMF of a fuel cell operating on carbon monoxide. In this case;

$\Delta^r G^\circ = -515$ kJ/mol for carbon monoxide

$F = 96485$ C/mol

$n^{el} = 4$ for ionisation of carbon monoxide

Substituting into Equation 2-6 gives a reversible voltage of 1.334 V.

2.4.4 Operational fuel cell voltages

The operational fuel cell voltage can be determined by analysing the various factors that reduce voltage from the theoretical values.

Activation Losses – These are related to the slow rate reactions at the electrode and electrolyte interfaces. The cathode material, typically LSM, has limited ionic conductivity. Reactions and electron transfers must take place at the three phase boundary between electrolyte, cathode and gases. If the three phase boundary contact area is increased, activation losses can be reduced [23].

Fuel Crossover and Internal Currents - Under open circuit conditions, oxygen ions should not diffuse through the electrolyte. If they do, the effect is called “fuel crossover”. This effect can be measured by monitoring fuel consumption and oxidant gases at open circuit conditions using equipment able to measure minute changes in gas flows. Fuel crossover creates a small current that alters operating efficiency. In low temperature fuel cells, particularly PEMFCs, fuel crossover can dramatically affect the open circuit voltage but this effect can be ignored in high temperature SOFCs [22].

Ohmic Losses - Electrical resistance of the electrodes and resistance to flow of the ions in the electrolyte contribute to Ohmic losses [22]. As the name suggests, voltage drop is proportional to the current,

$$\Delta V_{ohm} = i \cdot r \quad (2-7)$$

where i is the current and r is the resistance. This effect is dominated by electrolyte thickness so decreasing the electrolyte thickness will reduce voltage drop [23]. Electrolyte thickness, however, must still be sufficient and dense enough to prevent the anode short circuiting with the cathode. Highly-conducting electrode materials will also reduce internal cell resistance.

Concentration Losses - Fuel and oxidant concentration differences at their respective electrodes can produce a voltage drop. Some of the oxygen in the air being used on the cathode side of the fuel cell will be ionised and transferred through the electrolyte to the anode. As a result, oxygen partial pressure at the cathode decreases at a rate proportional to the current drawn from the cell. The Nernst equation (Equation 2-8) for the EMF can indicate the effect of pressure and/or gas concentration changes on the ideal voltage. The Nernst equation in its common form includes the reversible voltage and the modifier term:

$$V_N = \frac{-\Delta G}{n^{el} \cdot F} - \frac{R \cdot T \cdot \ln K}{n^{el} \cdot F} \quad (2-8)$$

Operating Voltage - Voltage drops from irreversibilities can be subtracted from the reversible open circuit voltage to obtain the cell's operating voltage:

$$V_{op} = V_{rev} - \Delta V_{ohm} - \Delta V_{act} - \Delta V_{conc} \quad (2-9)$$

The ratio of the operating voltage to the Nernst voltage gives an indication of the generators efficiency [41].

$$\eta = \frac{V_{op}}{V_N} \quad (2-10)$$

2.4.5 Current

Current is directly related to fuel consumption rate. The following analysis is for hydrogen but, as with the reversible voltage, can be easily extended to other fuels. Molar flow rate of electrons is twice the molar flow rate of hydrogen:

$$\dot{n}_{el} = 2\dot{n}_{H_2} \quad (2-11)$$

Faraday's constant is the multiple of elementary charge and Avogadro's constant:

$$F = e \cdot N_A \quad (2-12)$$

Electric current is directly proportional to molar flow rate of electrons, or molar flow rate of the spent fuel:

$$I = \dot{n}_{el} \cdot (-e) \cdot N_A = -\dot{n}_{el} \cdot F = -2\dot{n}_{H_2} \cdot F \quad (2-13)$$

For 50 mL/min of hydrogen, assuming 100% fuel utilisation, the current is 6.67 A.

2.4.6 Fuel utilisation

The current generated by a SOFC is related to fuel consumed [spent] at the anode. Fuel utilisation [ratio] is the ratio of spent fuel flow to inlet fuel flow:

$$U_f = \frac{\dot{m}_{FI} - \dot{m}_{FO}}{\dot{m}_{FI}} \quad (2-14)$$

Fuel utilisation ratio may also be defined using molar flow rates:

$$U_f = \frac{\dot{n}_{FI} - \dot{n}_{FO}}{\dot{n}_{FI}} \quad (2-15)$$

2.4.7 Reversible power output

Reversible power is the maximum theoretical power which can be produced assuming zero losses and is calculated by multiplying the current and reversible voltage together:

$$P_{rev} = I \cdot V_{rev} \quad (2-16)$$

When current is 6.67 A and reversible voltage is 1.229 V, maximum theoretical power output is 8.2 W.

2.4.8 Actual power output

Actual maximum power output is reduced by the overpotentials (Section 2.4.4) and can be calculated by multiplying current by operational voltage:

$$P_{actual} = I \cdot V_{op} \quad (2-17)$$

2.4.9 Thermodynamic efficiency

Thermodynamic efficiency is given by the ratio of the Gibb's free energy of the reaction to the corresponding enthalpy of reaction [42]:

$$\eta_{thermo} = \frac{\Delta G}{\Delta H} = \frac{\Delta H - T\Delta S}{\Delta H} \quad (2-18)$$

2.4.10 Thermal efficiency

Thermal efficiency of a conventional thermodynamic process is defined as the ratio of net work output to heat energy supplied:

$$\eta_{thermal} = \frac{W_{out}}{Q_{in}} \quad (2-19)$$

Adapting this efficiency for the SOFC, net work output is equivalent to electrical energy output plus any excess heat recovered for cogeneration purposes and the heat energy in is supplied by potential energy of fuel.

$$\eta_{fc} = \frac{I \cdot V_{op}}{\dot{Q}_{in}} \quad (2-20)$$

Energy of fuel entering the anode:

$$\dot{Q}_{in} = \dot{m}_{FI} \cdot \Delta H_{FI} = \dot{n}_{FI} \cdot M_{FI} \cdot \Delta H_{FI} \quad (2-21)$$

Fuel cell efficiency is:

$$\eta_{fc} = \frac{-2\dot{n}_{H_2} \cdot F \cdot V}{\dot{m}_{FI} \cdot \Delta H_{FI}} \quad (2-22)$$

2.4.11 Published data

This section discusses theoretical performance equations with published data for SOFC systems. Data from peer-reviewed journals and books for SOFCs and systems (some breadboard and some fully integrated) developed around the world are summarised (Table 2-5) in order of increasing fuel cell electrical output. The lower heating values (LHV) are generally-accepted values for specified fuels compiled from various sources.

No one report provided enough information to calculate total energy input and/or energy output, electrical, thermal, and/or overall efficiencies of the generator(s) so it is neither possible to compare systems nor verify claimed increased performance over that of earlier systems.

Developments in MT-SOFC technology are concentrated in low power generators ranging from 1 W_e to 10 kW_e. Most of the fuel input data for MT-SOFC systems only specify fuel consumption rate of the fuel cells and do not include energy required to heat the fuel cells to the operating temperature. As literature reports, high overall efficiency of SOFC systems will only be achieved by combining the SOFC module with a gas turbine generator. Efficiencies of small SOFC systems will be much lower than theoretical because these systems do not have a large amount of supporting equipment.

2.5 MINI-TUBULAR SOFC

Research into MT-SOFCs began in the early 1990s. One of their main benefits is their ability to resist thermal shocks [43, 44], so MT-SOFC systems can reach the operating temperature quickly. These systems are also resistant to physical shock, which allows MT-SOFCs to be considered for portable generators. Some novel applications for MT-SOFC include electric golf carts, auxiliary power units for cars and trucks and military applications [45, 46].

Table 2-5 Published data for SOFC systems

Organisation	Technology	No. of cells	Fuel	Fuel LHV [MJ/kg]	Feed rate [mL/min]	Energy input [W]	Fuel utilisation [%]	FC electrical output [W]	GT electrical output [W]	Thermal output [W]	Electrical efficiency [%]	Thermal efficiency [%]	Reference
Tohoku University, JP	MT	3	Butane	45.7	-	-	-	0.0165	-	-	-	-	[24]
Giftu, JP	MT	-	Butane	45.7	390	-	-	0.14	-	-	-	-	[12]
Keele University, UK	MT	3	Butane	45.7	25-80	-	-	0.1 - 1	-	-	-	-	[8]
Keele University, UK	MT	-	Butane	45.7	-	-	-	8	-	-	-	-	[4]
Nanodynamics, US	MT	-	Butane	45.7	-	-	-	50	-	-	-	-	[25]
Alberta Research Council, CA	MT	-	-	-	-	-	-	50-500	-	-	-	-	[26]
Birmingham University, UK	MT	20	Hydrogen	120	400	-	-	-	-	-	-	-	[14]
Connecticut University, US	MT	40	Hydrogen	120	4000	-	30	100	-	-	-	-	[15]
Keele University, UK	MT	400	Diesel	45.7	-	-	-	100	-	-	-	-	[27]
Keele University, UK	MT	1000	Methane	50	-	20,000	1	200	-	-	-	-	[23]
Ceramic Fuel Cells Ltd, AU	P	-	LPG	46	-	-	21	1,000	-	-	-	-	[28]
Sulzer Hexis, CH	P	-	Methane	50	-	-	-	1,100	-	2,500	25-30	-	[29]
Ceramic Fuel Cells Ltd, AU	P	-	LPG	46	10,000	-	-	5,000	-	-	-	-	[28]
Acumentrics, US	MT	-	Methane	50	-	-	-	5,000	-	-	45	-	[30]
Siemens Westinghouse, US	T	-	Methane	50	-	-	-	123,000	103,000	-	46	27	[23]
Siemens Westinghouse, US	T	-	Methane	50	-	-	-	172,000	22,000	-	52	-	[23]
Julich Research Centre, DE	P	-	Methane	50	-	-	80	200,000	-	-	-	-	[31]

It is relatively easy to manufacture a single MT-SOFC and make it work on a lab bench. Increasingly, development has focused on placing many cells together (a stack) and producing prototypes. There are several technical issues in scaling up from single cells to a functioning prototype including: having an even temperature distribution in the heated zone; determining the appropriate electrical and gas connections; selecting a fuel; and integrating a heater and fuel pre-processor.

2.5.1 Heating

Testing a single MT-SOFC is usually done inside an electrically-heated and controlled furnace. The heating filament is normally nickel-chromium wire, which may be wound around an alumina tube or rod. The advantage of using an electrically-heated and controlled furnace is that heating and cooling rates can be controlled and a stable operating temperature maintained. The position of the controlling thermocouple relative to the fuel cell and the heating elements is important so that it indicates the actual operating temperature. Single MT-SOFCs can also be tested within the confines of quartz tubing (Figure 2-8) using heat provided by an external combustion heater.

Temperature is controlled by the fuel flow rate. Regardless of the heating method, insulating the heated zone decreases heating load. Since the main objective of single cell testing is to determine electrochemical performance, there has been little effort into designing an insulated test facility.

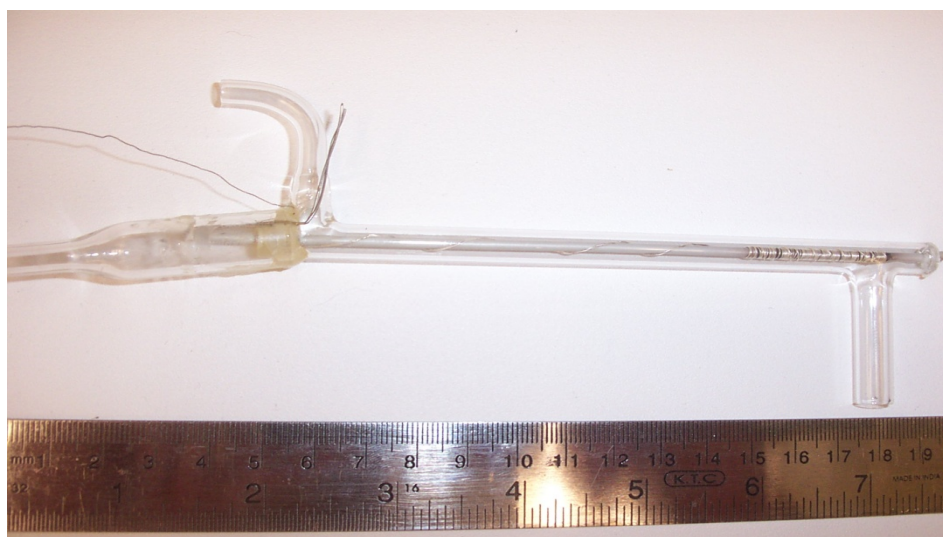


Figure 2-8 MT-SOFC encapsulated by quartz tubing

Electrical and combustion methods can also be used to heat small stacks. Electrical methods are normally used when electrochemical performance of the cells is the main consideration (Figure 2-9) whilst combustion techniques are used when demonstrating concepts of a fully-functional generator.

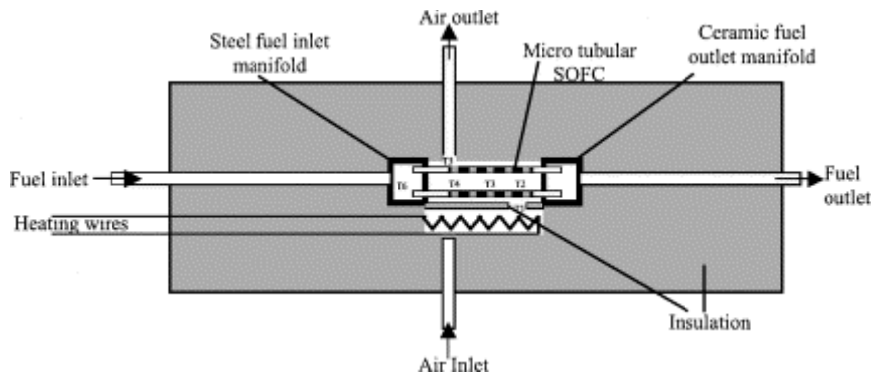


Figure 2-9 Schematic of MT-SOFC test rig [14]

The important characteristics of heating a MT-SOFC system are to maintain an even temperature profile across the fuel cells whilst minimising heat input and to allow a quick start up. Using electrical energy to heat a practical MT-SOFC system is not viable because more electricity would be used to heat the cells than would be generated. Therefore, it is better to develop a MT-SOFC system heated using conventional combustion or catalytic methods. This would allow a truly independent generator running on a single energy source.

An obvious solution is to use combustion reactions of a fuel to heat the system. An ideal MT-SOFC system will use the same fuel source for both heating the cells and fuelling cells directly or via a fuel reformer. Lockett's design (Figure 2-10) incorporates 20 MT-SOFCs in an array [14]. Cells are heated by exhaust gases from a catalytic fuel reactor located below the cells. This design could potentially expose the cathode to unreacted fuel from an incomplete reaction, which would decrease cell potential and efficiency as well as potentially damage the cathode.

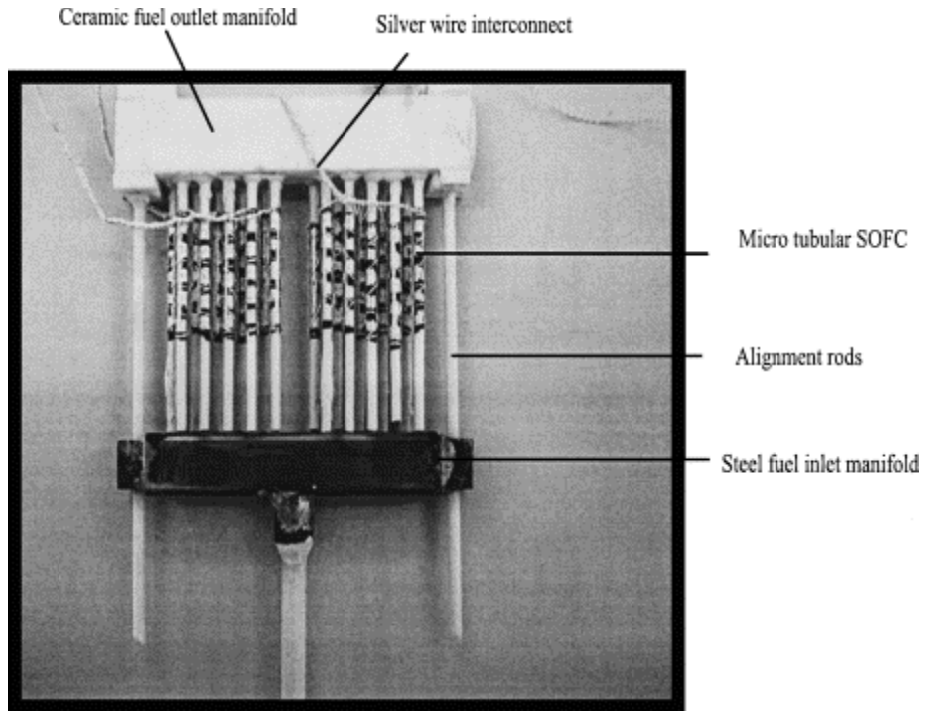


Figure 2-10 MT-SOFC module [14]

Alternative set-ups have also been investigated including retrofitting a commercially-available catalytic heating appliance with modified MT-SOFCs (Figure 2-11). To reduce set-up complexity, the anode of the modified cells was on the outside of the electrolyte tube, the cathode on the inside and air was blown through the tubes [47].

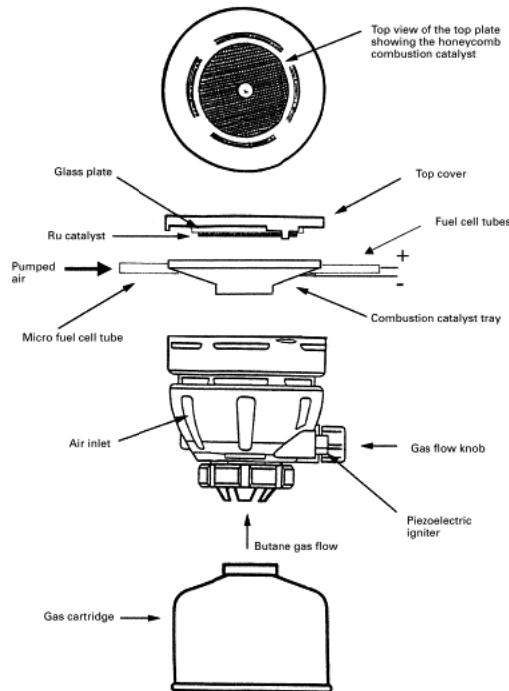


Figure 2-11 Schematic of the burner components of a modified MT-SOFC [47]

2.5.2 Manifolds and sealing

Leaks between the fuel and air sides of the fuel cell decrease the difference in oxygen partial pressure and thus lower fuel cell potential. Several methods for sealing MT-SOFCs from the gas supply have been investigated:

- Cold sealing with rubber and silicon tubing
- Hot sealing with ceramic pastes
- Compression seals with ceramic fibres
- Brazing with silver

Early MT-SOFC designs had a long electrolyte tube with a small active length at one end. Cold sealing involved inserting the opposite end through layers of insulation and sealing a silicon or rubber tube over the end. High-temperature ceramic paste can be used to hot-seal the ceramic tubes to metal tubes and manifolds but the paste can crack and subsequently leak [48]. Brazing in an anode-supported MT-SOFC stack [15] involves using silver between the anode tube and the metal manifold because of its good electrical conduction and similar coefficient of thermal expansion with the reduced nickel oxide-yttria-stabilised-zirconia cermet anode.

2.5.3 Electrical connections

Interconnecting the anode and cathode current-collection wires of MT-SOFCs in series is essential to increase the voltage. It is difficult to connect the anode current collector with the cathode current collector because the wires are in separated gas streams, the wires may be of different metals, or the wires may have to be brought out of the heated zone.

One method involves bringing all the wires outside the heated zone and connecting them with conventional terminal blocks or simply by twisting the appropriate wires together. This method can be cumbersome when connecting many cells. Attempts to keep the connections within the hot zone can be equally difficult as the wires must cross between the fuel and oxidant sides, presenting further sealing issues.

A newer technique of connecting MT-SOFCs in series is to use anode-supported tubes. Once the nickel oxide is reduced, the anode tube becomes electronically conductive. The cathode current collector of an adjacent cell can then be connected to an area on the outside of the anode tube that has not been coated with electrolyte and cathode. This keeps the connections within the hot zone and ensures the anode current collector maintains good physical contact with the anode.

2.5.4 Fuel and reforming

Initial MT-SOFC tests are usually done with hydrogen being used before running the cells on other hydrocarbon fuels. Stationary SOFC systems are generally designed to run on natural gas whilst portable systems tend to be developed to run on existing portable fuel supplies such as propane-butane gas canisters and liquid fuels such as methanol. The advantage of using a gaseous fuel source is that the gas pressure will drive the gas through the system. Liquid fuel systems need extra balance of plant over a gas fuelled system.

2.5.5 Balance of plant

Equipment that supports the stack of cells is required to make a complete system (Figure 2-12). Costs of designing and constructing all features of a SOFC system, including the extra balance of plant, can only be justified for large generators. Smaller SOFC systems need to operate without most of the extra balance of plant to minimise costs and complexity. This, however, decreases overall system efficiency.

The following aspects are important for both small and large systems:

SOFC Stack - The fuel cells need to be held at a high temperature so a furnace or other heating device is required. The furnace may be insulated and electrical and gas connections must pass into the heated zone.

Flow Control - Gaseous fuels are controlled with pressure regulators and needle valves. Air flow rates across the cathode are not always controlled, but may be controlled by fan motors.

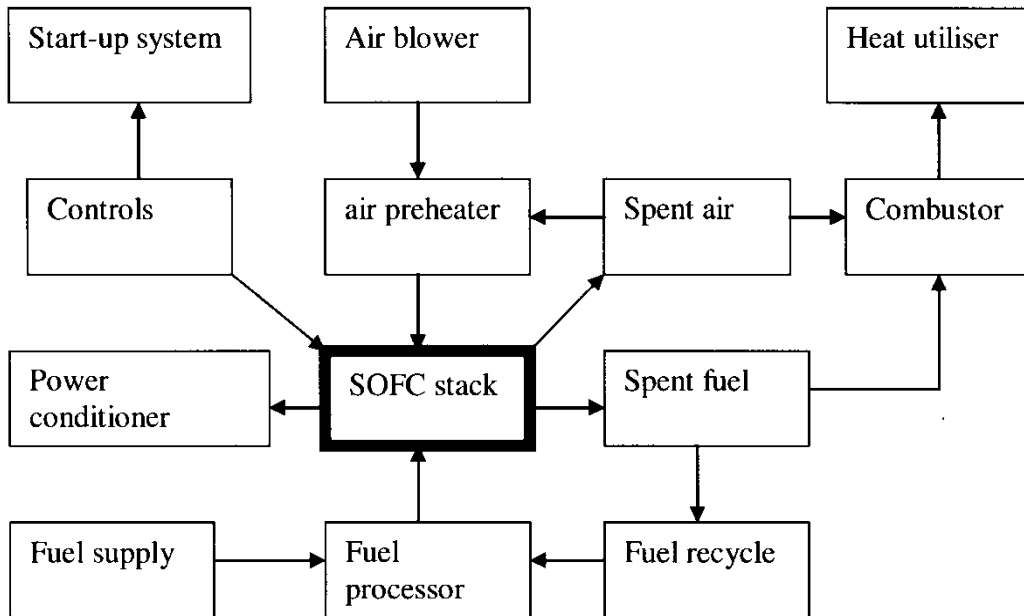


Figure 2-12 Schematic of SOFC stack and extra balance of plant [23]

Air Blower and Air Preheater - Exhaust gases can be used for preheating incoming air. A prototype and the associated mathematical model for heat transfer based on free convection and chimney effects has been developed [13]. Simple counter- or co-flow heat exchangers may be used, but the design must accommodate the gaseous water in the exhaust gas stream, which could condense within the heat exchanger

Filtration - The gas and air supply is filtered to remove particulate matter that may harm the system components. Filtering the air supply is largely overlooked in MT-SOFC systems.

Fuel Supply and Fuel Processor - Gaseous fuels normally have an odorant such as methyl mercaptan so leaks may be easily detected. However, the odorant will poison the anode of a SOFC [11] and may be removed with an adsorber. Some adsorbers work at room temperature and others need to be heated to approximately 250°C. Fuel deodorisation can be done with molecular sieves (Table 2-6). Molecular sieve 5A can remove methyl mercaptan at room temperature [24] and zinc oxide can remove odorants at higher temperatures [49].

Molecular sieves may be regenerated by being heated in air, nitrogen or hydrogen at 230-275°C for 12 hours.

Table 2-6 Molecules and compounds removed by molecular sieves

Molecular Sieve	Molecules Removed
3A	H ₂ O
4A	H ₂ S, mercaptans, H ₂ O, CO ₂ , MeOH, EtOH, SO ₂ , C ₂ H ₄ , C ₂ H ₆ , C ₃ H ₆
5A	Methyl mercaptan
13X	H ₂ S, mercaptans, CO ₂ , H ₂ O

Fuel Processing - The type of fuel reformation determines any extra balance of fuel processing plant. Partial oxidation requires an oxygen source, normally air. Filtering and flow control will be required. Steam reformation requires a water source and a heat source.

Fuel Recycling – A fuel-recycling design to ensure unspent fuel leaving the fuel cells was not wasted but used to heat the stack has been developed [23]. Unspent fuel leaving the fuel cell was ignited with air surrounding the cathode and used to heat the stack to operating temperature. Temperature control in this design is achieved by controlling fuel flow rate to the cells or by modifying the flow rate of incoming air. Large systems tend to recycle unused fuel gas from the anode or to burn the fuel and use it to heat the fuel cells or generate electricity using a gas turbine.

Spent Air - Air supplied to the cathode is normally preheated to approximately 650°C to eliminate a large drop in furnace temperature.

Combustor – Heat Utiliser - The combustor is used to ensure that any un-reacted hydrocarbons are fully converted to water and carbon dioxide.

Control System - Equipment to monitor stack voltage and current is normally required. Gas flows are normally controlled mechanically although pumps for head space vapour can be electronically controlled in liquid fuelled systems [10]. Electronic control of electrically heated systems is common practice.

Power Conditioning – The SOFCs produce direct current electricity. As voltage output may vary, power conditioning is required for voltage-sensitive appliances.

2.5.6 MT-SOFC system design

The literature indicates that the following criteria need to be considered when designing a MT-SOFC stack [46]:

- Thermal shock resistance
- Rapid heating system
- Low electrical losses due to current collection methods

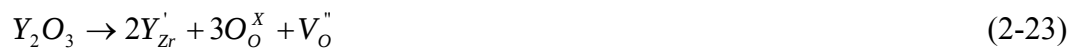
These points will be developed further in Section 2.7.

2.6 MT-SOFC COMPONENTS

2.6.1 Electrolyte

The electrolyte performs two key functions in an SOFC. Firstly, it separates fuel and oxidant gases. Porosity must be minimal so gases do not diffuse across the electrolyte. Secondly, it must allow good ionic conductivity at the SOFC operating temperature. The electrolyte most commonly used is manufactured from yttria-stabilised zirconia (YSZ).

Ionic conductivity of the electrolyte can be described by defect chemistry (Equation 2-23) using the Kröger-Vink notation [50].



The vacancies are responsible for the high ionic conductivity of YSZ. The electrolyte of the MT-SOFC is typically extruded [2, 6, 51], although some researchers have formed the tubes by iso-static pressing. The conditions for extruding thin YSZ tubes for MT-SOFC electrolytes have been optimised [52] and show that the maximum electrolyte wall thickness of 20 µm for an efficient MT-SOFC [53] is one-tenth the wall thickness of extruded electrolyte tubes, implying that electrolyte-supported MT-SOFCs would suffer large losses because they are too thick. Studies have also calculated that the electrolyte tubes should be no longer than 100 mm to limit electrical energy losses [53].

2.6.2 Anodes

At the anode, hydrogen is oxidised by oxygen ions to produce water and electrons. Anode coatings are typically applied to the inside of the electrolyte tube and usually a given mix of YSZ and NiO, which is later reduced to produce an YSZ Ni cermet. Factors influencing composition and hence performance of the anode layers are particle size, thermal expansion coefficients, three phase boundaries, and the number of anode coatings. Research on anode-supported MT-SOFC indicates they have the potential for higher current and power densities than electrolyte-supported MT-SOFCs [54, 55]. The tube is extruded from a nickel oxide and YSZ paste. An electrolyte layer of YSZ is applied to the outside of this tube followed by the cathode layers.

2.6.3 Anode current collection

The anode current collector must make good physical contact with the anode coating. Typically for MT-SOFC, 0.5-mm diameter nickel wire is wound into a spiral around a former and is then inserted down the inside of the fuel cell [43, 56]. In practice, thermal cycling between operating and room temperatures relaxes the nickel wire and so full contact with the anode coating can be lost. Firing the anode coating with the nickel wire *in situ* can overcome this decrease in contact. An alternative method of collecting electrical current for anode supported MT-SOFC involves reducing the nickel oxide in the anode to pure nickel, creating multiple electronic pathways between the nickel atoms in the anode cermet. Consequently, a nickel wire spring current collector is not required because the current can flow along the anode itself. Instead, a wire, typically the same silver wire used in cathode current collection, is wound around some uncoated anode tube. This method has an additional benefit of closer and tighter contact between the wire and the anode because it has been wound around the outside of the anode tube rather than being inserted into the tube.

2.6.4 Cathodes

Oxygen molecules are disassociated at the cathode with the aid of electrons from the anode reaction. The SOFC cathode is usually made of YSZ and lanthanum strontium manganate (LSM). Much work has been done on techniques to coat the cathode onto the electrolyte [57].

2.6.5 Cathode current collection

The cathode current collector is typically 0.25-mm diameter, 99.9% silver wire wound around the outside of the cathode and over the outside of the hot zone to a potentiostat or a load. Silver paste may be applied to the outside of the cathode before and/or after the silver wire has been wound around the fuel cell to increase electrical contact between the wire and cathode as well as to encourage oxygen to dissociate into ions [43, 58, 59].

2.6.6 Interconnects

Planar and tubular systems often use interconnects to provide electrical connections between adjacent cells and to separate fuel and oxidant gases streams. However, due to the way cells are stacked in a MT-SOFC system, interconnects are not usually used. The required electrical connection between cells is achieved by connecting the current collection wires.

2.7 MT-SOFC GENERATOR CONCEPT

A small portable generator based on MT-SOFCs is proposed, using propane-butane gas as the fuel. The generator would generate nominal power as a proof of concept. The prototype generator could be analysed and characterized to determine viability of portable generation using MT-SOFCs.

2.7.1 Integrated heating and fuel reforming

Developing a heating system for the fuel cells is essential for a MT-SOFC stack. For a portable MT-SOFC system, this issue can be approached from a different angle than the usual practice of combusting the unused fuel from the fuel cells [47]. Performance and reliability of MT-SOFCs is directly related to thermal management of the stack through the design and control systems [13]. Three operating modes can be defined for a stack: start-up, steady-state, and shut-down. One problem encountered in large-scale SOFC demonstrations is the long start-up time. One benefit of MT-SOFCs is their ability to withstand large changes in temperature over a short time. Hence, start-up time can be as short as one minute. Whilst a quick start-up time is advantageous, there may be detrimental effects. For example, the anode coating can delaminate from the electrolyte after several thermal cycles.

Once the fuel cell system has reached the desired operating temperature, the main objective is to maintain that temperature within a narrow range. One design controls core temperature of the stack by manually regulating gas flow rate [4]. Larger systems may use thermocouples and a computer to monitor temperatures and control heat and mass flows [23].

Controlled shut-down of the system is as important as start-up and steady-state operation. The anode must never be exposed to an oxidizing environment, which can cause the anode to delaminate from the electrolyte. Large SOFC systems sometimes pump inert gases past the anodes to exclude oxidizing gases [23].

2.7.2 Development

A laboratory prototype of a MT-SOFC generator was developed to test the heating and fuel reforming system as well as arrangement of fuel cells. The fuel cells were tested in an electrically heated furnace to measure electrochemical performance before being exposed to exhaust gases exiting the heating system.

2.7.3 Modelling

Developing a model of a MT-SOFC will help compare the theoretical performance of a small generator with actual performance measured in the laboratory. The important characteristics of the fuel cell system include:

- Fuel flow rate
- Electrical output
- Thermal profile

Other characteristics of SOFC systems such as the fuel utilisation ratio are difficult to measure in small systems, but are estimated from the electrical output.

2.8 SUMMARY

2.8.1 MT-SOFC knowledge

MT-SOFCs were first reported in the literature by Kilbride in 1996 [6]. These cells were based on extruded electrolyte tubes and their preparation and properties were reported. The main advantage proposed was the quick start-up time due to

the resilience of the small diameter cells to rapid changes in temperature. A range of fuels for MT-SOFC have been investigated including hydrogen, methane, propane, butane, ethanol, iso-octane and biogas from landfills [7, 10, 12, 36, 37, 60, 61]. Developing new materials and new materials processing techniques improved fuel cell performance as well as increasing the knowledge of how fuel cells work. Mathematical models of MT-SOFC systems first appeared in 2000 but few papers have been published since [13, 53]. Several small systems integrating up to 24 fuel cells, have been constructed and tested [4, 13-15, 46, 48]. Two larger systems constructed by Keele University and Acumentrics Corporation, have also been reported [23].

Electrochemical testing of single MT-SOFCs has provided data on how fuel, fuel flow rate, pre-reforming method, and operating temperature affect electrical output. The data provide insights on ideal fuel cell operating conditions. One potential problem is that these data are gathered under strictly controlled conditions, which may not be available in an actual fuel cell generator. Secondly, some data is incomplete so true single cell electrochemical performance cannot actually be measured. There is also a lack of reported comprehensive performance data for larger systems. Incomplete data means accurate comparisons of single cell tests or evaluation of fuel cell systems such as fuel to electrical efficiencies is difficult.

Mathematical models are useful because their results can be used to improve the design of future fuel cell systems. Current modelling does not seem to provide useful conclusions that can be integrated into system designs to improve electrical performance or system efficiencies.

2.8.2 Knowledge gaps

All aspects of MT-SOFCs could be improved. Initially, the role of MT-SOFC in electricity generation needs to be discussed. Just as alkaline fuel cells found a niche market in providing power and water for the space programme, there will be an application that particularly suits MT-SOFC generators. Some roles, such as power-assisted bicycles and golf carts, have been discussed in general detail [47].

Several engineering challenges not addressed in the literature become apparent when scaling from single cell experiments to testing fully functional generators. For example, there are no interconnects in a MT-SOFC system (Section 2.6.6). Instead, metallic wires are used to connect the anode of one cell to the cathode of the next cell when cells are connected in series. The cells could also be connected in parallel but there is little discussion of the series versus parallel electrical connection issue.

The fuel cell generator design will determine the number of seals required. Sealing is an acknowledged issue in planar systems but sealing fuel cells in tubular systems can be avoided completely. The system developed by Siemens Westinghouse is a prime example [62]. The MT-SOFC systems are usually manifolded at least at one end of the fuel cell and designs try to keep this seal in a relatively cool zone.

The fuel cell is a relatively small component of the MT-SOFC system. The balance of plant enables fuel cells to operate in optimum conditions but there is no discussion of balance of plant for a MT-SOFC system in the literature. Therefore, a comprehensive study of a MT-SOFC system is needed. Several MT-SOFC systems are presented in the literature, but neither the merits of each design nor whether the system designs could be too simple to gain the theoretical benefits of using SOFC technology to generate the electricity, have been discussed. Ideally, the control system would make it as simple as pressing a switch to start the generator, with power being available within a short time. Existing MT-SOFC prototypes involve many valves, switches, thermocouples and must be manually operated and monitored.

Most systems developed are one-off prototypes. Further development of these prototypes either by improving the designs or taking-on the lessons for future prototypes has not been reported. This may be due to lack of knowledge of how best to assemble a MT-SOFC system. This compares with the specification of the Siemens Westinghouse planar SOFC design and continued research and development of that design [23, 62] which may not be the best design and arrangement of cells.

Several technical issues need to be solved to develop a MT-SOFC generator but the technical challenges have not been prioritised by researchers. Although basic problems can be solved separately, the problems are often interrelated. For example: insulation is used to decrease heat loss from the hot zone but the type of insulation and its arrangement depends on the fuel cell arrangement. Therefore, fuel cell stacking must be solved first because it is partially dependent on how the cells will be heated as well as how the electrical and gas connections are made. Studying the better documented development of Siemens Westinghouse's larger tubular systems offers guidance on some of these issues. Larger fuel cells and interconnects allows a higher packing density than documented for MT-SOFC systems.

Cells can also be constructed into modules, which allows easier integration and stack assembly. The design of the fuel cells and interconnects provides a compact and simple method of electrically-connecting the cells in series. This method has not been attempted with mini-tubular cells.

MT-SOFCs have been fuelled by hydrogen and hydrocarbons. Normally, the hydrocarbons are premixed with steam or oxygen (air) before entering the fuel cells. Reforming the fuel over the anode of the SOFC is beneficial. Some studies have a SOFC system with a pre-reformer [63-65] but most studies conclude that internal reforming over the anode is preferred. There are some studies of exothermic reactions to reform fuel in a SOFC. If a mixture of full and partial oxidation reactions of propane and higher hydrocarbons are used, there could be enough heat to maintain fuel cells at the appropriate operating temperature. Fuel remaining after the incomplete reaction may be used to power the fuel cells. However, there are no published reports on MT-SOFC generator fuelled by propane and/or butane gas using exothermic reforming reactions to heat the cells.

Although fuel cells are theoretically more efficient than conventional generators, there will still be concerns about exhaust gases released into the atmosphere. Water and carbon dioxide will be produced from burning any hydrocarbon fuel but there is potential for carbon monoxide, nitrogen oxides (since air is being used for the oxygen source) and un-reacted hydrocarbons. Gas composition within a

MT-SOFC system has not been documented to the same extent as the electrochemical performance of the same fuel cells being fuelled by hydrocarbon fuels.

The design of a MT-SOFC generator needs to ensure noxious gases are not exhausted to atmosphere. The smaller the SOFC system, the more difficult to reduce these emissions; it will be equally difficult to remove them once they are produced. The advantage of larger systems is that their higher capital costs and longer lifetimes allow more efficient reformers and fuel cells as well as exhaust gas scrubbers to be developed and installed. Further research in MT-SOFC will allow a totally portable device to be designed, documented and improved. Such a system has not been described in the literature.

2.8.3 Scope

Designing and researching an entire generator based on SOFC technology is beyond the scope of one PhD thesis so this design brief has been restricted to:

- A generator will be developed based on MT-SOFCs, using LPG (a combination of propane and butane) as the primary energy source, and using an exothermic partial oxidation device as the primary heat source and fuel reformer.
- Electrochemical performance MT-SOFCs operated on hydrogen, propane-air mixes and exhaust gases from the heating system will be examined.
- The effect of various operational conditions on composition of gases at various points within the system will be analysed.
- The influence of thermal performance of insulation and other system components on the system design shall be examined.
- Improved documentation of a MT-SOFC system, component-by-component, to produce a standard starting point for future research in MT-SOFC.

2.8.4 Research questions

This thesis endeavours to answer the following general questions about MT-SOFC systems.

- Can a partial oxidation heating system provide enough heat to maintain MT-SOFCs at the desired operating temperature?

- Can the same partial oxidation heating system provide sufficient non-reacted fuel to allow the MT-SOFCs to recharge batteries or run low power devices?
- Can the features of the heating and fuel reforming system be integrated with the fuel cell manifolds to create a compact generating device that can be connected to common gas canisters?

2.8.5 Hypothesis

It should be possible to design and build a MT-SOFC system that can maintain a temperature of 800-900°C and in which electrical output is proportional to the number of fuel cells. The design has the following critical design features:

- It must use an existing fuel supply such as propane and/or butane gas commonly found in camping canisters.
- A non-flame catalytic reactor is used and developed to maintain the fuel cells at the operational temperature.
- The catalytic reaction must also produce an acceptable fuel for the fuel cells.
- The design will incorporate a suitable number of fuel cells dependent on physical attributes and volume restrictions.

Initially the research will focus on the catalytic reaction, which primarily heats the fuel cells to the operating temperature. Thereafter, the research will investigate the design requirements of a MT-SOFC that can operate on the by-products of the catalytic reaction.

The research has the following specific objectives:

- To investigate how to use propane and/or butane gas in a portable MT-SOFC.
- To develop a compact heating system suitable for a portable MT-SOFC system.
- To develop a fuel reforming system that minimises the harmful effects of hydrocarbon fuels and odorants on the fuel cells.
- To develop a mathematical model of the heat and mass transfers that can be used to design future generators based on MT-SOFCs.
- To identify the factors that affect performance and efficiency of a MT-SOFC generator and to measure their effects on a laboratory demonstration unit.

3 EXPERIMENTAL SET-UP & TRIALS

This chapter describes the materials, analytical techniques and experiments used to evaluate fuel cell systems, specifically gas analysis, electrochemical performance and thermal profiling. The development of manifolds to hold and provide fuel to the fuel cells is also presented.

3.1 GAS ANALYSIS

The objectives of the gas analysis were to characterise the gas compositions at the various stages of the mass flows through the MT-SOFC generator and to evaluate whether the experimentally determined gas compositions were suitable for operating MT-SOFCs in a low-power generator design. Fuels, air:fuel ratios and exhaust gases were analysed by gas chromatography. Gas analyses helped characterise performance of the catalytic reactor and the fuel cells.

3.1.1 Equipment

A Perkin Elmer AutoSystem XL gas chromatograph (GC) was connected to a Compaq personal computer running Microsoft Windows 2000 (Professional Edition) via a serial LINK cable. The software provided by Perkin Elmer was TurboChrom, version 6.1.1.0.0:K20. The carrier gas, argon, was supplied from BOC Gases New Zealand and was certified 99.999% pure. A stainless steel diaphragm gas regulator was used to maintain the gas line pressure at 100 kPa. The carrier gas was passed through a drier, oxygen and hydrocarbon traps, all sourced from Alltech NZ (now Grace Davison). A 10-port gas sampling valve (Vici) was supplied with the GC. Temperature was maintained at 120°C to prevent water condensing in the lines. The gas sampling valve was actuated using dry compressed air supplied at 500 kPa. Initially, a 1-mL gas sampling loop was used, but this sample size overloaded the columns. Thereafter, a 0.25-mL gas sampling loop was used. Three columns were used to separate the gases, 'Porapak Q', 'Molecular Sieve 13X', and a 'Hayesep Q'. Column arrangement is described in the method development section. A thermal conductivity detector (TCD) was used to detect the separated gases.

3.1.2 Overview of GC operation

The GC, columns, 10-port gas sampling valve and sampling loop were set up to provide loop sampling with two column sequence reversal (Figure 3-1), which is a standard arrangement recommended by the valve manufacturer (Vici Limited, www.vici.com). When the valve is switched to position B, the sample within the loop is introduced to the carrier gas line and forwarded to the first column (column 1). Once the fixed gases and methane have exited column 1, the valve is switched back into position A. This protects the molecular sieve column (column 2) from carbon dioxide, ethane and higher hydrocarbons, which are absorbed by the molecular sieve column and thus would not be detected (or only at a reduced amount). A third column was added between port 7 and the detector to delay retention time of the organic compounds.

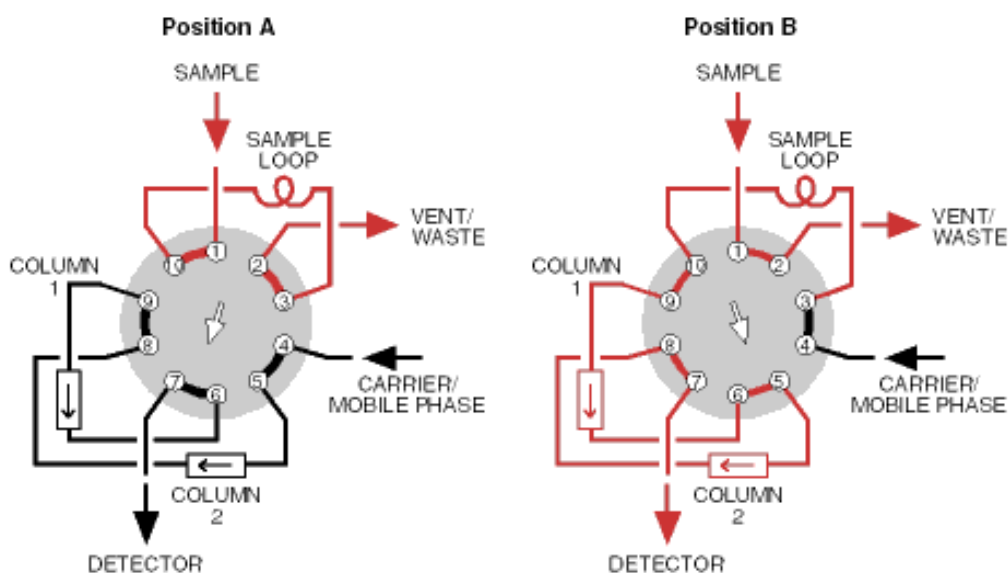


Figure 3-1 Loop sampling with two column sequence reversal.

The TCD is connected to a comparison circuit (Wheatstone bridge). The reference circuit is only exposed to carrier gas and the other circuit is exposed to the gas being analyzed after components have been separated by the columns in the GC oven. Each gas will cool or heat the TCD element by its thermal conductivity (Table 3-1) and/or the quantity of the gas present in the sample.

Detector output is plotted with time on a chromatogram, from which the peak areas may be calculated.

Table 3-1 Thermal conductivities of gases [66]

Gas	25°C	250°C
Argon	17.8	27.7
Carbon monoxide	24.8	40.7
Carbon dioxide	16.7	35.5
Ethane	20.9	57.7
Helium	154.6	230
Hydrogen	185.9	280
Methane	34.5	75.0
Nitrogen	25.9	39.6
Oxygen	26.2	42.6
Propane	17.9	49.2

3.1.3 GC method

The controlling parameters of a GC are referred to as the method. After investigating factors that affect GC analysis, the following conditions were used:

- Carrier and makeup flow rates. Flow rates for both the carrier gas and the make-up gas were set to 20 mL/min and were checked using an electronic flow meter
- Detector attenuation. The attenuation was set at -2.
- Detector range. Range was set at 1.
- Detector polarity. Polarity was set to negative because the carrier gas was argon.
- Oven temperature. This was set to 50°C.
- Valve switching time. This was influenced by the time required for carbon dioxide to pass through the first column. It was important to ensure carbon dioxide did not enter the molecular sieve (second) column, where it would be absorbed.
- Heating rate during a run (if necessary). After 10 minutes at 50°C, oven temperature was increased to 200°C at 45°C/min.
- Detector temperature. This was maintained at 250°C.

3.1.4 Constant quantity

To compare analyses of an unknown sample with those of a standard gas, it is essential the same quantity of gas was analysed. Rearranging the ideal/perfect gas law shows that pressure, volume and temperature must all be kept constant (Equation 3-1).

$$n = \frac{PV}{RT} \quad (3-1)$$

The easiest way to ensure a constant sample volume is to use a gas sampling loop connected to a gas sampling valve. Most gas sampling loops are in a small temperature-controlled oven maintained at 120°C so any moisture in the gas will not condense. Samples passed through the inlet and outlet lines of the gas sampling loop were allowed to equilibrate to atmospheric pressure before a slug of gas was introduced to the columns by activating the gas sampling valve. It was important to record atmospheric pressure during the analysis so pressure adjustments may be made to the raw data.

3.1.5 Calibration

For qualitative analysis, common gases were used to identify the gas peaks. For example, dry air was used to identify nitrogen and oxygen peaks, and reticulated natural gas was used to identify methane. Alpha standard gases are required for accurate quantitative analysis. The components in the standard gas should ideally be approximately the same as in the gas samples being analyzed ($\pm 10\%$) [67]. Three alpha standard gases were used during the trials: SG1 (Section 3.1.8), SG2 (Section 3.1.9) and SG3 (Section 3.1.10).

3.1.6 Analysis method

Each standard gas was analysed 10 times using the standard method. Areas under each peak were calculated automatically by the GC and entered into a spreadsheet for computational analysis. Data were adjusted for ambient pressure then mean values, range and standard deviations were calculated. Mean for each component was equated to concentration level while range and standard deviation indicated analysis error.

3.1.7 Calculating gas concentrations

To calculate concentration of a component in an unknown gas sample, area of the component must be compared with area for that component in a standard gas.

$$X_{component} = \frac{x_{sg} \cdot A_{component}}{A_{sg}} \quad (3-2)$$

Where

$x_{component}$ is the unknown concentration of component X in the sample.

x_{sg} is the known concentration of component X in the standard gas.

$A_{component}$ is the known area of component X from the GC analysis.

A_{sg} is the known area of component X in the standard gas.

Component concentration varied with ambient pressure, which was accounted for by a simple pressure ratio (Equation 3-3).

$$X_{component} = \frac{x_{sg} \cdot A_{component} \cdot P_{sample}}{A_{sg} \cdot P_{sg}} \quad (3-3)$$

Where

P_{sample} is the atmospheric pressure at the time the sample was analysed.

P_{sg} is the atmosphere pressure at the time the standard gas was analysed.

3.1.8 SG1 - Standard gas #19792

Standard gas one (SG1) was sourced from Alltech NZ (Catalogue #19792), who had obtained it from Matheson Tri-Gas, 1650 Enterprise Parkway, Twinsburg, OH 44087, USA. The certificate of analysis (Appendix V1) provided information on the components and their concentrations. Mixture accuracy is specified at $\pm 2\%$ and is NIST traceable by weights or gaseous standards. The cylinder, which contained 14 L at 240 PSIG, was filled in August 2005. The GC analysis of a gas sample showed that all the expected components were present (Figure 3-2).

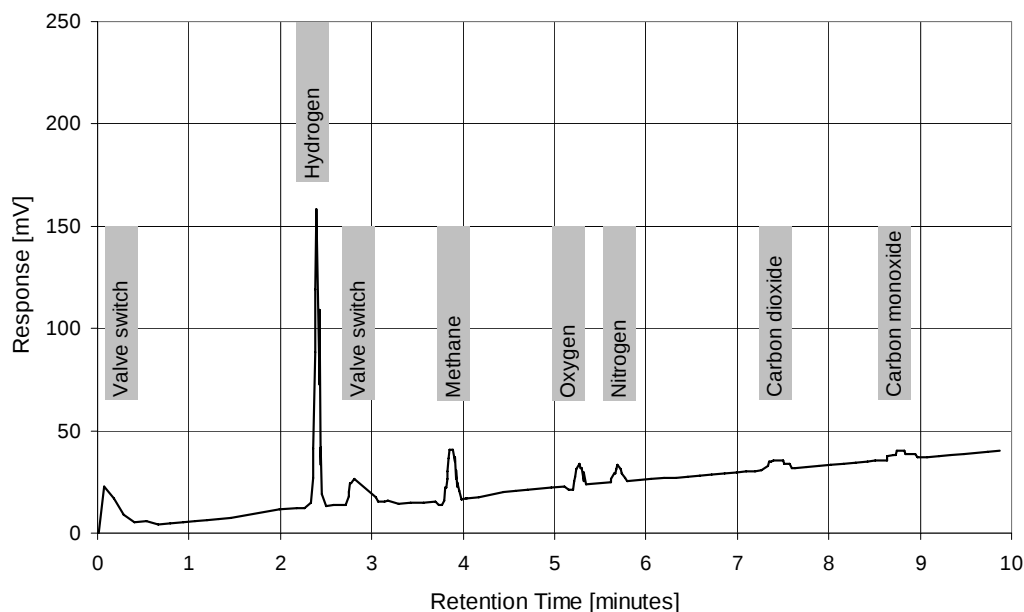


Figure 3-2 Chromatogram of SG1

Mean area can be equated to the specified concentration for each component of the standard gas (Table 3-2). The balance of gas in the standard was helium.

Table 3-2 Peak areas and composition of SG1

Gas	Retention time [min.]	Mean [mV·s]	Range [mV·s]	Standard deviation [mV·s]	Specified concentration [mol·%]
H ₂	2.41	430,000	34,091	8,520	4.137
CH ₄	3.87	153,000	2,773	1,030	4.058
O ₂	5.27	68,000	1,742	511	4.850
N ₂	5.69	50,200	4,662	1,440	5.015
CO ₂	7.40	49,100	1,356	421	5.023
CO	8.76	38,500	865	319	5.000
He	2.20	n/a	n/a	n/a	balance

3.1.9 SG2 - Standard gas #M7014

Standard gas two (SG2) was sourced from Alltech NZ (Catalogue #M7014) who had obtained SG2 from Matheson Tri-Gas, 1650 Enterprise Parkway, Twinsburg, OH 44087, USA. The certificate of analysis (Appendix VI) indicated propane was the only documented component, with a minimum concentration of 99 mol·%. The mixture accuracy is specified at $\pm 2\%$ and is NIST traceable by weights or gaseous standards. The cylinder, which contained 14 L at 240 PSIG, was filled in

June 2006. The calibration gas was certified until May 2008. The GC analysis of a gas sample showed propane and ethane were present (Figure 3-3).

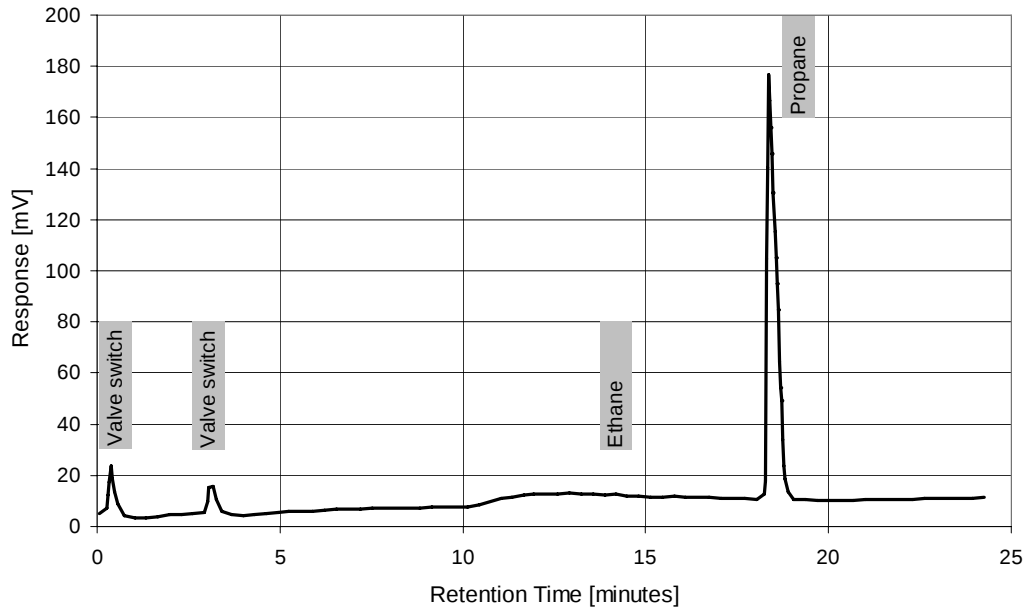


Figure 3-3 Chromatogram of SG2

Area under the propane peak indicated propane concentration was 99 mol·%. Ethane concentration could not initially be calculated due to lack of a suitable gas standard. Standard gas three (SG3), which contained 2.03 mol·% ethane, was obtained and allowed ethane concentration in SG2 to be calculated as 0.2 mol·%. Therefore, by difference, propane concentration was 99.8 mol·% (Table 3-3).

Table 3-3 Peak areas and composition of SG2

Gas	Retention time [min.]	Mean [mV·s]	Range [mV·s]	Standard deviation [mV·s]	Specified concentration [mol·%]
C ₂ H ₆	14.12	6,960	5,902	1,820	0.2
C ₃ H ₈	18.27	2,960,000	106,035	38,300	99.8

3.1.10 SG3 - Standard gas #MA84047

Standard gas three (SG3) was sourced from BOC Gases NZ Ltd (Catalogue #MA84047) to replicate the approximate concentrations of propane and butanes in liquid petroleum gas (LPG). This standard gas also contained methane and ethane (Figure 3-4). A copy of the certificate of analysis is in Appendix VI.

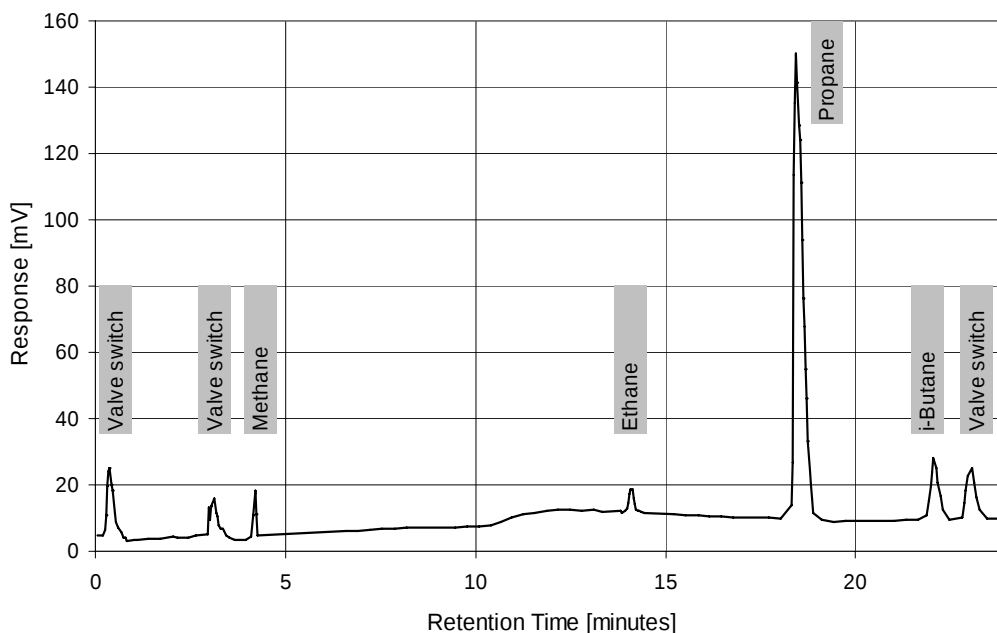


Figure 3-4 Chromatogram of SG3

The mean area indicated specified concentrations for each minor component of the standard gas (Table 3-4). The balance of the gas was propane and is equated to 75.68 mol·% by difference.

Table 3-4 Peak areas and composition of SG3

Gas	Retention time [min.]	Mean [mV·s]	Range [mV·s]	Standard deviation [mV·s]	Specified concentration [mol·%]
CH ₄	4.18	82,100	6,520	2,320	2.02
C ₂ H ₆	14.09	61,200	3,440	1,310	2.03
C ₃ H ₈	18.37	2,290,000	54,000	16,200	75.68
i-C ₄ H ₁₀	22.03	278,000	17,000	7,050	10.30
n-C ₄ H ₁₀	22.98	244,000	28,600	11,500	9.97

3.1.11 Ethane

An attempt to use a gas cylinder containing mostly ethane as a standard gas was made. If components other than ethane could have been identified and quantified, then the ethane composition could have been calculated by difference. The only information known about the gas cylinder was that the major component was ethane. Three peaks were identified by GC - ethane, nitrogen and an unknown component (Figure 3-5). As the latter could not be identified using any of the available standard gases, ethane composition could not be calculated initially.

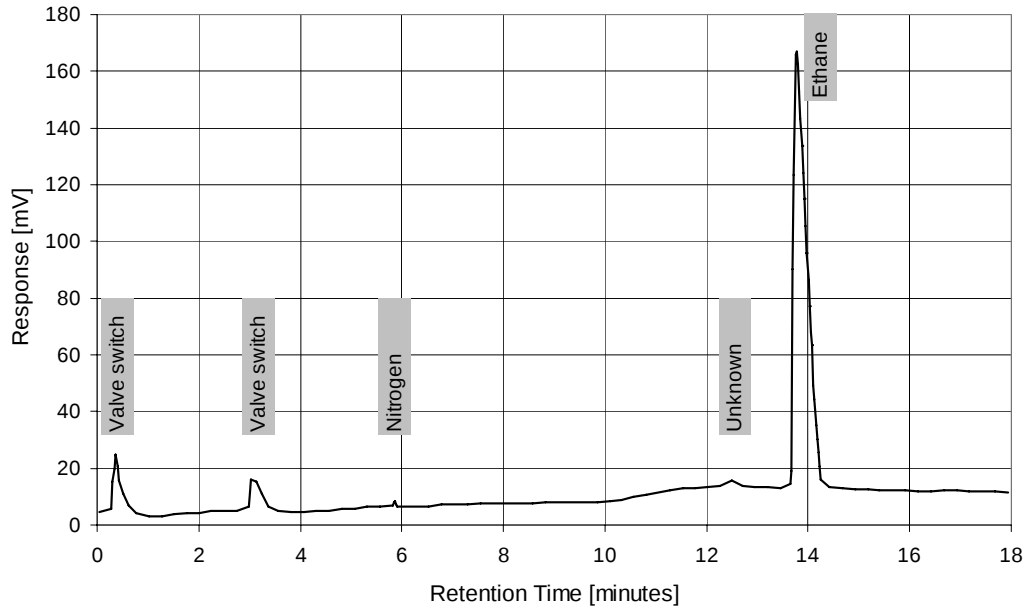


Figure 3-5 Chromatogram of ethane standard gas

Nitrogen in this gas could be calculated using SG1 (0.9 mol-%). By using the known ethane content of SG3 and assuming TCD response was linear from zero to 100 mol-%, the ethane standard gas was estimated to be 92.5 mol-% ethane and, by difference, 6.6 mol-% unknown component (Table 3-5).

Table 3-5 Peak areas and concentrations for ethane standard gas

Gas	Retention time [min.]	Mean [mV·s]	Range [mV·s]	Standard deviation [mV·s]	Concentration [mol-%]
N ₂	5.87	9,280	3,219	948	0.9
Unknown	12.50	13,900	10,935	3,600	6.6
C ₂ H ₆	13.74	2,790,000	30,316	10,200	92.5

3.1.12 Nitrogen

A sample from an oxygen-free nitrogen cylinder analysed by GC confirmed nitrogen was the only constituent (Figure 3-6). Therefore, the TCD response for nitrogen of 1,040,000 mV·sec was equated with a 100 mol-% concentration (Table 3-6).

Table 3-6 Peak area and composition of nitrogen standard gas

	Retention time [min.]	Mean [mV·s]	Range [mV·s]	Standard Deviation [mV·s]	Concentration [mol-%]
N ₂	5.83	1,040,000	4,875	1,750	100

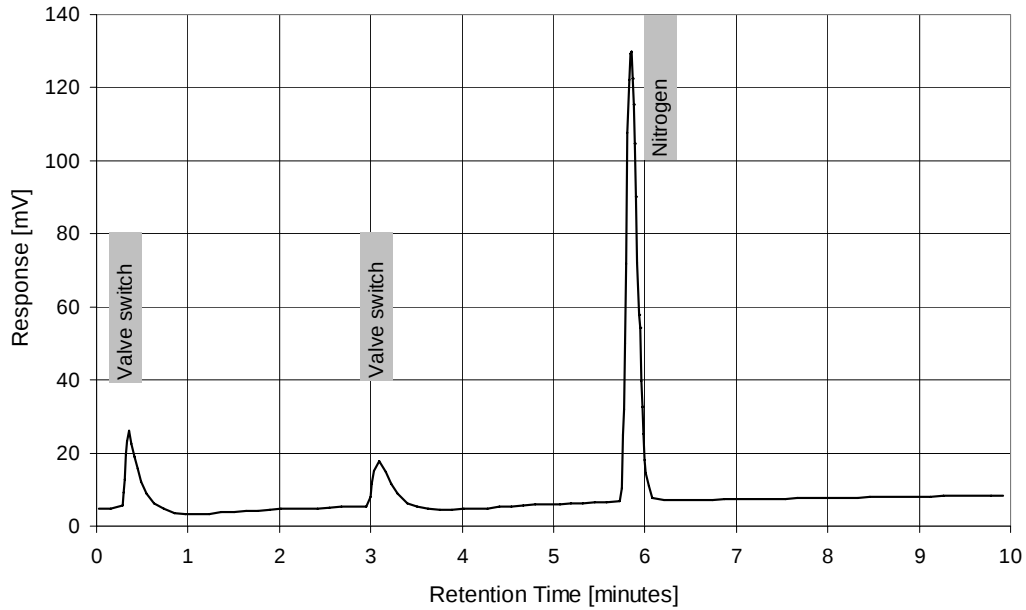


Figure 3-6 Chromatogram of nitrogen standard gas

3.1.13 Dry air composition

A GC analysis of a dry air sample from the BOC cylinder indicated only oxygen and nitrogen (Figure 3-7). As argon was the carrier gas, any argon in the atmosphere or the dry air gas cylinders would not be measured. Argon is approximately 0.934 mol-% of the atmosphere [67].

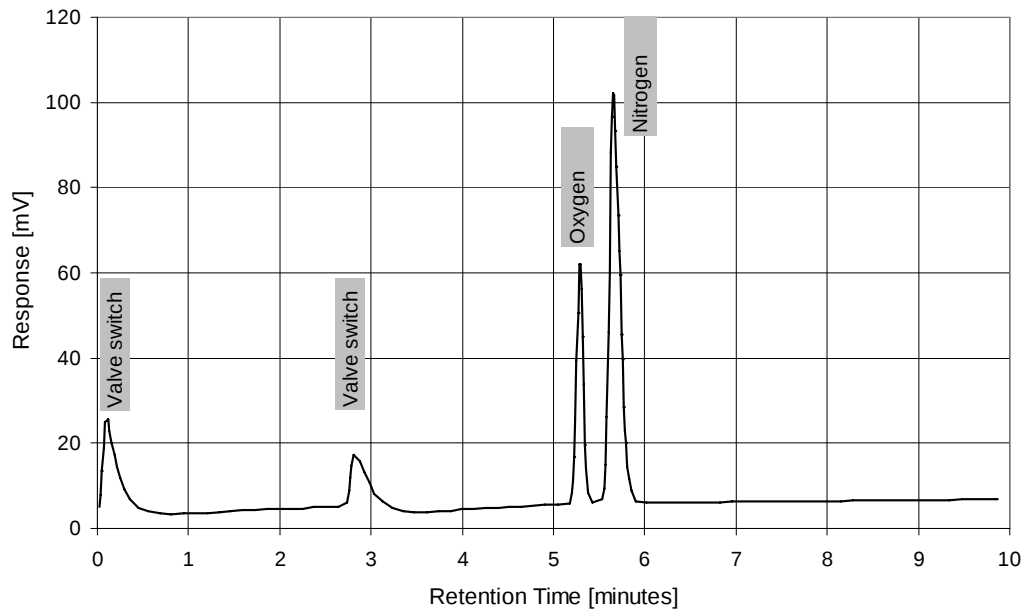


Figure 3-7 Chromatogram of dry air standard gas

By using SG1, oxygen and nitrogen in the dry air were calculated as 21.68 mol-% and 81.62 mol-% respectively compared with measured values of 20.95 mol-%

and 78.08 mol-% (Table 3-7). The totals of 103.30 mol-% by calculation and 100.07% by analysis indicate more than 10% error. If the 100 mol-% nitrogen standard gas were used for the calculation, nitrogen concentration was 78.5 mol-% and the oxygen concentration (by difference) 21.5 mol-%, which were much closer to published data for air composition.

Table 3-7 Peak areas and composition for dry air

	Retention time [min.]	Mean [mV·s]	Range [mV·s]	Standard deviation [mV·s]	Concentration [mol-%]
O ₂	5.28	304,000	4,034	1,220	20.946
N ₂	5.65	817,000	3,140	1,090	78.084

3.1.14 Carbon dioxide

Only carbon dioxide was detected in a gas sample taken from the carbon dioxide cylinder (Figure 3-8).

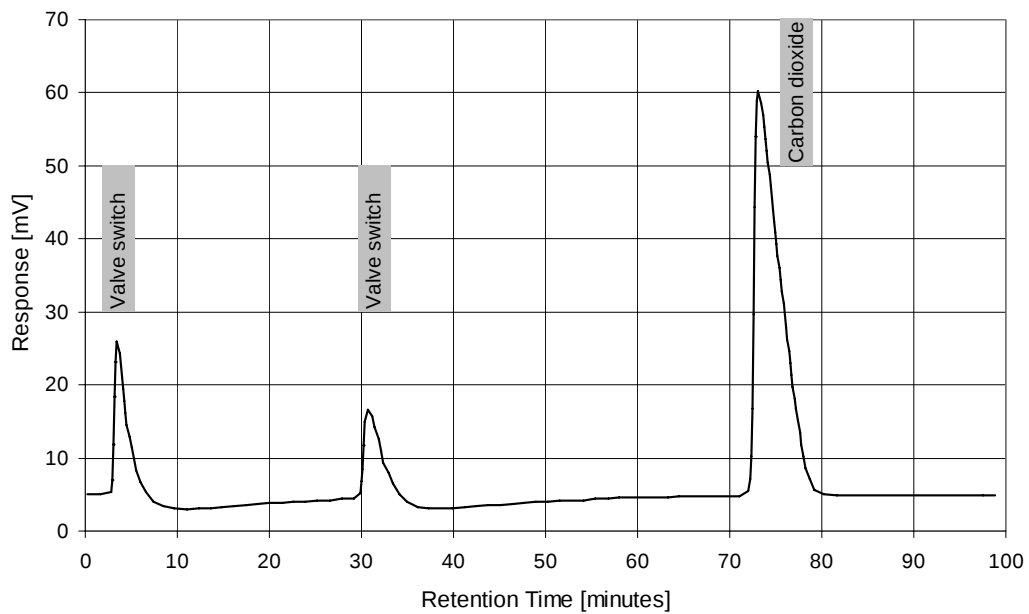


Figure 3-8 Chromatogram of carbon dioxide standard gas

The TCD response of 1,090,000 mV·sec was equated with 100 mol-% carbon dioxide (Table 3-8).

Table 3-8 Peak area and concentration for carbon dioxide standard gas

	Retention time [min.]	Mean [mV·s]	Range [mV·s]	Standard Deviation [mV·s]	Concentration [mol-%]
CO ₂	7.29	1,090,000	6,406	1,770	100

3.1.15 Linearity of TCD response

A TCD does not necessarily have a linear response. For example, if the response area for a gas component at 25 mol·% is 25,000 mV·s, the detector may not necessarily have a response area of 50,000 mV·s for 50 mol·% gas. Linearity of the TCD was determined by analysing several standard gases with different concentrations of known components and plotting the TCD response for each component using data from the calibration gas analyses (Figure 3-9). Response lines for oxygen, nitrogen and carbon dioxide were linear as the limited data could be extrapolated to intersect the origin.

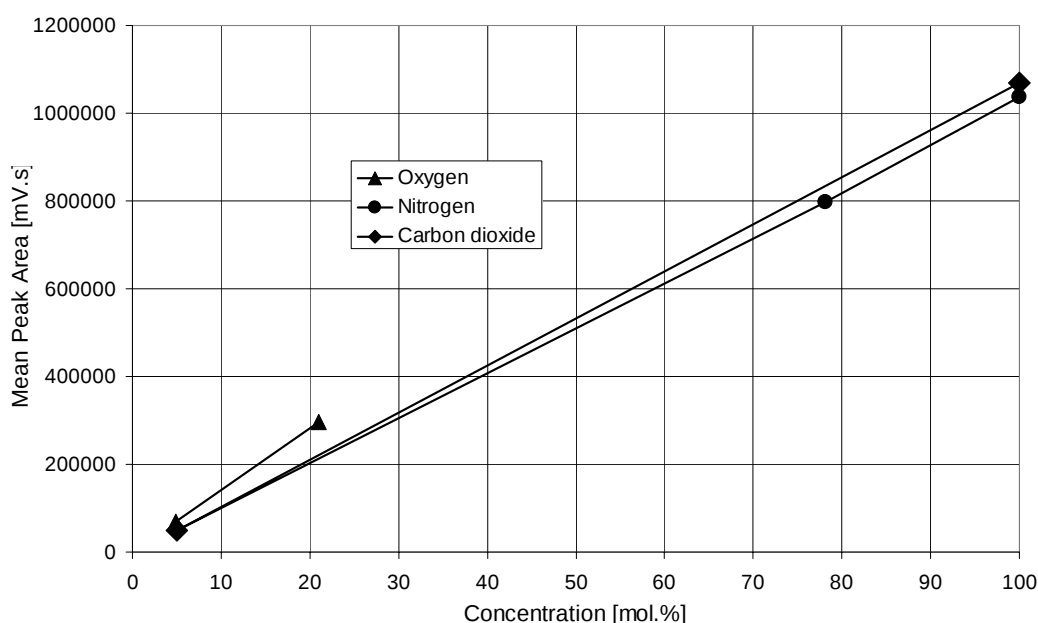


Figure 3-9 Linearity of TCD response

3.1.16 Experimental set-up

Previous research has demonstrated the practicality of operating MT-SOFCs on LPG gas canisters but failed to characterise the gaseous reactants and products [4, 48]. Compositions of the gas stream in the system were evaluated to give an accurate picture of the internal chemical reactions (Figure 3-10).

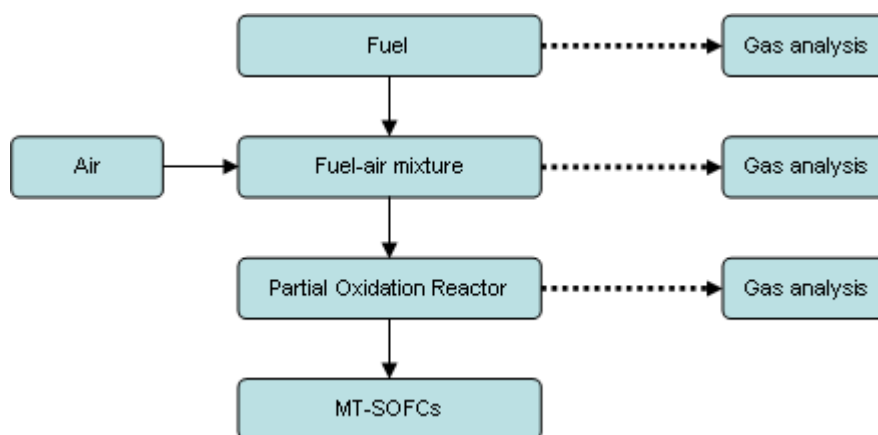


Figure 3-10 Schematic of gas sampling points for MT-SOFC generator

The LPG with a 80:20 propane-to-butane ratio was obtained from a local supplier. Reticulated natural gas in the laboratory was used as the natural gas supply. Gas composition data for natural gas was obtained from the gas company to confirm gas analysis results. Moisture in gas samples was removed using molecular sieve 4A before the analyses.

3.1.17 Sampling technique

The sample loop volume was 0.25 mL and the volume of the connecting tube was calculated to be approximately 0.3 mL. Residual gases in the sample loop and connecting tube were removed by flushing with excess gas from new gas samples. A flushing volume of 20 times the sample loop and inlet line volumes (approximately 11 mL) was estimated to be adequate before starting the analysis. In some instances, a 60-mL syringe was used to collect gas samples. Because of the larger volume, multiple analyses could be taken from the one gas sample.

3.2 ELECTROCHEMICAL ANALYSIS

Various factors affect electrochemical performance of fuel cells. The main factors investigated included electrode form and composition, thermal profiles and operating temperatures, and performance variations across a batch of MT-SOFCs.

3.2.1 Objective

The objective of electrochemical testing is to quantify electrical output of a fuel cell and investigate how it has been affected by the materials, material properties,

manufacturing techniques and/or fuel cell system. However, there is no standard test procedure for electrochemical testing of SOFC, even though the American Society for Testing and Materials (ASTM) has formed a subcommittee (C28.04.05) to write a standard for the “measurement of electrochemical performance of single planar solid oxide fuel cells” (WK7637). Likewise, there is no standard testing procedure for MT-SOFC. The MT-SOFC literature indicates some commonalities for electrochemical testing, which were used to develop the standard method for this research. These experiments were done early in the research because they influenced the manifolding and thermal profiling experiments. The MT-SOFCs were run under various operating conditions and the electrochemical performance was correlated. Results can be evaluated by ranking the parameters influencing electrochemical output of the MT-SOFCs.

3.2.2 Fuel cells

Three cell variations were used: Lemming, GT and HS types. Cell variations were determined as well as testing the operating conditions of the cells. A commercial (Advanced Ceramics Limited) supply of 8YSZ electrolyte tubes, 4.1 mm outside diameter with 0.2 mm wall thickness were obtained. The electrodes and current collectors were attached to the tubes using a standard fabrication process (Figure 3-11).

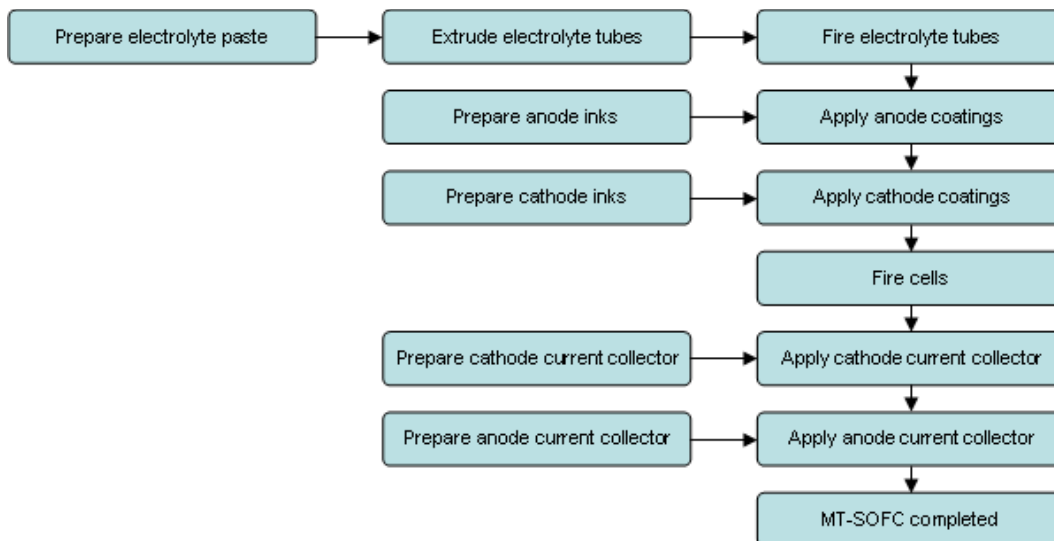


Figure 3-11 MT-SOFC fabrication processes

The Lemming cell design had a segmented cathode (Figure 3-12) made up of five 10-mm segments separated by 2-mm gaps. The anode was based on the standard ink formulations and applied using the conventional technique [48].



Figure 3-12 Lemming design MT-SOFC

The GT1 cells were based on 3.4-mm diameter, 0.2-mm wall thickness electrolyte tubes. Commercial electrolyte tubes (Advanced Ceramics Limited) were used in the GTn (where $n = 1$ to 5) cells. The GT1 cell had a novel anode current collector made by inserting a nickel felt within the cell. The GT2 (Figure 3-13) cell had a 0.11 mm nickel mesh anode current collector. Two methods of collecting current at the cathode were also evaluated on the GT2 cell; either two or four silver wires being used.

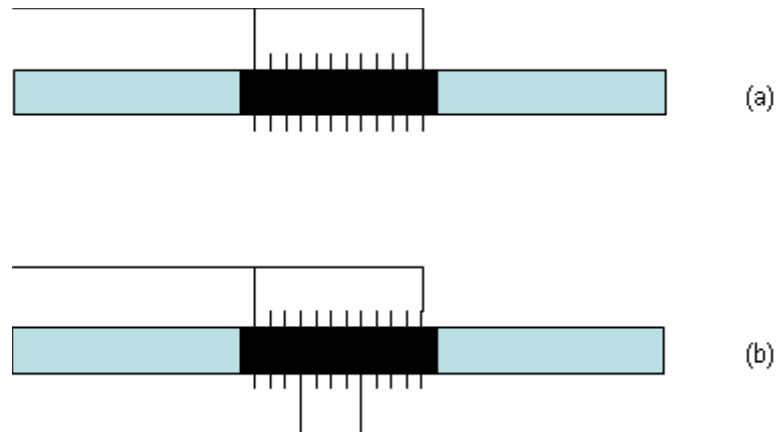


Figure 3-13 GT2 design MT-SOFC, two wire (a) and four wire (b)

A 1-mm diameter nickel wire was used as the anode current collector for the GT3 cell. The wire was wound around an appropriately-sized former to create a coil, which was then inserted into the cell. The HS type cells (Figure 3-14) were the same as GT cells except the cathode was completely painted with silver conductive ink before winding the standard strand of silver wire around the cell.

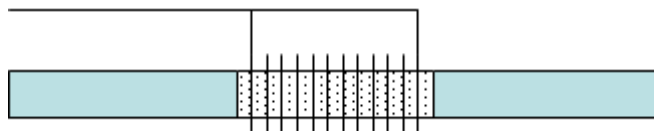


Figure 3-14 HS2 design MT-SOFC

3.2.3 Anode ink compositions and preparations

The anodes consisted of two layers, A1 and A2, each with their own composition. The key layer (A1) had 60:40 weight% ratio nickel:yttria-stabilised zirconia while the current collection layer (A2) had a 90:10 weight% ratio nickel:yttria-stabilised zirconia. The key layer was applied to the supporting electrolyte surface and allowed to dry. The current collection layer was then applied and also allowed to dry.

A1 Preparation Procedure – The ingredients (Table 3-9) were processed using a standard technique for preparing the anode inks [6, 57]. The nickel oxide was pre-treated by calcining at 650°C for five hours in air and the 8YSZ was calcined at 1500°C for three hours in air. The pre-treated nickel oxide, acetone and dispersant (KD1) were milled on a vibro-mill for 25 hours. Particle size distribution was checked to ensure it was between 0.4 and 0.8 microns. The 8YSZ was milled in a second container until 20 g could pass through a 1-micron sieve. The remaining 8YSZ was further milled until five grams were between 10 and 30 microns. Then 5.5 g of 1-micron 8YSZ was added to the nickel oxide and acetone and milled for a further five hours. Particle size distribution was re-checked to be approximately 1 micron. Half a gram of 10-30-micron 8YSZ was now added and milled for a further two hours. Binder (PVB) was then added and milling continued for a further 30 min. Once prepared, the ink was stored in an appropriately sealed container.

Table 3-9 A1 ingredients and suppliers (60:40 weight% Ni/YSZ)

Mass	Ingredient	Supplier
10.5 g	Nickel oxide	Alfa #12359
3.5 g	Acetone	Aldrich #A4206
0.5 g	KD1	Uniqema Hypermer PS-3
6.0 g	8YSZ	MEL/TOSOH

A2 Preparation Procedure – All ingredients except for the extra two grams of nickel oxide and the 0.3 grams PVB (binder) were placed in a milling container and milled for 23 hours (Table 3-10). The extra nickel oxide and binder were then added to the container and milled for a further one hour.

Table 3-10 A2 ingredients and suppliers (90:10 weight% Ni/YSZ)

Amount	Ingredient	Supplier
15 g	Nickel oxide (Green – F')	Alfa
1 g	Ceria oxide	Rhodia
14 g	Acetone	Aldrich #A4206
0.6 g	KD2	Uniqema
1.9 g	8 mol% YSZ	Tosoh
2 g	Nickel oxide	Alfa #12359
0.3 g	PVB	BM18

3.2.4 Anode coating technique

The electrolyte tubes were cleaned with acetone and then dried in a 70°C oven for one hour. The A1 ink was sucked up the inside of the electrolyte tube to a pre-determined mark using a syringe connected to the electrolyte tube with a short piece of silicone tubing. Once the ink had reached the mark, the silicone tube was disconnected and excess ink allowed to run out of the tube. The coated electrolyte tube was then dried in a 70°C oven for one hour. The second anode coating (A2) was then applied in the same way. Any anode ink on the outside of the electrolyte tubes was removed using acetone and the tubes were allowed to dry before applying the cathode.

3.2.5 Cathode ink compositions and preparations

The cathode consisted of a key layer (C1) of 0.5,0.5 lanthanum strontium manganate (LSM) and a current collection layer (C2) of 0.82,0.18 LSM.

C1 Preparation Procedure – All ingredients (Table 3-11) were placed in a suitable milling container and milled for 25 hours. Particle size was checked to, ensure maximum particle size was sub one-micron.

Table 3-11 C1 ingredients and suppliers

Quantity	Ingredient	Supplier
6.5 g	0.5,0.5 LSM	Praxair
6.5 g	8 mol-% YSZ	Tosoh
20 g	Acetone	Aldrich #A4206
0.5 g	KD2	Uniqema
0.2 g	Triolein glycerol trioleate	Aldrich #T7140

C2 Preparation Procedure – All ingredients except the trioleate were placed in a milling container and milled for 24 hours. The trioleate was then added and the slurry was milled for a further 10 min Table 3-12.).

Table 3-12 C2 ingredients and suppliers

Quantity	Ingredient	Supplier
20 g	0.82,0.18 LSM	Merck
14 g	Acetone	Aldrich #A4206
0.7 g	KD2	Uniqema
2 g	Triolein glycerol trioleate	Aldrich #T7140

3.2.6 Cathode coating technique

The technique used for coating the cathodes was based on previous research [43, 57, 68]. The key layer (C1) was applied to the outside of the electrolyte tubes with a small paintbrush and allowed to dry before applying the current collection layer (C2).

3.2.7 Firing

Anode and cathode electrodes, suitably supported on alumina oven furniture, were fused to the electrolyte tubes by firing. The firing regime of an initial low heating rate up to 500°C followed by a higher heating rate was based on previous research [2, 3]. Cells were co-fired at a maximum temperature of 1300°C (Figure 3-15).

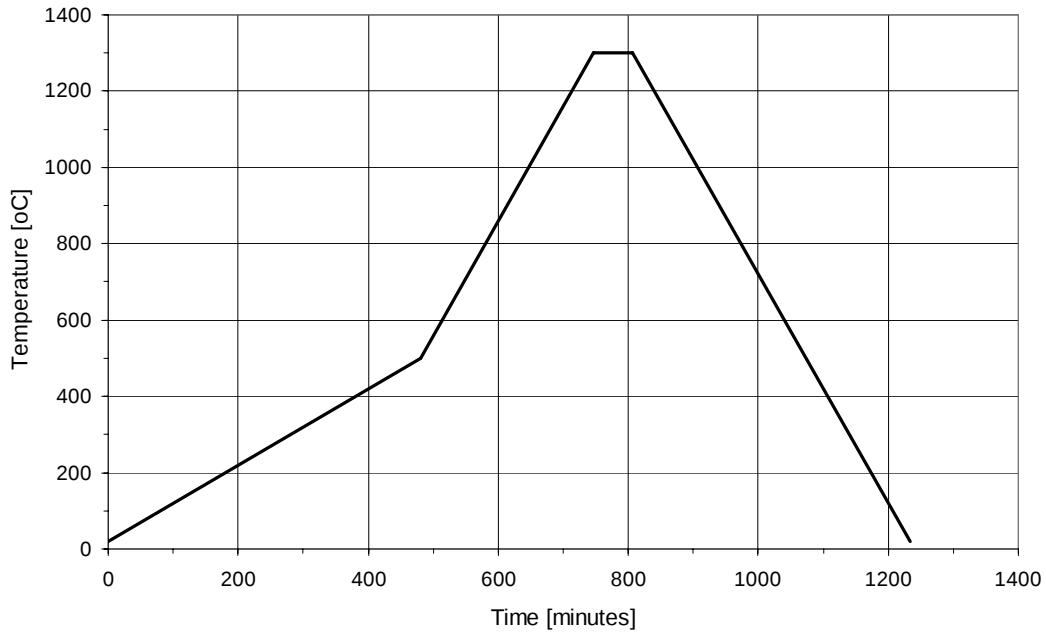


Figure 3-15 MT-SOFC co-firing regime

3.2.8 Anode reduction

The anode of each cell was exposed to reducing conditions by flowing 30 mL/min hydrogen over the anode for 15 min at 850°C. Some tests were done on different reducing conditions by holding the cell at 600°C for 15 min and then increasing the temperature to 850°C.

3.2.9 Open circuit voltage measurement

The OCV was monitored using a standard multi-meter and a Keithley 2420 High-Current Source Meter during the reducing process. Once the OCV had stabilised, the OCV was recorded and loading experiments were started.

3.2.10 Under-load voltage and current measurements

The Keithley 2420 meter also acted as the loading device. The loading regime involved loading the cell until the voltage dropped to pre-determined values, typically in steps of 0.1 V between OCV and 0.5 V. Current at predetermined voltage values was measured and recorded. The OCV would be checked after loading each cell and compared with the original measurement.

3.2.11 Operational parameters

Initial tests investigated performance variations within a batch of MT-SOFCs. Thereafter, MT-SOFC performance was evaluated at the following operating parameters:

- Operating temperature: 800°C, 850°C, 900°C
- Fuel flow rate: 30 mL/min, 50 mL/min, 70 mL/min
- Active length of cathode: 30 mm, 50 mm
- Cathode segmentation:
 - One 30-mm segment, three 10-mm segments
 - One 40-mm segment, two 20-mm segments, six 5-mm segments
- Number of wires for cathode current collection: two wires, four wires
- Silver conductive ink on the cathode
- Silver nitrate on the cathode
- Anode current collectors: nickel wire coils, nickel felt, nickel mesh, pinned anode coils
- Nickel nitrate solution on the anode
- Platinum solution on the anode
- Fuel: hydrogen, methane, propane

Experiments were also done to compare a basic MT-SOFC design with fuel cells having several of the above enhancements.

3.2.12 Equipment

Fuel test gas – Hydrogen gas (99.9% purity), supplied by BOC Gases in a G-sized bottle, was fitted with a hydrogen regulator and flashback device. The regulator was set to deliver hydrogen at 100 kPa.

Gas lines – 1/8" OD Swagelok stainless steel tube was used from the regulator to the fuel cell test rig. Stainless steel fittings such as valves and t-joints were also sourced from Swagelok.

Physical connections – A silicon tube was connected to the end of the MT-SOFC with the anode current collecting wire. The wire was pierced through the silicon tube. The MT-SOFC was placed inside the furnace, but the end with the silicon tube attached was kept just outside the heated zone.

Furnace – A custom-built furnace was used to house the fuel cells. Heating was provided by nickel-chromium heating elements wrapped around small alumina tubes. Temperature was maintained at the set point by an electronic controller.

Multi-meter – A commonly-available multi-meter was used to measure the open circuit voltage (OCV) of the cell.

Potentiostat – A Keithley 2420 High-Current SourceMeter and a Hewlett Packard 34401A meter were used to measure current generated by the fuel cells. Electrical connections between the cell's wires and the potentiostat were made using crocodile clips and/or spring loaded hook grips.

3.2.13 Test conditions

Fuel flow rate – A range of fuel flow rates were tested. Flow rates reported in literature range from 10 mL/min to 100 mL/min per MT-SOFC [8, 43, 44, 57, 69].

Temperature – Most electrochemical testing of MT-SOFCs is reported to occur at 850°C [8, 15, 43, 57, 69]. However, test furnace design is not described so the thermal gradient across the furnace is unknown.

Anode reduction – The anode of every MT-SOFC required a reduction treatment to convert the nickel oxide-zirconia ceramic to a nickel-zirconia cermet. Reduction was done at 850°C at a fuel flow rate of 20 mL/min. The open circuit voltage (OCV) was monitored during the reducing process. Once the OCV had stabilised near the expected value, electrical loading experiments could start.

Electrical loading – Current would be drawn from the fuel cell until the potential reached a predetermined level. Current was then measured and recorded.

3.2.14 Data and results

The OCV was recorded once fuel flow rate and operating temperature were reached for each fuel cell. Current and power results were normalised against the active area of the anode before graphing against the fuel cell voltage.

3.3 MANIFOLD DESIGN

Single cell tests have been performed and grouping cells together has been attempted [8, 13, 14, 27, 48, 61]. However, manifold techniques have not been fully documented even though manifold design is one of the key issues on scaling MT-SOFCs from lab-scale into prototype generators. This section outlines

objectives for the trials done to group several MT-SOFCs in a stack arrangement. Manifold materials are listed together with their respective suppliers (Table 3-13) and the construction techniques are documented. Finally, the experiments undertaken are described.

Table 3-13 Materials for manifold development

Material	Application	Supplier
Micro-porous block	Insulation	Microtherm
Alumina fibre-mat & board	Insulation & manifold	Saffil
Fibre-board	Insulation & manifold	Kaowool
Controller	Measurement & control	University
Ni-Cr wire	Heating element	Goodfellow
Quartz tube	Reactor	University
Nickel mesh	Reactor	Goodfellow
Platinum-impregnated alumina beads	Reactor	Alfa
Aluminium, tube and plates	Containment	Mico Metals
K-type thermocouples	Measurement & control	RS NZ
TC-08 thermocouple data logger	Logging	University
Rotameters	Measurement & control	University
LPG gas supply	Fuel	Ongas
Dry air gas supply	Oxidant	BOC Gases

3.3.1 Objectives

The manifold design should fulfil the following criteria:

- Ensure oxidising and reducing gas flows are kept separate
- Hold fuel cells in tight formation
- Be flexible to avoid stressing the cells during heating and cooling cycles
- Ensure each fuel cell is supplied with adequate fuel flow

Experiments were done to:

- Evaluate performance of the manifolds in physically holding the fuel cells in their correct location
- Test how much fuel was being delivered to each cell

- Measure effectiveness of the seals
- Check for electrical isolation
- Measure heat losses from the hot zone
- Identify manifold design features that can be modified and adapted for a new stack design

The research extended the application of single-cell testing and manifold techniques to multi-cell testing and manifolding techniques.

3.3.2 Machined-metal manifolds

Stainless-steel metal manifolds were machined in the University workshop. Two manifolds were required, one at each end of the MT-SOFC. The two halves of the manifold were fixed together using cap screws. A 3.18 mm stainless steel tube was welded to one half of each manifold for gas flows. Silicone tubes were connected to these pipes outside the containment vessel. Two variations of machined-metal manifolds were evaluated, one holding up to three MT-SOFCs and a second holding between 10 and 12 MT-SOFCs.

3.3.3 Sheet-metal manifolds

Manifolds were fabricated from 0.5 mm stainless-steel sheet-metal that was folded and formed over mandrels and fixed by spot welding. Two sheet-metal manifold sizes were manufactured, one holding three MT-SOFCs and one holding six MT-SOFCs.

3.3.4 Alumina fibre-board manifolds

Alumina-fibre board manifolds were fabricated primarily to support the MT-SOFCs and secondly as a barrier between the fuel and oxidant gases. Alumina-fibre boards were cut to size using standard workshop tools. Holes for the fuel cells were drilled using a drill press and CNC milling machine.

3.4 THERMAL PROFILES

As temperature gradients across the fuel cells and across the generator as a whole could lead to poor performance, it is important to understand the thermal profiles and how the profiles may be modified to improve generator performance. The

experimental set-up was based on the final prototype design and aimed to characterise thermal performance of the generator as well as the energy streams in and out of the system.

3.4.1 Objectives

The objective of these experiments was to measure the heat required to heat fuel cells to temperature and to maintain that temperature within the confines of the final prototype generator. Initially an electrical heating element was used but in later trials an exothermic catalytic reactor was fuelled by liquid petroleum gas (LPG).

The objectives for thermal profiling a MT-SOFC generator were:

- To produce/understand the thermal conditions of the MT-SOFC system using an electrical heater and a partial oxidation heater, and compare data with theoretical analyses.
- To verify whether a partial oxidation reactor could provide the heat required to maintain MT-SOFCs at the operational temperature.
- To quantify the energy required to maintain MT-SOFCs at operational temperature and to compare actual energy used with theoretical predictions.
- To establish whether the partial oxidation reactor could generate electricity within five minutes of start-up.
- To determine performance characteristics of the partial oxidation reactor so its performance may be matched to performance characteristics of MT-SOFCs and hence electricity generating capacity of the MT-SOFC generator.

3.4.2 Equipment

Thermocouples – K-type thermocouples sourced from RS Components were used to measure temperatures within and outside the generator.

Data logging – An eight channel temperature data logger (Pico TC-08) was used to measure and record the temperatures. The data logger was connected to a personal computer. The Pico proprietary software exports data in a suitable format for Microsoft Excel.

Heating element – The 12.5-mm diameter, 120-mm long electrical heating element (Tempco Ltd, www.tempco.com) was suitable for temperatures up to

900°C and rated at 500 W at 240 V, thus drawing a maximum of 2.1 A. Approximately 60 mm from the mounting point was unheated. Mounting was achieved using a circular mounting flange at the unheated and wired end of the heating element. A K-type thermocouple was incorporated into the heating element with the tip located and grounded at centre of the heated end.

Controller – A Shinho MCD-130 Microcomputer Based Temperature Indicating Controller was used to control heating rate and to maintain the desired temperature.

Power and energy meter – The electric heating element and controller were plugged into the mains power via an EMU 1.74 (Landis & Gyr) power and energy meter that could measure various parameters relating to electricity consumption, including logging total energy used.

Catalytic reactor – The catalytic reactor was manufactured at the University of Waikato and consisted of platinum-impregnated alumina beads held by nickel mesh within a quartz tube. The alumina beads with 0.5 wt% platinum catalyst were sourced from Sigma-Aldrich, part # 520705.

3.4.3 Data and results

Several characteristics of the prototype generator were investigated:

- Warm-up and steady-state profiles from (a) ambient to beginning electricity generation or (b) ambient to operating temperature, 850°C.
- Energy consumption during steady-state.

Different insulation configurations were tested as well as the influence of fuel cells operating conditions, including entry and exit of air, fuel and exhaust gases.

The test apparatus design, materials used, processes investigated and operating procedures are detailed. The objectives for each of the experimental areas are reviewed.

3.4.4 Construction and operation

The partial oxidation reactor was contained with a 14-mm diameter, 120-mm long quartz tube. A nickel mesh was held in place by slightly reducing the diameter of the tube approximately 40 mm from one end. Platinum impregnated alumina spheres were held in place by the nickel mesh. The air-fuel premix was passed

over these catalyst spheres. The reactor was initially heated by an external flame to initiate the reaction inside the reactor where fuel passed over the catalyst (the spheres glowing red-hot) radiating heat energy to the surroundings. It was assumed that some fuel and oxygen remain from incomplete reaction.

3.4.5 Operational parameters

Thermocouples were placed at strategic locations within the generator (Figure 3-16) and temperatures were recorded with time. An energy meter measured energy input for the electrically-heated experiments. Fuel mass flow rate was measured to determine energy input for the partial oxidation reactor-heated experiments.

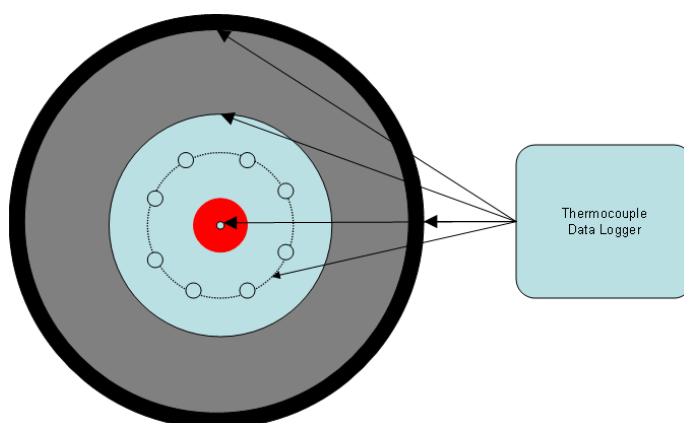


Figure 3-16 Plan view of thermocouple locations

Thermal profiles were obtained for both the electrically-heated and partial oxidation reactor-heated regimes. The most important thermal profile was across the fuel cell zone where the active volumes of the MT-SOFCs were located. These profiles were taken during steady-state operation, which was ascertained by minimal temperature fluctuations across the thermal insulation barriers. Secondary thermal profiles during transient processes such as start-up and shut-down were also recorded.

3.5 SUMMARY

This chapter has described the materials, analytical techniques and experiments used to evaluate a MT-SOFC generator. The next chapters present the results from the experiments and development work testing the fuel cells and the prototype stacks.

4 ELECTROCHEMICAL ANALYSIS

4.1 INTRODUCTION

Electrochemical testing measures the currents and potentials generated from electrochemical reactions and is used primarily to evaluate performance of new materials when developing SOFCs. A secondary role is to determine SOFC performance under different operating conditions such as fuel type and flow rate and operating temperature. The electrochemical testing methods used in this research had been developed by previous researchers at the universities of Waikato and Keele [70-73]. Several areas of electrochemical testing can relate to the design of a small portable generator. Experiments were designed to determine the effect of fuel flow rate, thermal gradients, current collection methods, type of hydrocarbon fuel, air-fuel ratios and cathode design on sensitivity of fuel cell electrochemical performance. The objective was to determine the importance of the parameters so that each could be assigned a weighting when designing a portable generator. The data could also be used to indicate possible fuel cell design changes that would help improve performance. The effect of each parameter on currents and potentials was measured. Data is normalised for the physical characteristics of the fuel cells such as diameter and surface area to present graphs showing current and power densities. Results are compared with reported values and discussed.

4.2 BATCH VARIATIONS

Several factors can produce a wide range in performance of cells from the same batch. Input materials and processes used to fabricate the MT-SOFCs were examined to help understand the reasons for variations. Several core materials are used and the fabrication processes are complex. Materials were sourced from reputable scientific suppliers but poor mixing when making the electrolyte tubes and the electrode inks may contribute to poor performance. Milling times of three to five hours have been reported as adequate [48]. Ink morphology was also checked before the ink was applied to the electrolyte but the method for applying electrodes to the electrolyte tube may also contribute to large differences between

performances of individual cells. Cathode coatings were painted on the outside of the electrolyte tubes and allowed to dry in air and ink was drawn up the inside of the tubes to create the anode (Section 3.2.4). Tubes were dried vertically to help produce a uniform coating. (Excess anode ink pooled along the tubes when the tubes were allowed to dry horizontally.) The anode ink dried quickly and it could block the bottom of the tubes; any excess anode blobs were removed after approximately 10 minutes.

Examination by microscope of 10-mm sections of tubes after firing indicated a uniform film had been applied. However, a previously unsuspected problem was observed - the anode coatings were delaminating from the electrolyte tube during the firing process. This could have been caused by factors such as not preparing the inks properly or using too rapid a firing regime. A cracked or delaminated anode can give poor ionic conduction from the electrolyte to the anode and also contribute to poor electronic conduction through the anode. Some of the supplied electrolyte tubes were very shiny and smooth, which made it difficult to apply the anode and cathode inks. To increase adhesion, the inks were thickened.

Because the fabricating method produced variations, performance of cells from a single batch differed. Therefore, each cell had to be tested individually (by a method akin to identifying batteries for performance). The electrochemical performance of six of the 12 fuel cells fabricated from a single batch of electrolyte tubes with identical electrodes and current collectors was ascertained at 800°C, 850°C and 900°C with 60 mL/min of hydrogen. The remaining six fuel cells had broken during fabrication, usually when the nickel wire coil was being inserted into the fuel cell, highlighting the difficulty of connecting current collectors to the electrodes and general cell frailty. Four fuel cells (AJH3, AJH6, AJH11, AJH12) performed within 10% of each other at 900°C (Figure 4-1 & Figure 4-2). Cell AJH10 had approximately 60% of the high-performing cells and AJH4 had very poor performance even though it did not have any visual faults. Differences in performance increased when currents greater than 50 mA/cm² were drawn. Mean power density of the four fuel cells was 58 mW/cm². Further research is needed to identify the reasons for high variability in cells produced within a single batch.

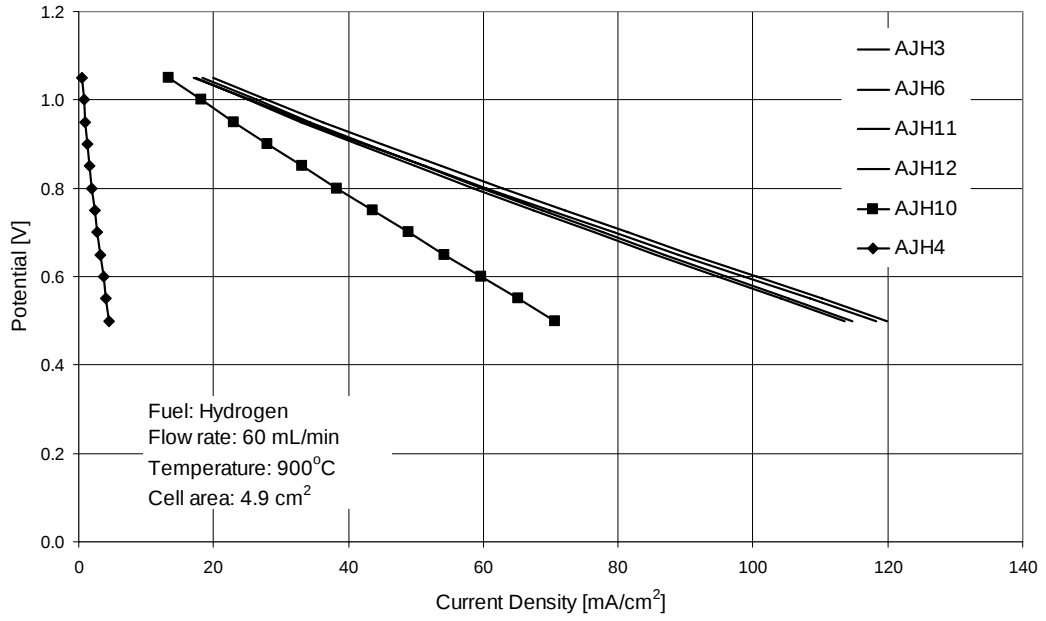


Figure 4-1 IV performance at 900°C. Cells AJH3, AJH6, AJH11 and AJH12 are presented in the order given in the legend.

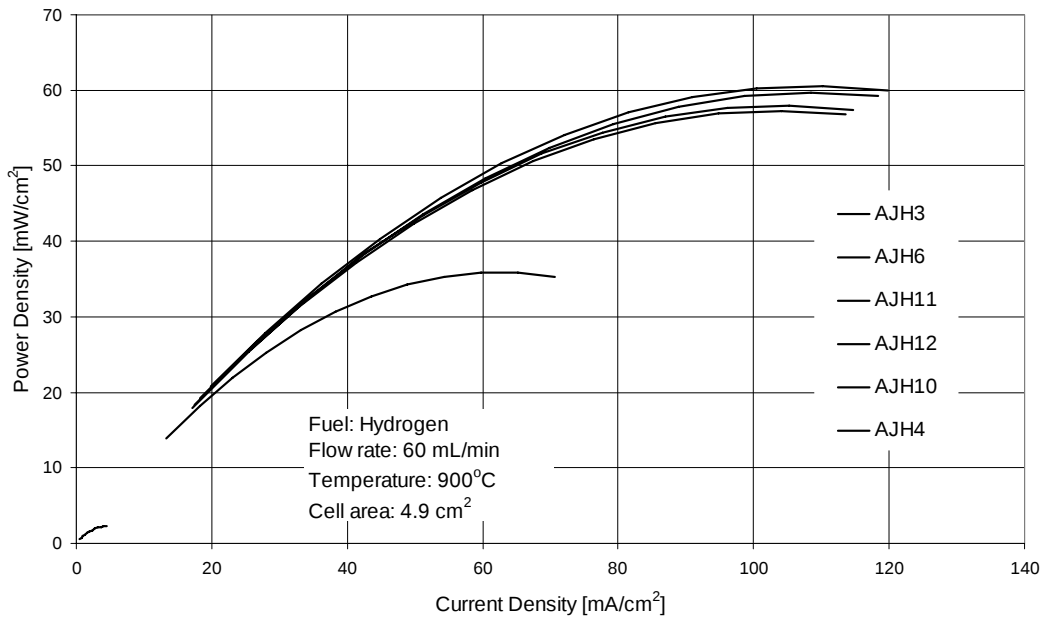


Figure 4-2 IP performance at 900°C. Cells AJH3, AJH6, AJH11 and AJH12 are presented in the order given in the legend.

4.3 FUEL FLOW RATE

Published electrochemical results normally report performance level at a specified flow rate, and other specified operating conditions. Electrochemical performance for a MT-SOFC can be almost constant for a range of fuel flow rates. This will establish the lower and upper limits and help system engineers design a generator. Experiments were done to determine how fuel flow rate affected fuel cell performance using the same fuel cell to eliminate the inter-cell variation.

4.3.1 Reynolds Number

Flow regime within the fuel cell (laminar, transitional, or turbulent) may affect cell performance. This regime may be determined from Reynolds number. Hydrogen gas density at 100 kPa and 850°C may be calculated using the ideal gas law (Equation 3-1).

$$\rho = \frac{m}{V} = \frac{M \cdot P}{R \cdot T} = \frac{(2 \times 0.00100794) \cdot (100000)}{(8.314) \cdot (850 + 273.15)} = 0.022 \text{ kg / m}^3 \quad (4-1)$$

Mean velocity of hydrogen may be calculated from volumetric flow rate (60 mL/min) and internal /cross sectional area of the fuel cell 0.002 m (Equation 4-2).

$$v = \frac{V}{A} = \frac{\left(\frac{60}{60 \cdot 1000000} \right)}{\left(\frac{\pi (0.002)^2}{4} \right)} = 0.318 \text{ m/s} \quad (4-2)$$

Dynamic viscosity of hydrogen (μ) is 18.78×10^{-6} kg/m·s [74]. Thus, the Reynolds number was 0.75 (Equation 4-3), indicating laminar flow. This is comparable with a calculated Reynolds number of 0.63 for a similar-sized and operated MT-SOFC [75].

$$\text{Re} = \frac{\rho \cdot v \cdot d}{\mu} \quad (4-3)$$

This analysis does not allow for the effect of chemical reactions occurring within the fuel cell or the effect of the nickel wire coil used for current collection. Fuel was reacting with the oxygen ions at the anode, producing water and possibly carbon dioxide. When hydrogen is the fuel, one mole of hydrogen produces one mole of water. If hydrocarbon fuel is used, more than one mole of product gas is produced per mole of fuel. The 1-mm diameter nickel wire reduces internal diameter of the cell, which increases mean gas velocity gas and Reynolds number.

4.3.2 Experimental

Variation in performance at 30 and 50 mL/min hydrogen were very similar but performance at 70 mL/min was approximately 3% higher (Figure 4-3 & Figure 4-4). Performance is very similar when little current is drawn (near the OCV) but diverge slightly as higher currents are drawn.

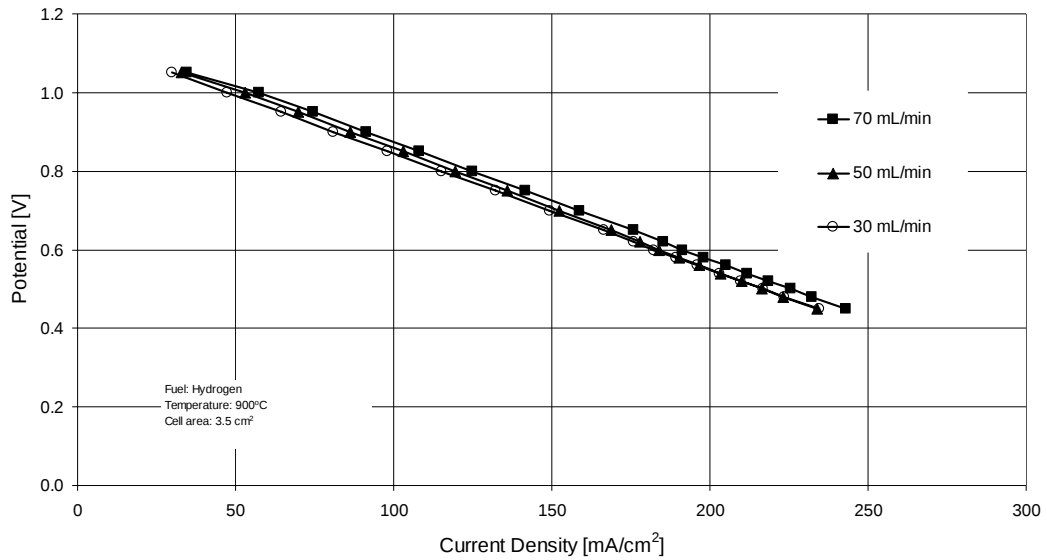


Figure 4-3 Effect of fuel flow rate on current density

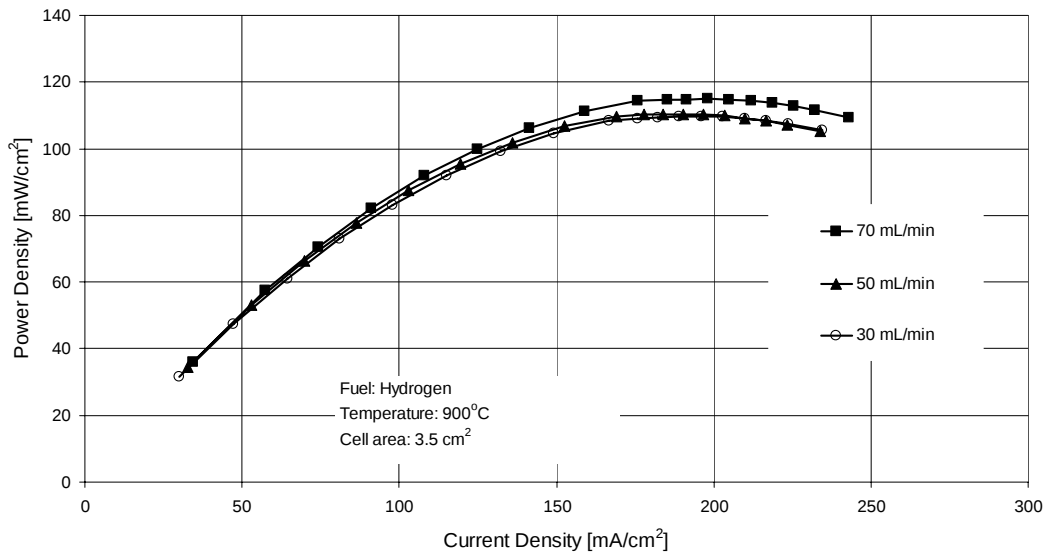


Figure 4-4 Effect of fuel flow rate on power density

The maximum current recorded was 641 mA, which is equivalent to a hydrogen consumption of 3.3×10^{-6} mol/s (approximately 9.1 mL/min). Therefore,

maximum fuel utilisation was approximately 30% at 30 mL/min and 13% at 70 mL/min, indicating excess fuel was available for further reaction at all flow rates. It was initially hypothesised that fuel cell performance would vary with fuel flow rate, especially because it is important to present fresh fuel to the reaction site and to remove the water and carbon dioxide produced. Further tests with air:methane fuel mixes, indicated little variation in maximum power output between 20 mL/min and 90 mL/min (Figure 4-5). Operational temperatures caused variations in performance. Performance at 900°C was approximately double that at 800°C and 850°C. This may be due to two factors: the increased ionic conductivity of YSZ at higher temperatures, and possibly the higher rate of internal reforming of the air-methane mixture producing hydrogen and carbon monoxide at the three phase boundary where the electrochemical reactions are occurring. One benefit of operating a fuel cell generator in a region where flow rate is not critical to electrical output is the possibility of recirculating the exhaust gas back to the fuel cells. This allows unspent fuel to be recycled and the water vapour produced can assist in steam-reforming hydrocarbon fuels. This concept is discussed further in the Chapter 6.

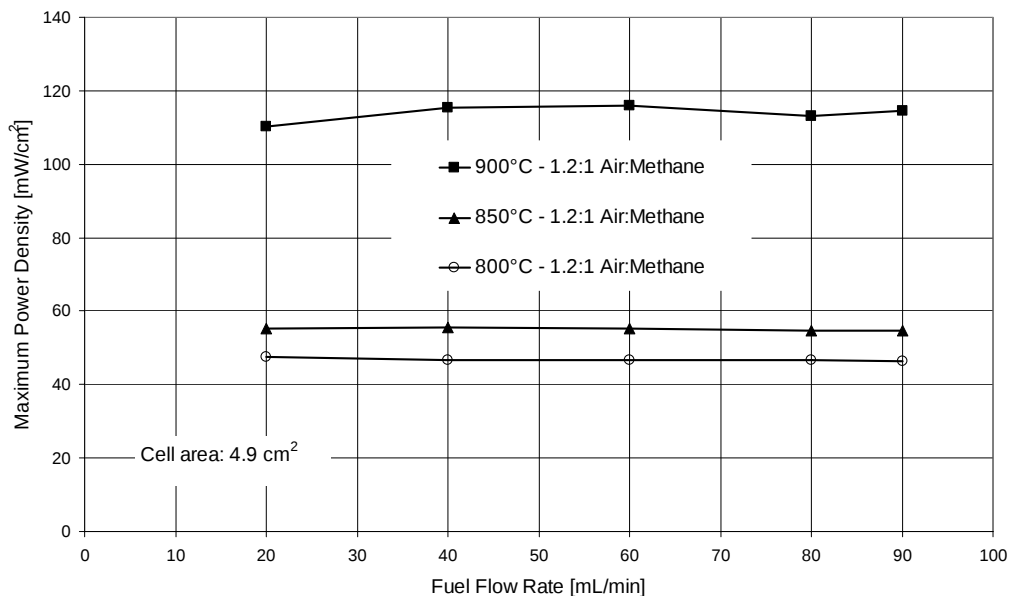


Figure 4-5 Effect of fuel flow rate and temperature on power density

Data showing electrical output was independent of fuel flow rate differ from cell performance data at similar fuel flow rates presented by Sammes *et al.* [15]. Their data indicate an almost linear increase of current density and power density with

flow rate (Figure 4-6 & Figure 4-7). Larger diameter cells (13.2 mm compared with 3.4 mm in this study) were used so mean fuel velocity was lower for the same volumetric flow rate. Also, anode-supported cells rather than electrolyte-supported cells were used and the anode current collection method involved metal tubes brazed to the fuel cell tubes, which eliminated the need for a nickel wire coil. Data for different fuel flow rates start at different points and the values obtained by extrapolating the current density lines to zero current density (i.e. OCV), are different (Figure 4-6). If a cell is performing consistently, its OCV at various flow rates should be very similar, as was observed in almost all results produced during this research. The differences in the reported data indicate Sammes *et al.* may have used different cells in their experiments.

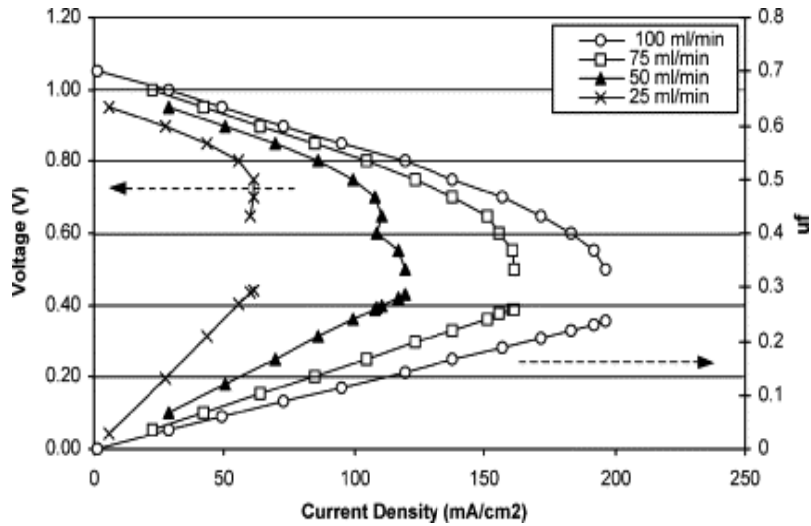


Figure 4-6 Effect of fuel flow rate on current density [15]

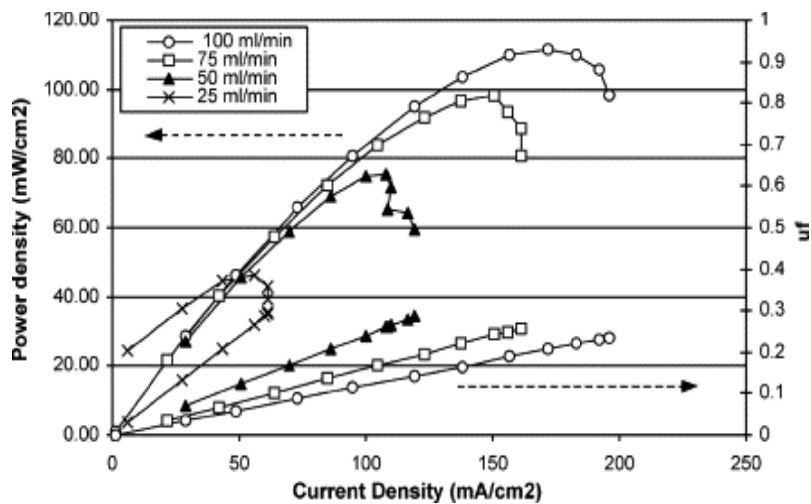


Figure 4-7 Effect of fuel flow rate on power density [15]

The analyses, including calculating Reynolds numbers, had not accounted for the reaction chemistry occurring within the fuel cell tube. Limits for molar increase of gas may be easily calculated if it is assumed fuel gases oxidation goes to completion. Complete reaction of one mole of hydrogen gives one mole of water vapour and no substantial change in gas volume or pressure is predicted. Molar ratios can be used for fuels such as methane, propane and butanes. Complete reaction of one mole of methane, propane or butane gives three, seven and nine moles of product gases respectively. The product gases are produced at the three-phase boundary and need to be removed to allow access for the non-reacted fuel. The best way to remove the product gases would be to have turbulent flow in the fuel cells, thus mixing product gases with the remaining fuel. To change flow from laminar (Reynolds number = 0.75) to turbulent (Reynolds number > 2000) requires a four-fold change. This could be achieved by increasing cell diameter and/or flow rate. Fuel cell diameter can be increased by one order of magnitude and tubular fuel cells ranging from 17 mm to 35 mm are reported in the literature [1, 62, 76]. Fuel flow rate could be increased but there then is insufficient time for the fuel to react at the three-phase boundary. Electrochemical performance decreased dramatically when fuel flow rate was above 100 mL/min.

Ideally fuel cells for a portable generator should run efficiently on a range of fuel compositions whereas a tighter fuel composition could be specified to optimise a large steady-state generator. Compounding the problems of introducing an ideal fuel gas mixture to fuel cells is the change in gas composition as it moves along the fuel cell. The product gases and decreasing fuel content could oxidise the zirconia-nickel cermet and also decrease electrochemical performance. These factors indicate fuel cells could be shorter rather than longer to minimise these effects and have larger diameters to encourage better mixing. Flow rates could also be increased but there must still be sufficient time for the reactions to occur.

4.4 HYDROCARBON FUELS

The fuel cells were tested using internal reforming of methane and propane because these are major components of natural gas and LPG respectively. The results were compared with using hydrogen. The preferred method of internal

reforming was partial oxidation as this would be the likely method for small portable generators. Partial oxidation premixes fuel with oxygen or air to react over the nickel-zirconia anode and can be easily implemented in a portable MT-SOFC system whereas steam reforming requires additional plant to store and add water to the fuel gas stream. Hydrocarbon fuels are only used with partial oxidation or steam reforming to prevent rapid formation of carbon deposits within the fuel cells, which would cause cell blockages. However, carbon deposition can also occur under partial oxidation or steam reforming conditions.

4.4.1 Methane

Methane was premixed with dry air in ratios of 1:1.1 and 1:1.5 on a volumetric basis. A 1:1.5 methane-to-air volume ratio is approximately a 3:1 methane-to-oxygen molar ratio. Partial oxidation is when methane reacts with a limited supply of oxygen to produce carbon monoxide and hydrogen (Equation 4-4).



The MT-SOFC performance deteriorated with increasing air-methane ratios, with a large drop between 1.4:1 and 1.5:1. Highest performance was at an air:methane ratio of 1.1:1 (Figure 4-8).

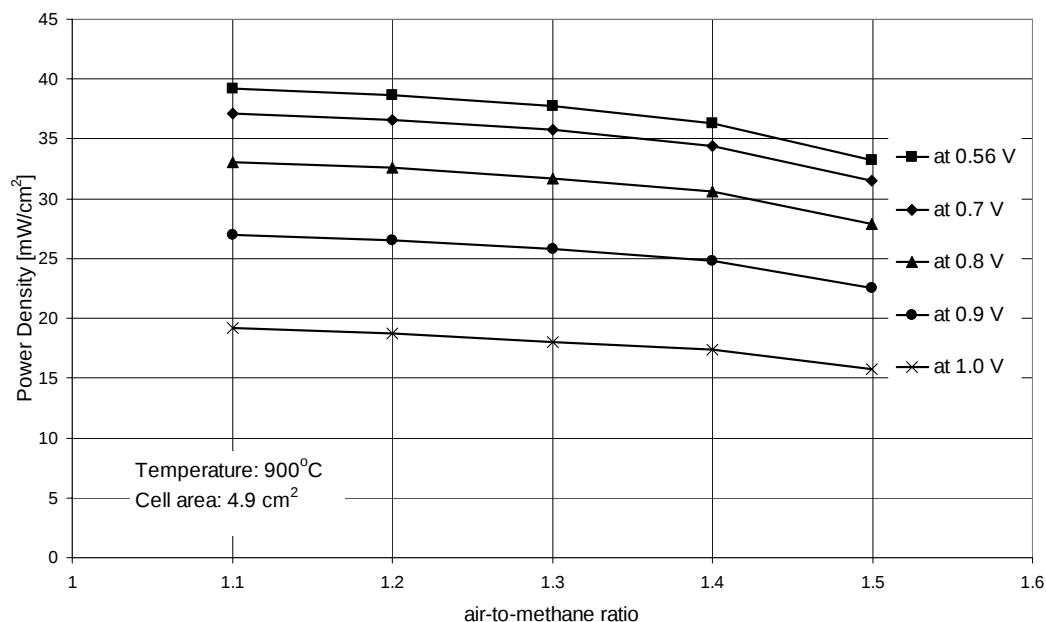


Figure 4-8 Effect of air-to-methane ratios on power density

Mixing methane with air diluted the fuel molecules approximately 50%. If the reaction chemistry is even slightly based on species concentration, then this will

lower electrical output. However, if the air:methane mixture is being partially reformed over the anode, three fuel molecules are produced for each methane molecule, giving a higher total fuel species concentration as well as diminishing the diluent effect because oxygen in the air was used up.

The MT-SOFCs produced less electricity when run on air:methane fuel mixtures than at similar hydrogen fuel flow rates. The minimum difference was 8% current and 10% lower power density (Figure 4-9 & Figure 4-10).

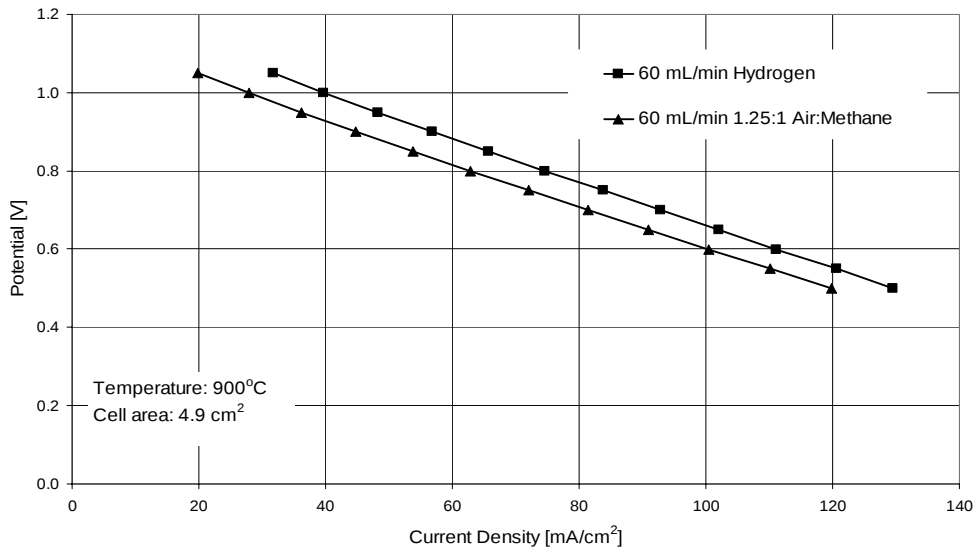


Figure 4-9 Effect of using hydrogen or methane on current densities

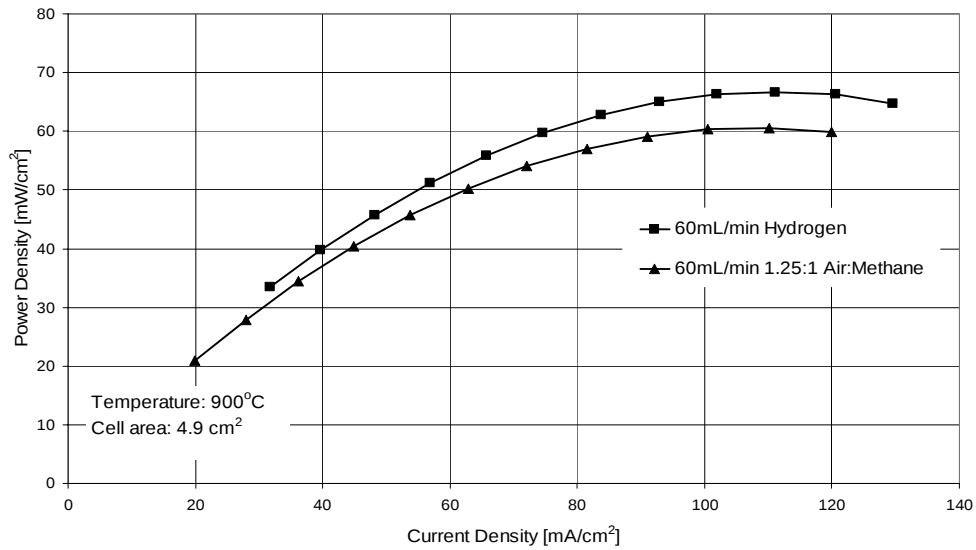


Figure 4-10 Effect of using hydrogen or methane on power densities

4.4.2 Propane

Current was 6% lower and power density 8% lower when the fuel cell was operated on 1:1 air:propane rather than hydrocarbon-air (Figure 4-11 & Figure 4-12). The propane was diluted with air so partial oxidation could occur at the anode. This should give double the hydrogen than when operating on methane so performance should be closer to that of hydrogen. The anode may be deteriorating in the presence of oxygen before it can react with propane, reducing fuel cell performance at the inlet.

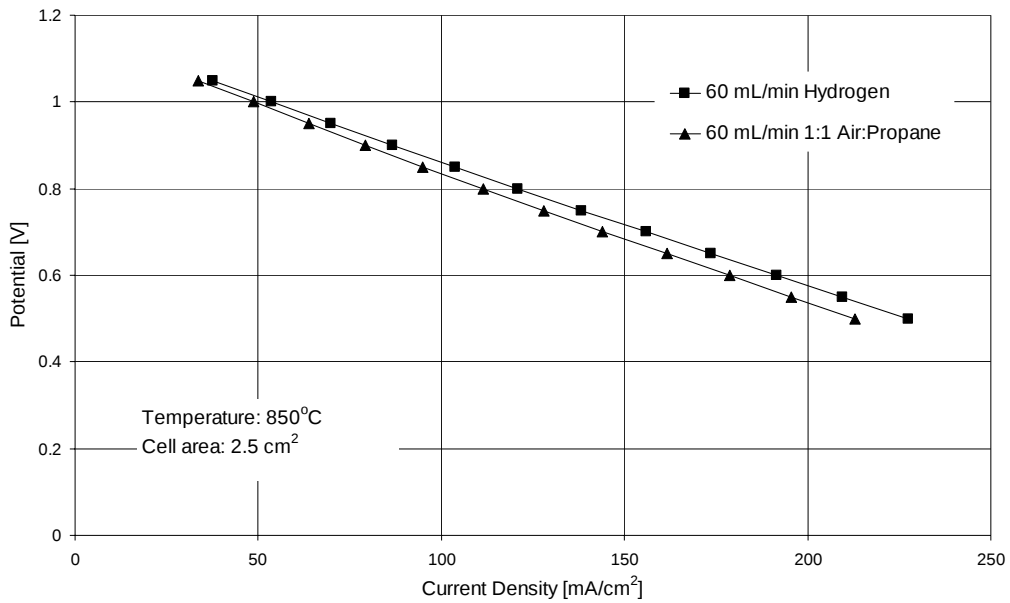


Figure 4-11 Effect of hydrogen and propane on current densities

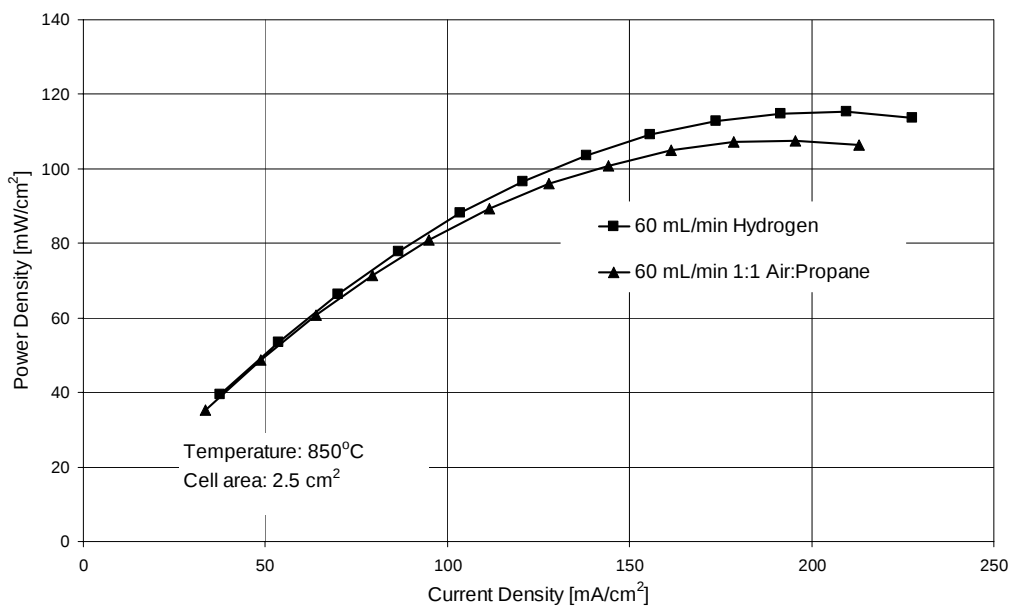


Figure 4-12 Effect of hydrogen and propane on power densities

4.5 OPERATING TEMPERATURE

Temperature affects ionic and electronic conductivities of materials and therefore SOFC performance. The OCV with 50 mL/min hydrogen were similar at 800°C, 840°C and 880°C (Figure 4-13 & Figure 4-14). Increasing operating temperature improved current and power densities by 54% and 44% respectively. Current density at 880°C was approximately 12.5% higher than at 840°C and the power density at 880°C was approximately 25% higher than at 840°C. The substantial increase in fuel cell performance with operating temperature indicates generators should operate at the highest temperature the supporting materials permit.

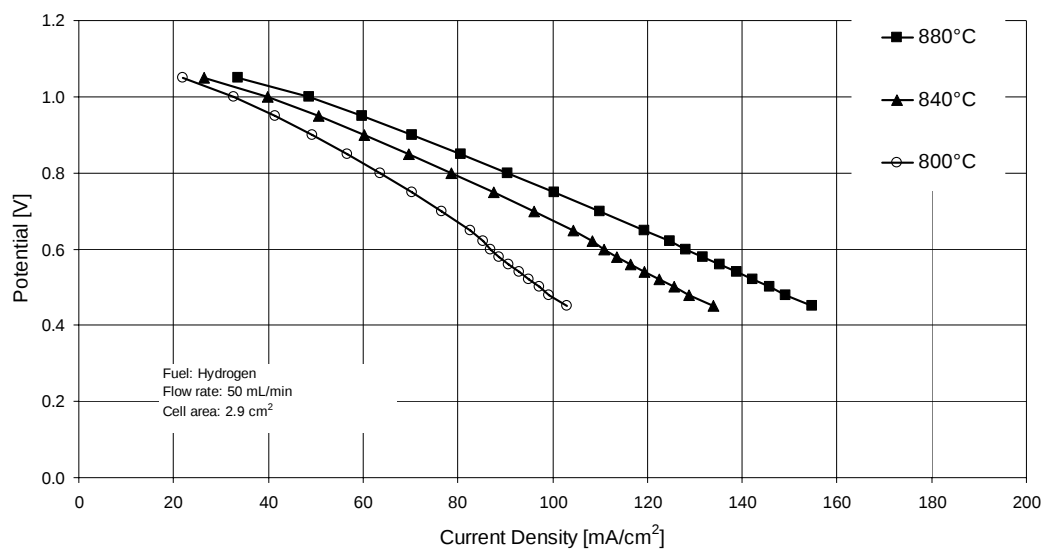


Figure 4-13 Effect of operating temperature on current density

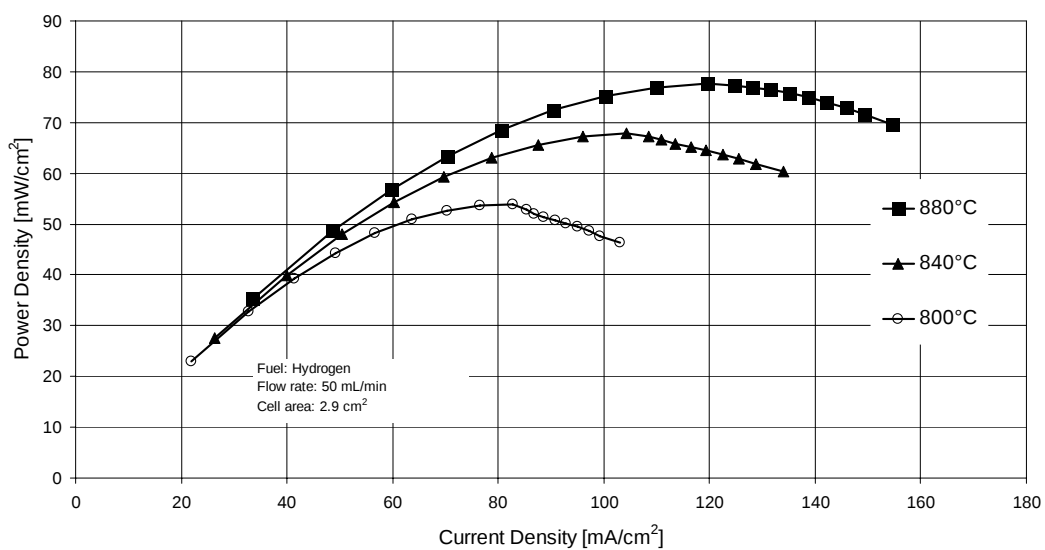


Figure 4-14 Effect of operating temperature on power density

4.6 FUEL CELL ACTIVE LENGTH

The active length of an electrolyte-supported MT-SOFC is governed by the length of cathode coating on the outside of the electrolyte tube. Anode coating does not affect active length because the entire inside surface of the electrolyte tube is usually coated. Performance of a 30-mm active length fuel cell was significantly higher (approximately 40%) than for a 50-mm active length fuel cell (Figure 4-15 & Figure 4-16).

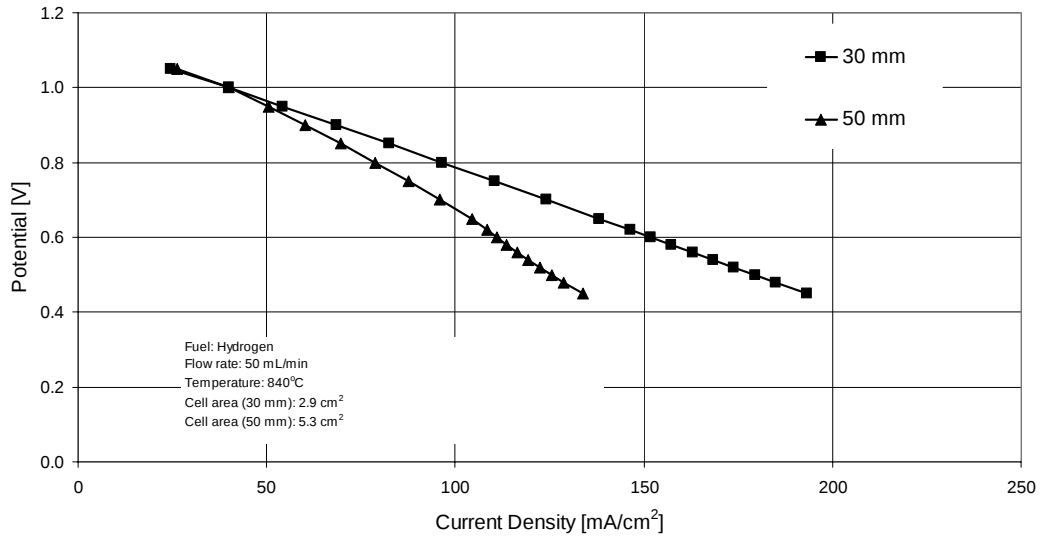


Figure 4-15 Effect of fuel cell active length on current density

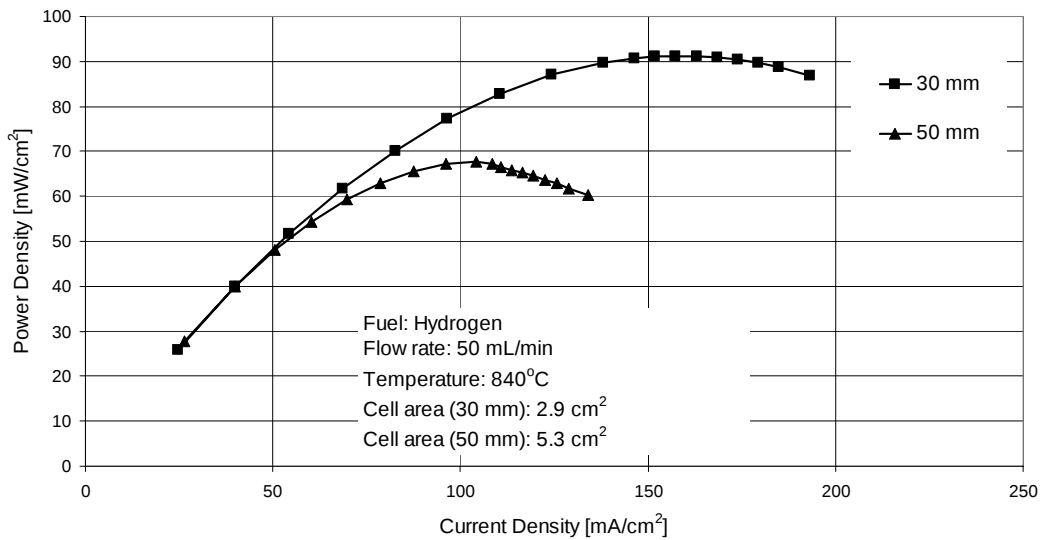


Figure 4-16 Effect of fuel cell active length on power density

Something unusual was occurring as longer cells should perform at least as well as short cells. Either cell length affected performance or there was some difference between these cells. Another explanation is that the longer cell had insufficient fuel along its complete length and therefore was not performing optimally. Higher electronic resistances in the cathode and anode could have loaded the cell *in situ* and reduced power output. The results support decreasing the active length of the fuel cell but the limit is whether the fuel cell can generate enough power to be useful.

4.7 CATHODE SEGMENTATION

Segmenting the cathode coatings on the electrolyte (Section 3.2.2) increased current density from 150 mA/cm² for unsegmented cathode to 210 mA/cm² and power density from 70 mW/cm² to 100 mW/cm² when cells were run at 885°C with 60 mL/min hydrogen (Figure 4-17 & Figure 4-18). Increased performance may be from two effects. Cathode current collection may be improved as each cathode segment has its own current collection wires. Alternatively, any unreacted fuel and product gases can mix without electrochemically reacting in the short distance between each cathode segment, moving water and carbon dioxide from the three-phase boundary and opening up other active sites so fuel could react with the incoming oxygen ion flux.

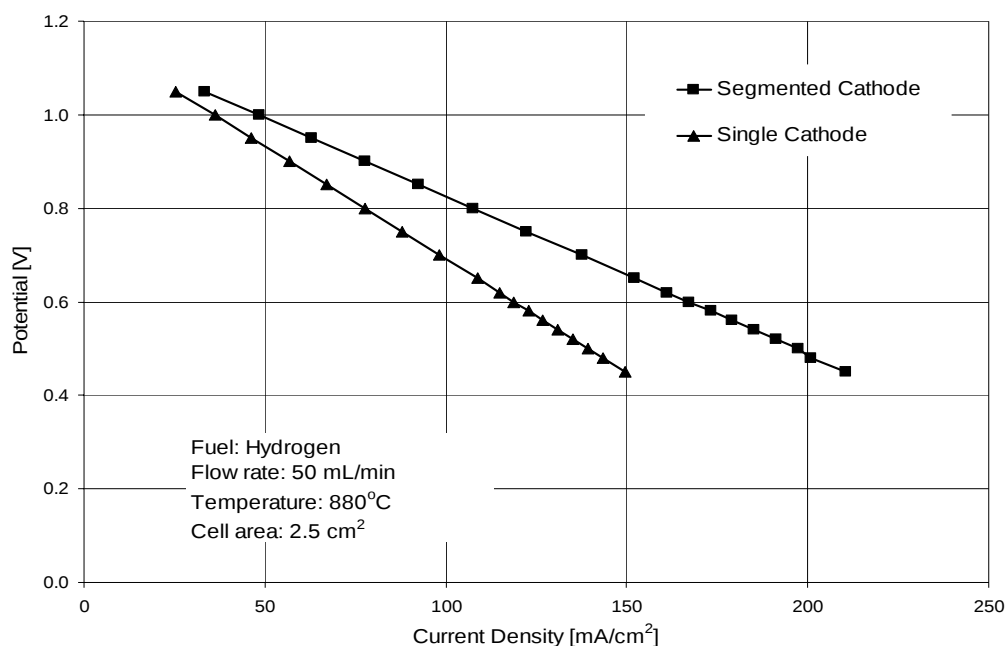


Figure 4-17 Effect of cathode segmentation on current density

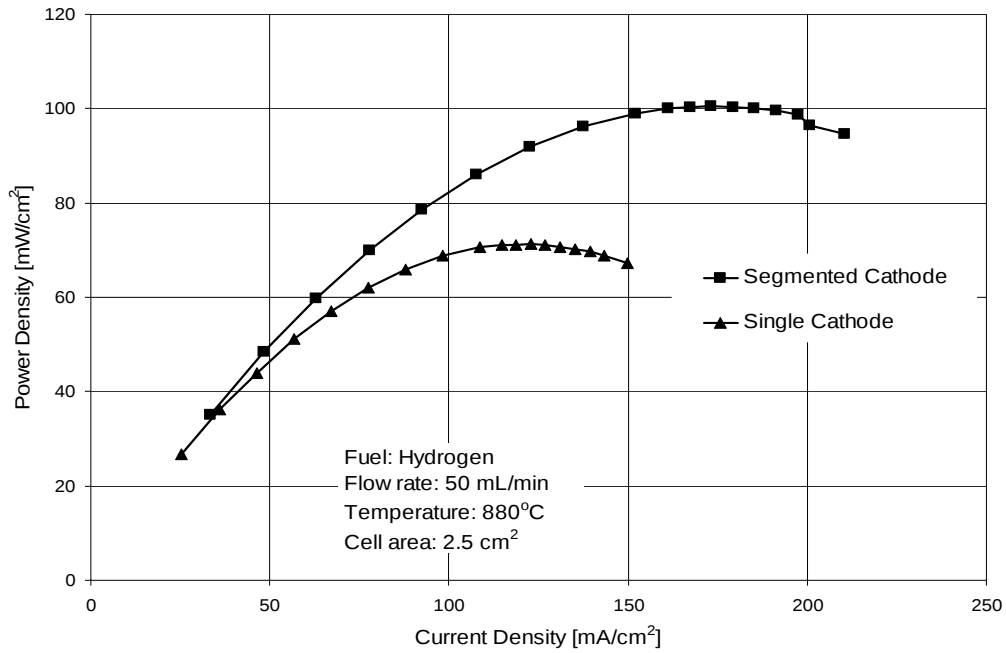


Figure 4-18 Effect of cathode segmentation on power density

Because segmenting the cathode improved performance, a batch of MT-SOFCs was manufactured with six segments. Three cathode configurations were investigated: fuel cells with standard 40-mm cathode; fuel cells with two 20-mm segments, and fuel cells with six 5-mm segments (Figure 4-19 & Figure 4-20). The two types of segmented cells had current and power densities within 5% of each other and 144% higher than the standard cell, emphasising that segmenting the cathodes increased performance.

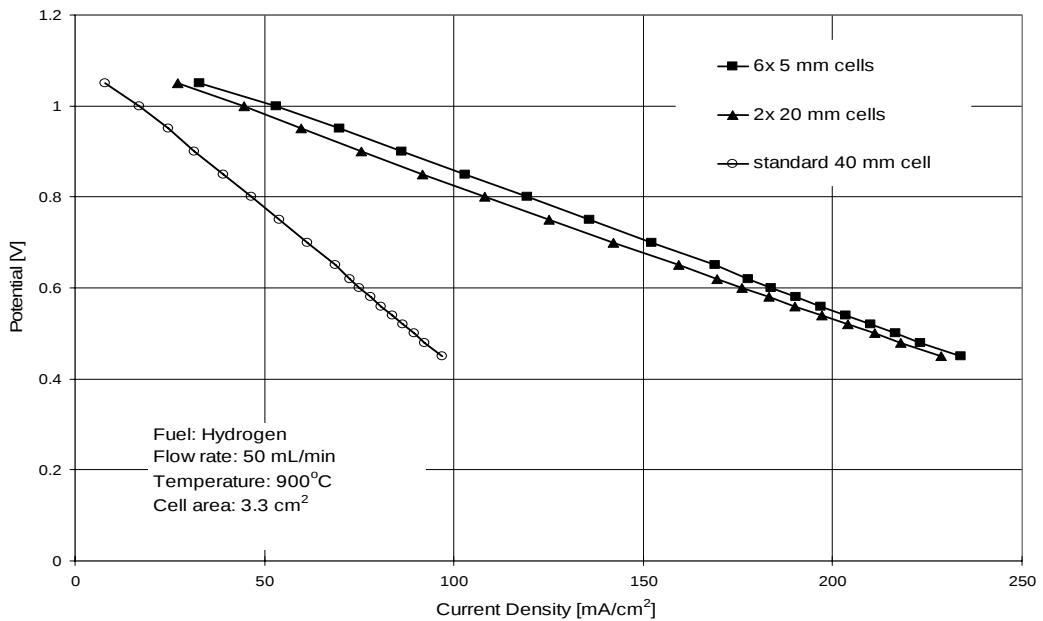


Figure 4-19 Effect of cathode segmentation on current density

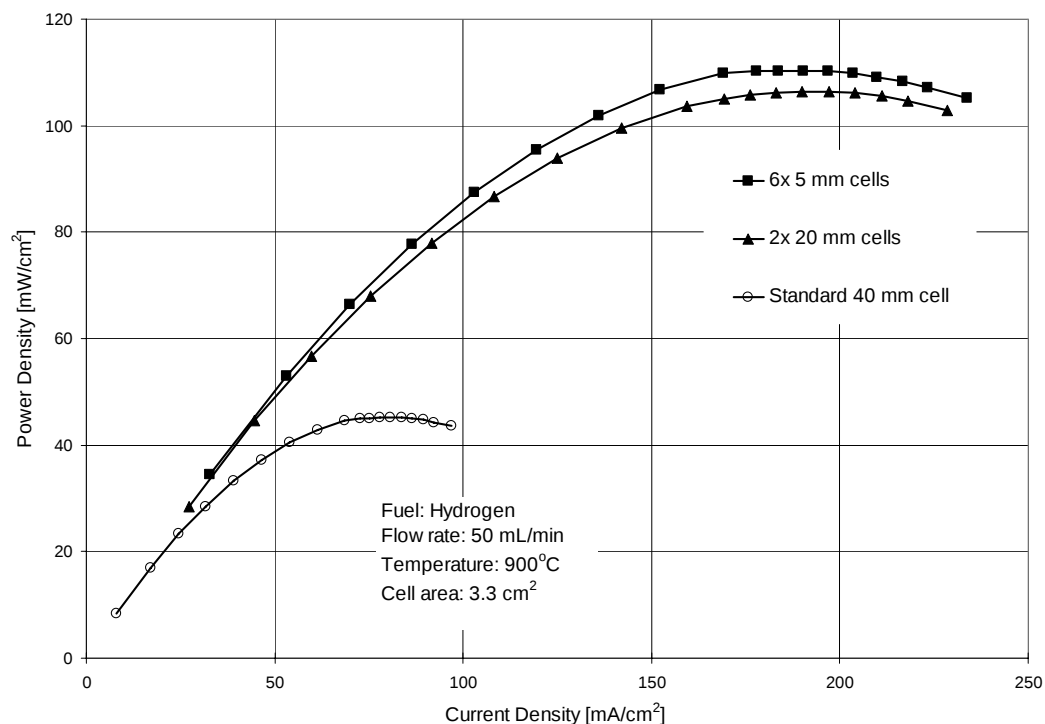


Figure 4-20 Effect of cathode segmentation on power density

4.8 CATHODE CURRENT COLLECTION WIRES

Trials were done with different numbers of silver wires wound around the cathode. Electronic resistance will decrease if wire cross sectional area is increased. Instead of increasing wire diameter, additional wires were added to the cathode current collection, effectively increasing the current pathway area. This also increased the contact area between the silver wires and cathode, which may also have increased cell performance. The current and power densities increased significantly from 70 mA/cm² for one wire, to 165 mA/cm² for two wires, and to 275 mA/cm² for four additional current collection wires (Figure 4-21 & Figure 4-22). The respective power densities were 36 mW/cm², 82 mW/cm² and 140 mW/cm². Thus, doubling the number of wires doubled performance and increasing from one to four wires gave an overall performance increase of 300%. The data indicate that the contact area between wires and the cathode should be increased or that cathode electronic conduction could be improved.

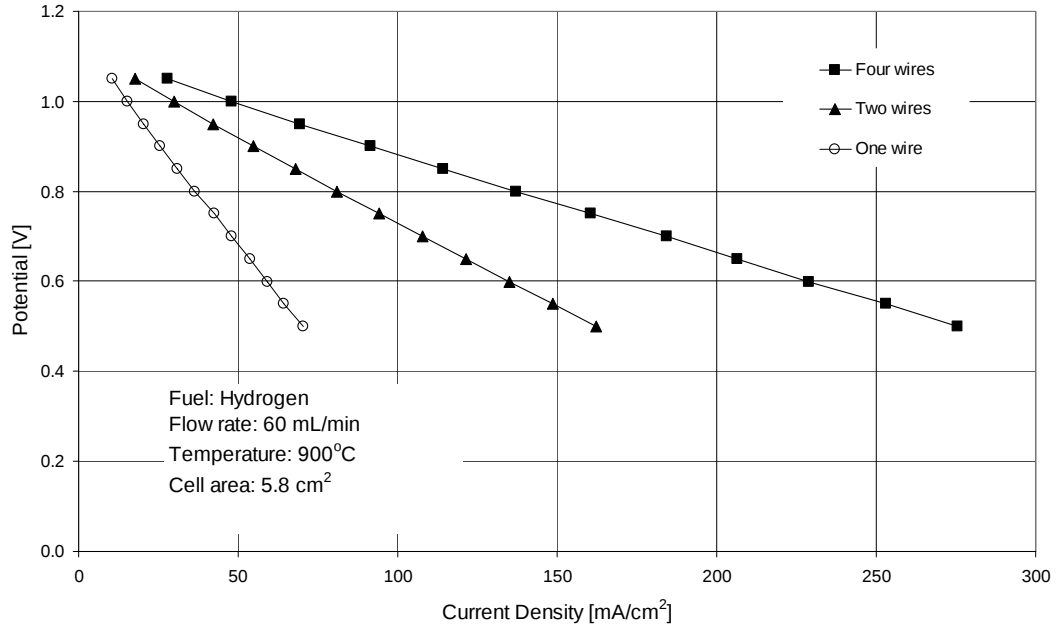


Figure 4-21 Effect of number of wires on current density

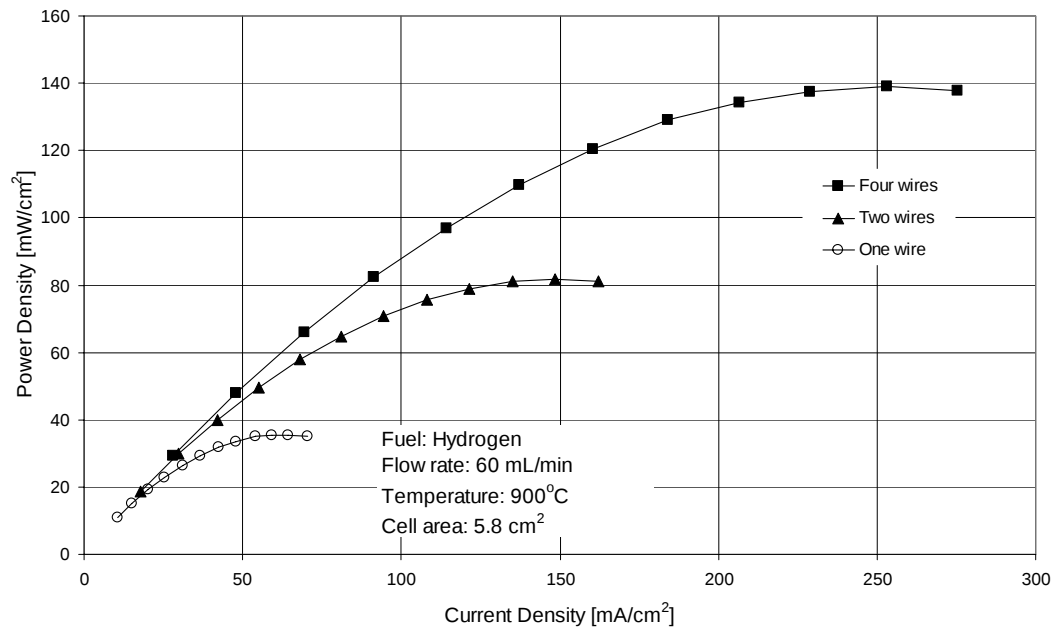


Figure 4-22 Effect of number of wires on power density

4.9 SILVER CONDUCTIVE INK

In an attempt to improve electrochemical performance, silver conductive ink was applied to the cathode after the silver current collection wires had been wound around the fuel cell. The silver conductive ink could benefit fuel cell performance in three ways: assist dissociation of oxygen molecules into ions at the three-phase

boundary with the YSZ and LSM; improve electronic pathways along the cathode; or improve the connection between the cathode and the silver current-collection wires. However, it is difficult to determine which had the major effect on improved performance. The ink (Alfa Aesar # 41823) contained 64% silver, 17% 2-butoxyethyl acetate, 10% diethylene glycol monomethyl ether acetate and 9% proprietary epoxy resins. Applying the silver conductive ink improved maximum current density by 10% (Figure 4-23) and maximum power density by 13% (Figure 4-24).

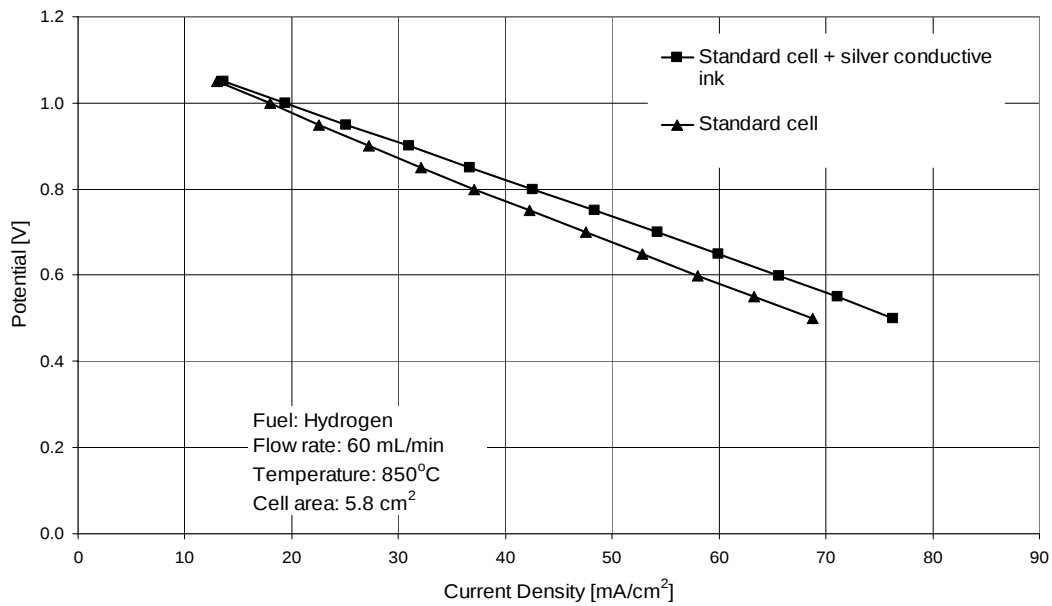


Figure 4-23 Effect of silver conductive ink on current density

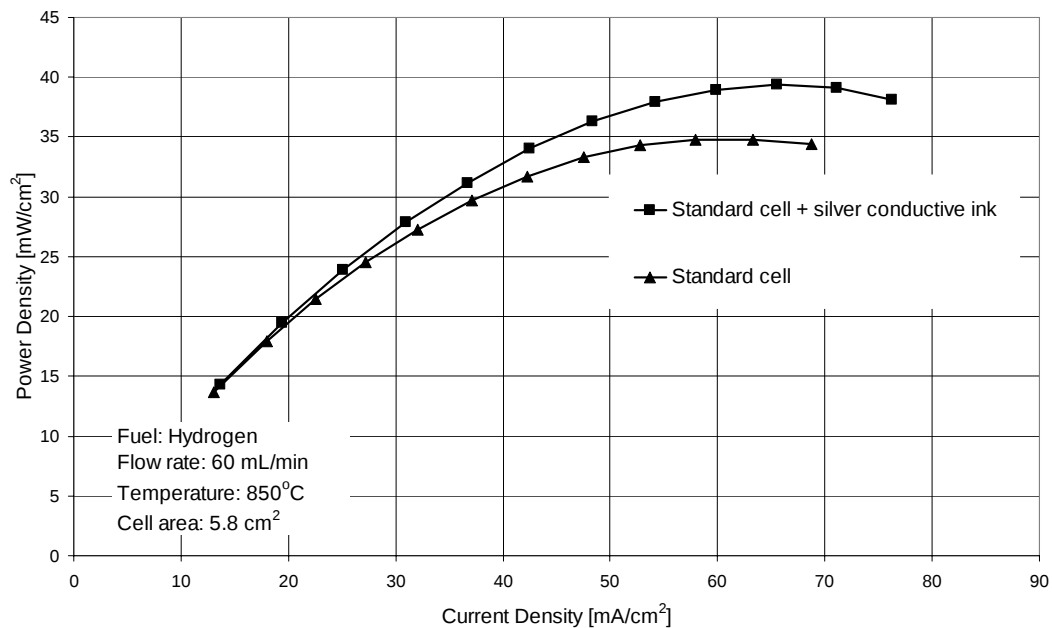


Figure 4-24 Effect of silver conductive ink on power density

Increase in performance is not as large as achieved by increasing the number of current collection wires. Conductivity measured along the cathode at room temperature indicated that the silver conductive ink provided more electronic pathways than in cells without the ink, although conductivity of the latter could not be measured. Although silver conductive ink improved electronic conduction along the cathode, a limitation for fuel cell performance is still the number of current collection points along the cathode, especially compared with the continuous current collection in the Siemens Westinghouse design, where the interconnect is fixed along the entire fuel cell tube.

4.10 SILVER NITRATE WASH COAT

Silver nitrate solution was used as a wash coat over the cathode to help improve electrochemical performance. It was theorised that the silver nitrate solution would be able to penetrate deeper into the cathode and help the oxygen dissociate to ions as a primary function at the three-phase boundary. A 2-wt% silver nitrate aqueous solution was applied to the cathode before drying at room temperature overnight. Current and power densities both increased by 11% (Figure 4-25 & Figure 4-26), which was less than for silver conductive ink. Silver nitrate had a different effect on cell performance compared with silver conductive ink - performance increased by a step amount (10 mA/cm) across the current range and OCV increased from 1.17 V to 1.22 V.

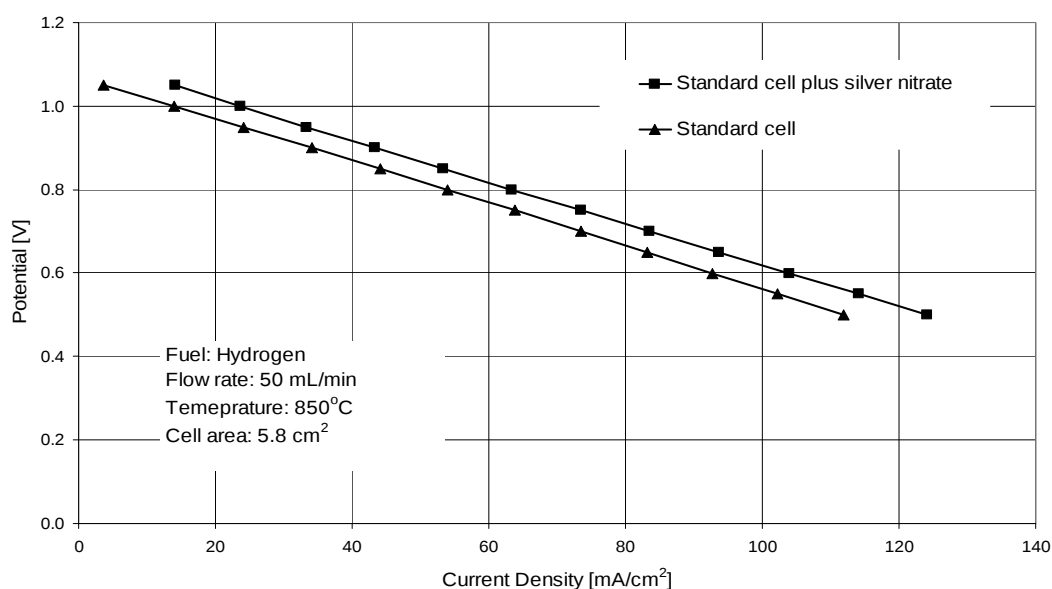


Figure 4-25 Effect of silver nitrate on current density

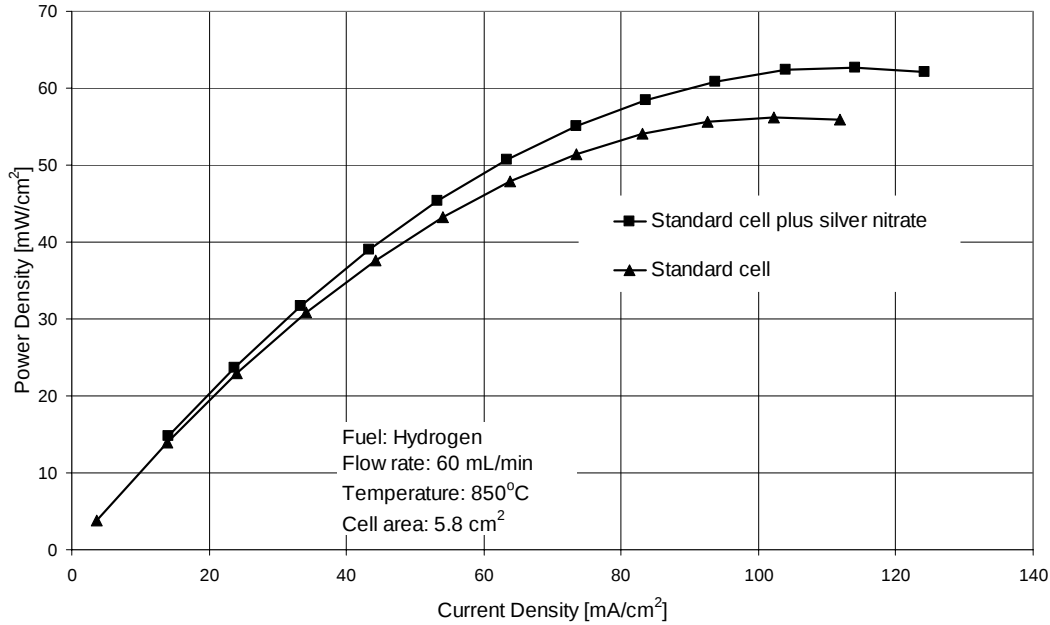


Figure 4-26 Effect of silver nitrate on power density

4.11 ANODE CURRENT COLLECTOR

Data from early trials indicated poor contact between the anode collection wire and the anode cermet. Sometimes the wire could be removed from inside the MT-SOFC with very little applied force. The looseness of the anode current collection wire and the amount of play within the MT-SOFC could remove part of the anode coating. Nickel has a coefficient of thermal expansion of $16.5 \mu\text{m}/\text{m}\cdot\text{K}$ and the coefficient of thermal expansion of 8YSZ increases from approximately $7.5 \mu\text{m}/\text{m}\cdot\text{K}$ at room temperature to approximately $10.1 \mu\text{m}/\text{m}\cdot\text{K}$ at 873K [77]. The nickel oxide in the anode, which was reduced to nickel metal, and the nickel wire current collector should have approximately the same expansion rate. The YSZ electrolyte does not expand as much as nickel metal so the nickel wire and the anode should remain in contact at high temperature.

Nickel metal softens considerably at 850°C so firm physical contact with the anode could decrease. The difficulty of maintaining firm physical contact between the electrode and the current collector occurs wherever metal is used at high temperatures so alternative methods need to be investigated. Trials were done to improve anode current collection and the contact between the wire and the cell. Several methods including nickel felts, wires, co-firing techniques and

pinning of nickel springs within the MT-SOFC were tested on a single batch of electrolyte tubes (Figure 4-27 & Figure 4-28).

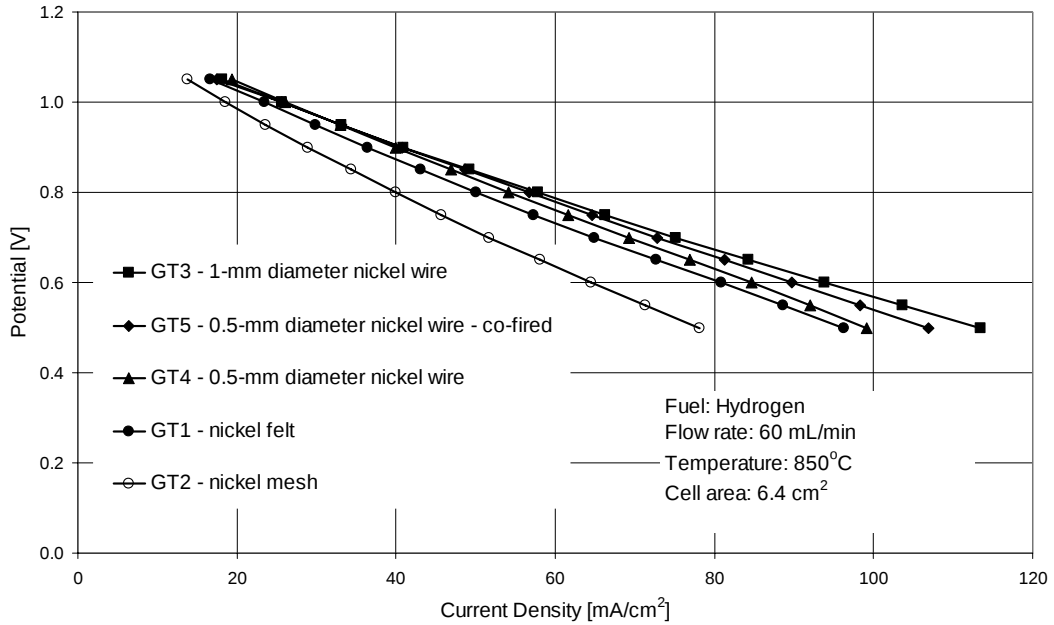


Figure 4-27 Effect of anode current collection method on current density

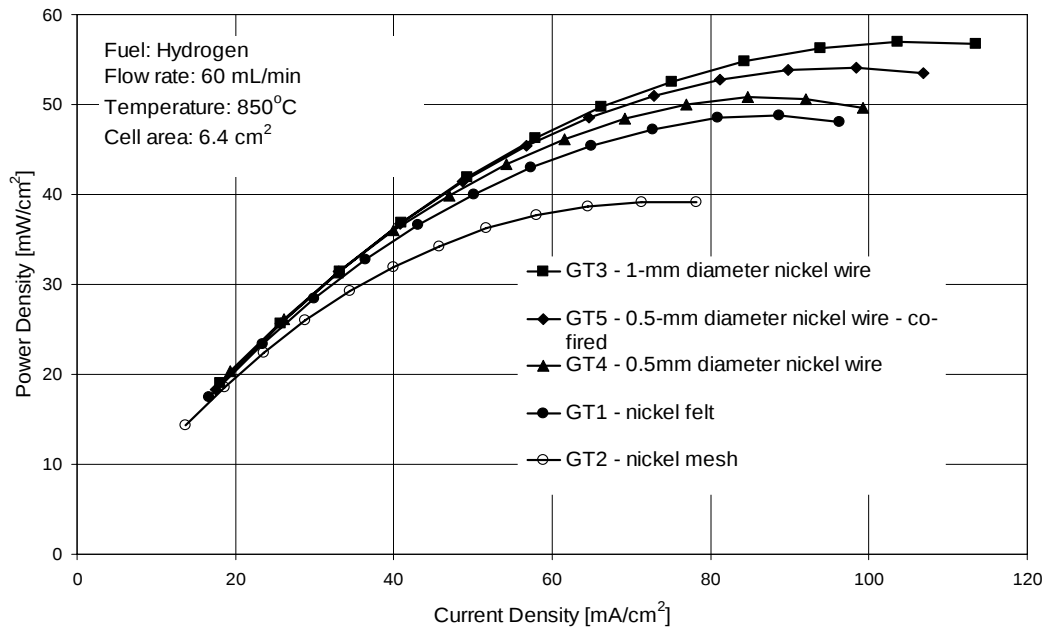


Figure 4-28 Effect of anode current collection method on power density

Current and power densities ranged from 78 mA/cm² to 115 mA/cm² and 39 mW/cm² to 57 mW/cm² respectively. Cell GT5 had a 0.5-mm nickel coil in the cell and had been washed with additional anode slurry before firing the cell. The

firing process fused the nickel coil to the anode, increasing contact area. The best cell had a 1-mm diameter coiled nickel wire insert. There was a 46% variance in cell performance across the anode current collection methods investigated, highlighting the need to develop a more consistent method. The results also emphasize that poor MT-SOFC performance was often due to poor physical connections and hence poor electronic conduction rather than poor ionic conduction and poor mass diffusion within the fuel cell, which is commonly the focus of research [78-80].

4.12 PINNED ANODE CURRENT COLLECTORS

After operating at high temperature, the nickel-coil anode current-collectors relaxed and firm physical contact with the anode diminished. An attempt to re-establish good physical contact between the anode and the current collector was made by carefully positioning some nickel pins between the coil and the anode. Poor performance of the unpinned cell was attributed to poor physical contact between the anode and the current collector. Once firm contact was re-established using the pinning technique, cell performance was at the expected level (Figure 4-29 & Figure 4-30).

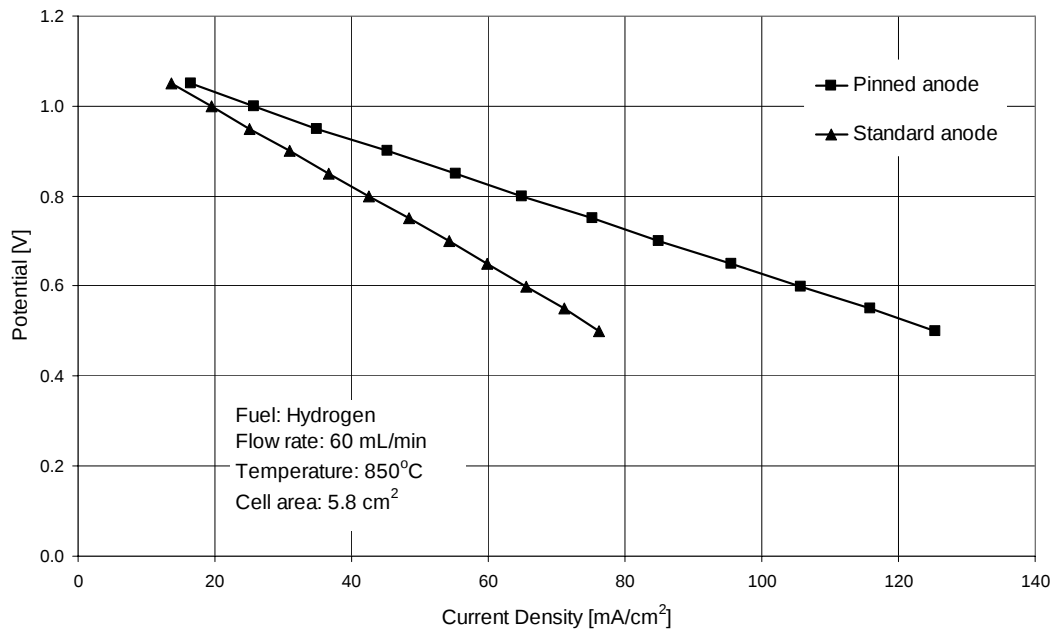


Figure 4-29 Effect of pinned anode current collection on current density

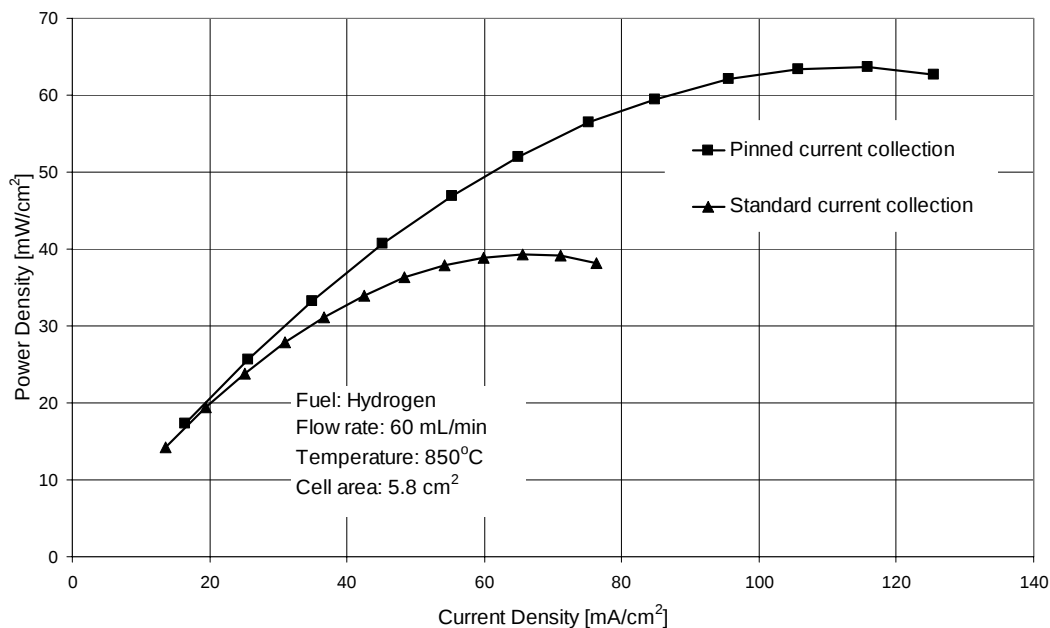


Figure 4-30 Effect of current collection methods on power density

Pinning the anode coil increased current density from 76 mA/cm² to 125 mA/cm² and power density from 39 mW/cm² to 63 mW/cm² and gave more consistent performance. There were some problems with inserting pins, especially when uneven and rough anode coatings within the MT-SOFCs led to cells fracturing. Inserting an additional wire did not guarantee firm connection between the anode and wire; sometimes several pins had to be inserted to establish firm contact. Each cell had to be checked after each thermal cycle because the nickel coils would become loose, even after as few as one thermal cycle; consequently, additional pins were required.

4.13 PLATINUM WASH COAT

Current at the anode could have been collected with platinum rather than nickel wires. As platinum has a higher catalytic activity, internal reforming of the hydrocarbon fuels would have been improved. The expense of platinum excludes its use as a current collector so an alternative method was proposed that involved a platinum wash over the anode before re-reducing the fuel cell. The platinum creates electronic pathways in the porous anode to the nickel wire current collector. Current and power densities increased from 60 mA/cm² to 76 mA/cm² and from 31 mW/cm² to 38 mW/cm² respectively (Figure 4-31 & Figure 4-32).

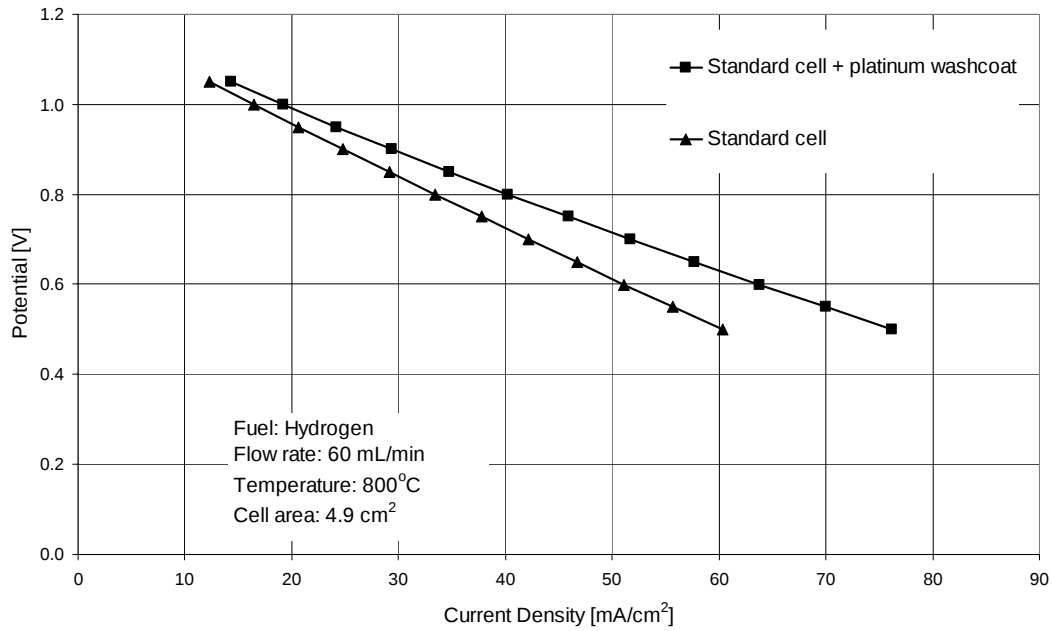


Figure 4-31 Effect of platinum wash coat on current density

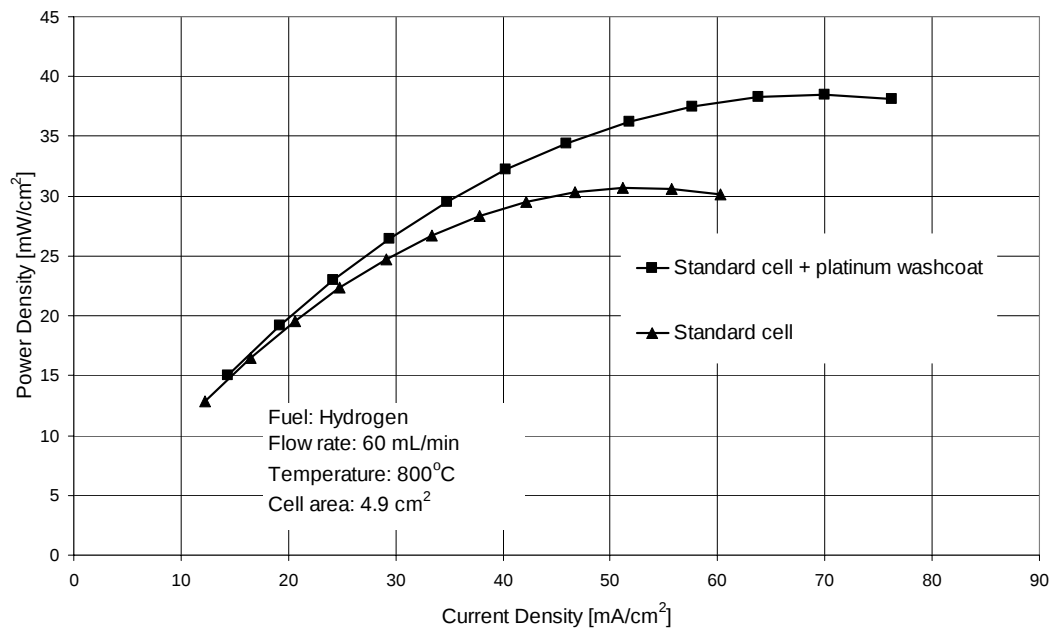


Figure 4-32 Effect of platinum wash coat on power density

4.14 COMBINED IMPROVEMENTS

Two batches of cells were fabricated. Batch A were prepared using the standard procedure with 50-mm long cathodes, silver wire wound around the cathode, a single strand of silver wire connected to the potentiostat, and a nickel wire coil for collecting current from the anode. Batch B incorporated the following improvements: the cathode segmented into five 10-mm sections with a 2-mm gap

between each section, five silver wires attached equally along the cathode and braided together before leading out of the hot zone of the testing furnace, a nickel wire coil for anode current collection and an extra nickel wire pin between the anode and the wire coil to establish a firm connection between wire and anode. Each fuel cell was fed 60 mL/min hydrogen. The improved design had 70% greater current and power densities (Figure 4-33 & Figure 4-34), which was less than the increase in performance by summing the effect of each improvement.

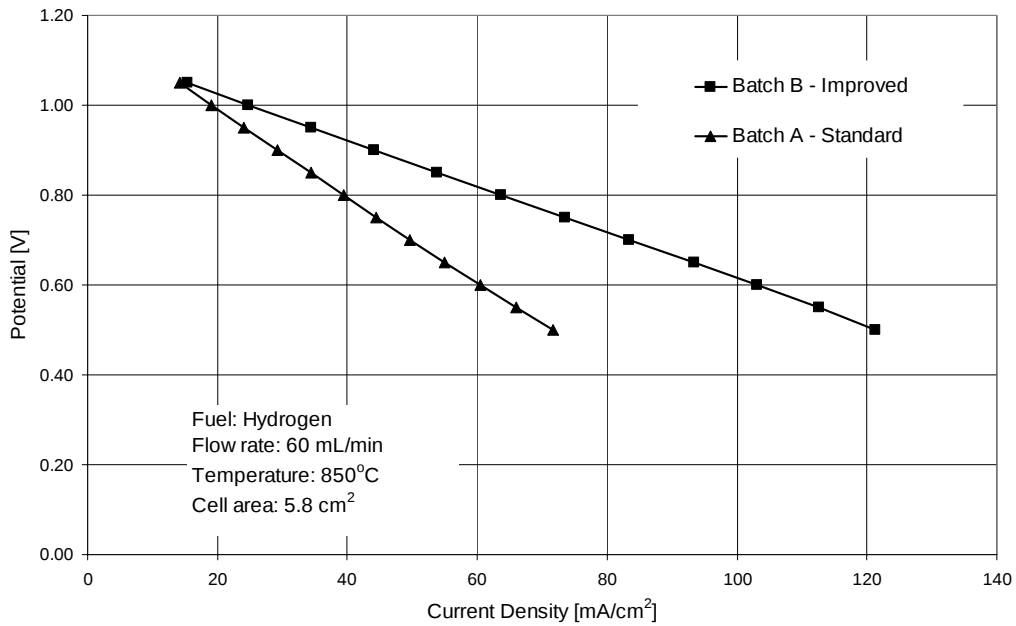


Figure 4-33 Effect of combined improvements on current density

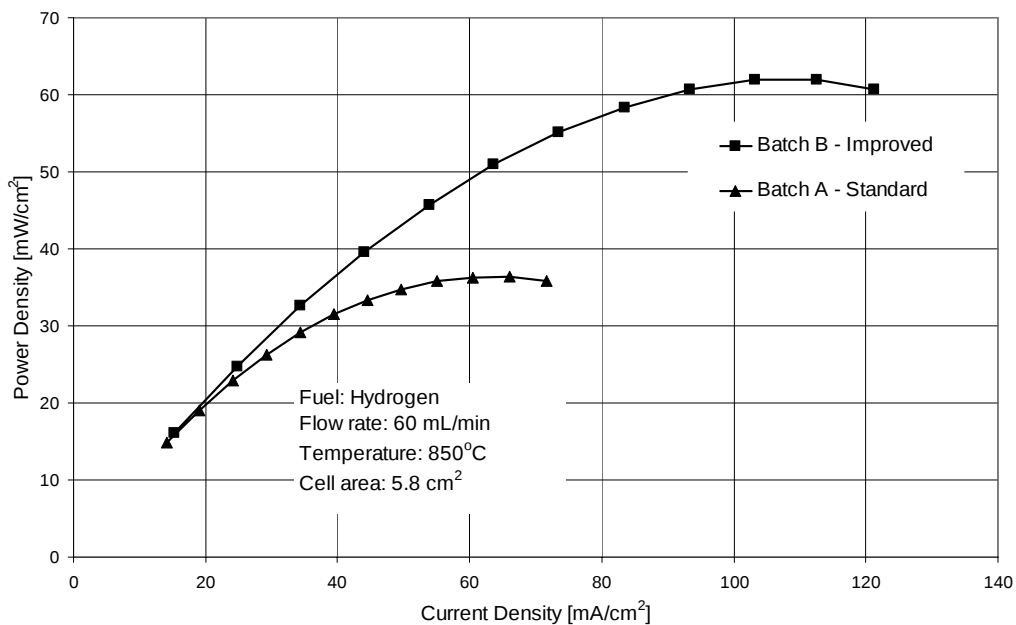


Figure 4-34 Effect of combined improvements on power density

4.15 SUMMARY

The electrochemical performance of MT-SOFCs was evaluated from various operating conditions and novel current collection techniques were developed to understand power production and to identify factors that limit fuel cell performance. Data indicate that electrolyte-supported MT-SOFCs can produce up to 480 mW of electrical power and that if sufficient number of cells were combined, useful power could be produced. Performance within a batch of fuel cells can vary widely and further work is required to identify processing conditions that will reduce this variability.

The MT-SOFCs fuelled with methane and propane gases mixed with air had similar electrochemical performance characteristics as when fuelled with pure hydrogen. Operating MT-SOFCs on hydrocarbon fuel and air mixtures, and using exhaust gases from a partial oxidation reactor allows greater flexibility for designing a generator that can be fuelled by commonly-available fuels such as natural gas and liquid petroleum gas (LPG). Electrochemical data showed that controlling flow rate within the fuel cells is not critical to power output so simplified flow control techniques can be used in a generator design.

There appears to be no advantage in having active length of cells longer than 30 mm, although this limit could be further investigated. Cells with less than 30-mm active length were not investigated in this research but could be investigated in future research. There was little or no increase in performance in cells with longer active length, which is thought to be due product gases not being removed. This led to poor mixing under the laminar flow conditions within the cells. Breaking the fuel cell active length by segmenting the cathode significantly increased cell performance. The small gaps in the cathode break the electrochemical performance along the cell and also allow gas mixing without electrochemical driving forces between the segments.

Identifying a reliable anode current collection technique is vital; methods used in this research were unreliable. If anode-supported MT-SOFCs are fabricated other options are possible such as leaving a portion of the anode tube without electrolyte or cathode coatings, which allows wires to be wound around the tube.

An alternative method would be to braze a metal tube to the zirconia-nickel cermet but this makes building up stack voltage difficult and creates further design issues to overcome electrical short-circuiting. Temperature can influence electrochemical performance dramatically so a major criterion in designing a portable MT-SOFC generator is to control and maintain high and even temperature and thermal profiles across the active lengths of the fuel cells.

5 PROTOTYPE DEVELOPMENT

When developing a functional prototype there are a range of features such as manifolds, fuel system and heating system which need to be incorporated. This chapter discusses development of manifolds, fuel systems and heating systems implemented in seven prototype generators. The prototypes developed are discussed in terms of the future direction of portable generators based on MT-SOFC technology.

5.1 MANIFOLDS

Manifolds are required to hold the MT-SOFCs in place and to provide channels for the inlet and exit gases. Three types of manifolds were developed with the physical security of the MT-SOFCs being of prime interest and the gas and electrical connections considered thereafter.

5.1.1 Machined-metal manifolds (P1, P2 & P3)

Three systems containing 1, 3 or 12 MT-SOFCs were constructed using machined-metal manifolds. The ability of the machined-metal manifolds to collect the power from the MT-SOFCs was also investigated. The manifolds were machined from stainless steel (304) in two pieces. Gaskets were fabricated from alumina fibre mat and were used to seal and insulate between the MT-SOFCs and manifolds as well as between the two halves of the manifolds (Figure 5-1).

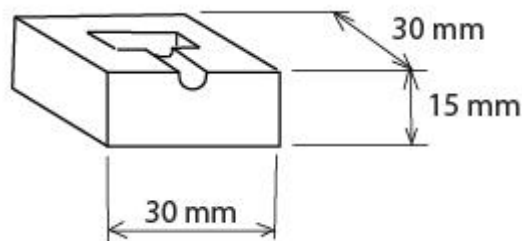


Figure 5-1 Machined metal manifolds (P1 & P2)

The P2 prototype used the same manifolds as P1 but incorporated three MT-SOFCs packed closely and connected in parallel. Developing the machined-metal manifolds from single cell (P1) to multi-cell (P3) capabilities required a new design to hold and seal the MT-SOFCs (Figure 5-2). The P3 manifolds were

machined from 304 stainless steel flat bar. Alumina fibre mat was cut into appropriate sized gaskets to seal the fuel cells against the machined-metal manifolds in a compressive type arrangement similar to that used in the P1 and P2 prototypes. The cells were electrically isolated from the metallic manifolds by ensuring that current collection wires were kept between layers of alumina fibre mat. This allowed the MT-SOFCs to be connected in series hence building up the voltage of the prototype. The design of the P3 manifold was modified at a later stage to allow threaded rod to connect the two opposing manifolds together which provided and maintained the correct location for the MT-SOFCs.

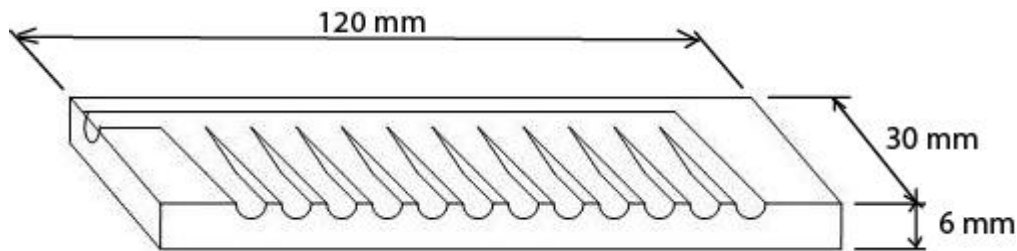


Figure 5-2 Multi-cell metal manifolds (P3)

Assembling a single MT-SOFC into the P1 manifold was relatively easy compared with later attempts at assembling multiple cells into manifolds. Care was taken to ensure that the alumina fibre gaskets sealed completely around the MT-SOFCs and over the two halves of each manifold. The fuel cell did not have to be perfectly straight because only MT-SOFC had to fit between the manifolds and the mounting holes were larger than that required allowing variance in the MT-SOFC dimensions. The two halves of the each manifold were screwed together with cap screws which was an effective method of holding the manifolds together and providing the sealing force. The MT-SOFCs performance could only be evaluated as a whole due to the metallic manifolds and nickel current collecting wires being linked together.

Using metallic manifolds and gaskets to hold and seal the fuel cells was effective initially but the rapid heating of the hot zone led to large thermal gradients across the MT-SOFCs and manifolds. The effect of coefficient of thermal expansion mismatches between the metal manifolds and the ceramic MT-SOFCs became evident from the number of fractured cells. MT-SOFCs did not usually break the

very first time heated but after several cycles between room and operating temperatures, typically five. Most MT-SOFCs broke at the point where they exited the metal manifolds. This led to fuel leaks to the cathodes and reduced fuel delivery to the unbroken MT-SOFCs. The MT-SOFCs fractured frequently and this was attributed to the extra stresses placed upon the MT-SOFCs by the heavy manifolds at each end of the cells. This was due to the difficulty in forming the exact shape required by the manifolds in the micro porous insulation block. If only one manifold was fully supported then the weight of the other manifold would be taken by the MT-SOFCs. To overcome this two threaded rods were placed between the manifolds, but this resulted in the MT-SOFCs fracturing due to tensile and compressive forces along the MT-SOFCs due to the difference in thermal expansion between the stainless steel and ceramic components. The linear coefficients of thermal expansion for stainless steel ($17.3 \times 10^{-6} \text{ K}^{-1}$)(0-100°C) [81] is greater than for YSZ ($10 \times 10^{-6} \text{ K}^{-1}$). Thus for a temperature increase of 800°C, stainless steel would expand by 1.4% whilst YSZ would only expand by 0.8% for the same temperature increase. Hence thermally induced forces were exerted on the MT-SOFCs by the manifolds.

Using compressive seals with alumina fibre mat gaskets proved to be an effective method of sealing the MT-SOFCs into the manifolds. Evidence of leaks was not readily apparent in the P1 and P2 prototypes, and consequently the use of compressive seals also was considered for the larger manifolds in the P3 prototype. Extra care was required in assembly of the P3 manifolds but thereafter in operation, leaks were not detected. Leaks were normally initially detected by changes in electrochemical performance of the MT-SOFCs and thereafter by visual inspection. Nevertheless the decision was made to continue with metallic manifolds but to design manifolds which did not contain so much metal as the machined ones.

5.1.2 Sheet-metal manifolds (P4 & P5)

Two manifolds, P4 and P5, holding four and six MT-SOFCs respectively were fabricated from 0.7-mm stainless steel sheet. The stainless steel sheet was folded in half and then pressed over steel formers of the appropriate shape and size to match the MT-SOFCs. Edges were seam welded where possible and silver

conductive ink was used to seal the MT-SOFCs into the manifolds. The MT-SOFCs were connected in parallel because of the silver conductive ink sealing the cells to the manifolds and because each nickel wire collecting current from the anode had to pass through a small pre-drilled hole in the manifold and these connections were also sealed using silver conductive ink. A stainless steel tube was inserted into the manifold's side entry for fuel delivery or exhaust gas extraction (Figure 5-3).

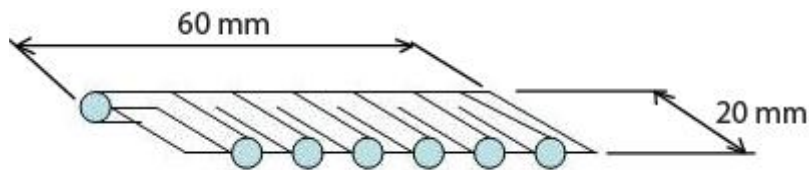


Figure 5-3 Folded sheet-metal manifold system (P5)

The main advantage of the folded sheet-metal manifolds over the machined-metal manifolds was less metallic mass connected to the MT-SOFCs. The key disadvantage was the inability to electrically connect the cells in series. If a poor performing MT-SOFC is connected to a good performing MT-SOFC the poor one will essentially be acting as an electronic load to the good one. Secondly the current increases due to the MT-SOFCs being connected in parallel and therefore higher resistances are encountered further reducing the electrical output. The manifolds had a low profile with the thickness being only slightly thicker than the diameter of the MT-SOFCs which led to lower heating requirements, and if larger stacks used these manifolds then a higher stacking density would be possible. The MT-SOFCs could not have any curvature otherwise assembly of the MT-SOFCs into the manifolds was near on impossible. Care was taken to avoid contact between the thermocouples and manifolds to prevent short-circuiting. This problem led to, on occasion, malfunctioning temperature controls and loss of electricity production. Folded sheet-metal manifolds reduced MT-SOFC failures due to thermal mismatches with the manifolds, but did not help resolve issues in building up the electrical potential and consequently alternative methods were sought to manifold the MT-SOFCs.

5.1.3 Alumina fibre-board manifolds (P6 & P7)

Cell fracturing using machined-metal and folded sheet-metal manifolds was frustrating in addition to the difficulties in inserting the MT-SOFCs in the manifold assemblies. It was also noted that single MT-SOFC testing involved resting each end of a MT-SOFC on a bed of alumina fibre mat contained within a cavity with firebricks. This concept was extended to incorporate several MT-SOFCs inserted through alumina fibre boards. This concept was further developed from preliminary work where cells were supported in furnaces using alumina fibre mat. Prototype P7 incorporated eight MT-SOFCs which were equally spaced on a 50-mm pitch circle diameter. The MT-SOFCs were held in place by two 12-mm thick, 60-mm diameter alumina-fibre discs with 4-mm holes drilled through for mounting the fuel cells. Eight 1-mm holes were drilled in one of the discs to allow the cathode current collection wires to exit the hot zone (Figure 5-4).



Figure 5-4 Alumina fibre manifolds (P7)

The alumina fibre boards have a similar thermal expansion to the MT-SOFCs. The alumina fibre boards did not form a perfect seal around the cells but at low fuel pressures there was no evidence of poor cell electrochemical performance due to cross contamination of air and fuel supplies. Leaks, if detected, were overcome by applying platinum catalyst solution to the alumina fibre boards around the cells which encouraged reaction of fuel to combustion products. The alumina fibre boards were also effective in insulating the hot zone with a thermal resistance

value of 2.4 m·K/W. A further advantage is that the alumina fibre board can be easily shaped with common workshop tools. Future work to improve the seals may look to form the boards around the fuel cells. The separation of physically holding the cells in position from provision of fuel to the cells could also be investigated.

5.1.4 Summary

Using metallic manifolds for MT-SOFCs was investigated but found to complicate thermal expansion issues and electrical connections between cells, especially if series connections were desired. A fully rigid system incorporating fragile ceramic fuel cells increased the risk of cell failures. Using alumina fibre gaskets to seal the cells was extended to fully support the fuel cells. The overall trend was to move away from rigidly holding the fuel cells in place, and to allow freedom of movement longitudinally as the stack heats up and cools down. Sealing may then be provided by ensuring sufficient length of contact between the ends of the cells and the alumina fibre boards. Assembling the cells into racks and manifolds identified issues of quality control in manufacturing the cells, specifically the roundness and straightness of the cells.

5.2 FUEL SYSTEM

Traditionally fuel cell tests and small stacks have used gaseous fuels directly from storage cylinders which could be described as a straight-through fuel system. Excess fuel, however, had to be sent through each cell to avoid oxidation of the anodes. An alternative design was to recycle the exhaust gases back through the cells. This system is known as anode-gas-recycling

5.2.1 Anode-gas-recycling

Recycling the anode exhaust gas is advantageous as the excess fuel put through the MT-SOFCs is not wasted. The system design was based on an anode-gas-recycling principle which involved a closed loop incorporating the anode side of the fuel cells (Figure 5-5). To avoid oxidation of the anode a reducing atmosphere was provided to the fuel cells. Fuel was added to the circulating gas flow using two methods; one being a simple bubbling arrangement and secondly by taking the head space vapour above the stored fuel. Iso-octane, methanol and

ethanol were used in the fuel reservoir. All of the gas would be bubbled through the liquid fuel, evaporating some of the fuel which would be carried through to the fuel cells.

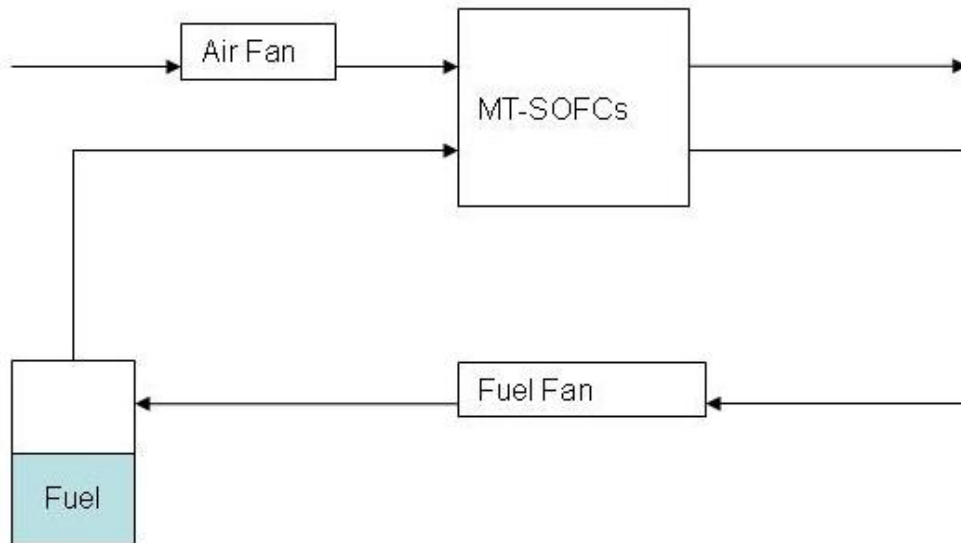


Figure 5-5 System design showing anode recycling

Later a bypass line was added so that the bubbler could be switched in and out of the main loop (Figure 5-6).

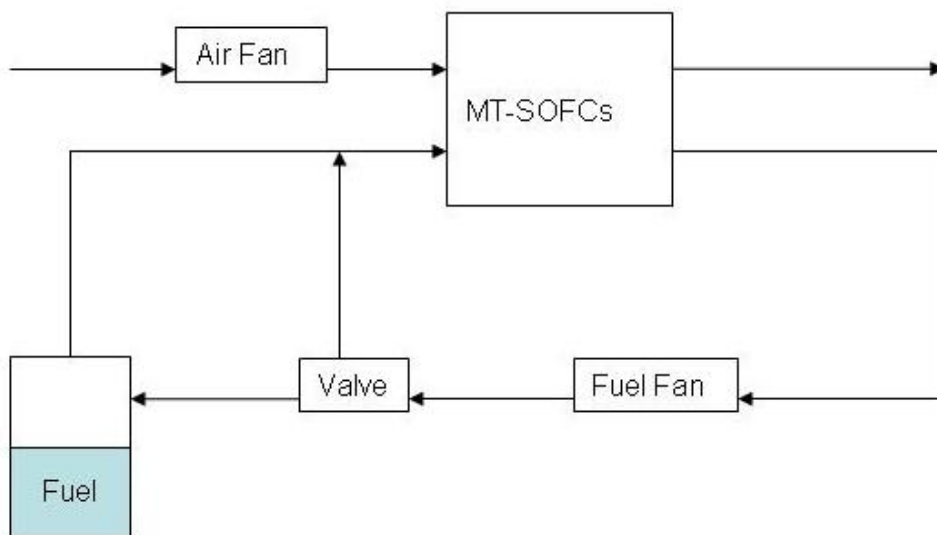


Figure 5-6 System design showing valve to turn off the bubbler

A vessel with large internal area was placed at the outlet of the hot zone to condense water from the gas stream. Carbon particles would sometimes be seen in the condensed water re-iterating the carbon deposition problems within the

MT-SOFCs. No means of removing the carbon dioxide produced was incorporated into this system and would need to be designed into future systems, possibly through membrane technologies. One of the main benefits of incorporating an anode-gas-recycling loop is the lesser chance of oxidising the anode during operations because the anode is never exposed to air.

The fuel cells and manifolds were placed within cavities machined out of micro-porous insulation block. The fuel cells, heater and insulation were housed within modified plastic boxes. Only the electrical wires and gas tubes passed into and out of the boxes.

Two small diaphragm pumps (ASF Thomas #50040 and #50042) were used to circulate the gas in the anode-recycling loop. The pump's throughput was adjusted by changing the power supply voltage and was measured using a bubble flow meter (Figure 5-7).

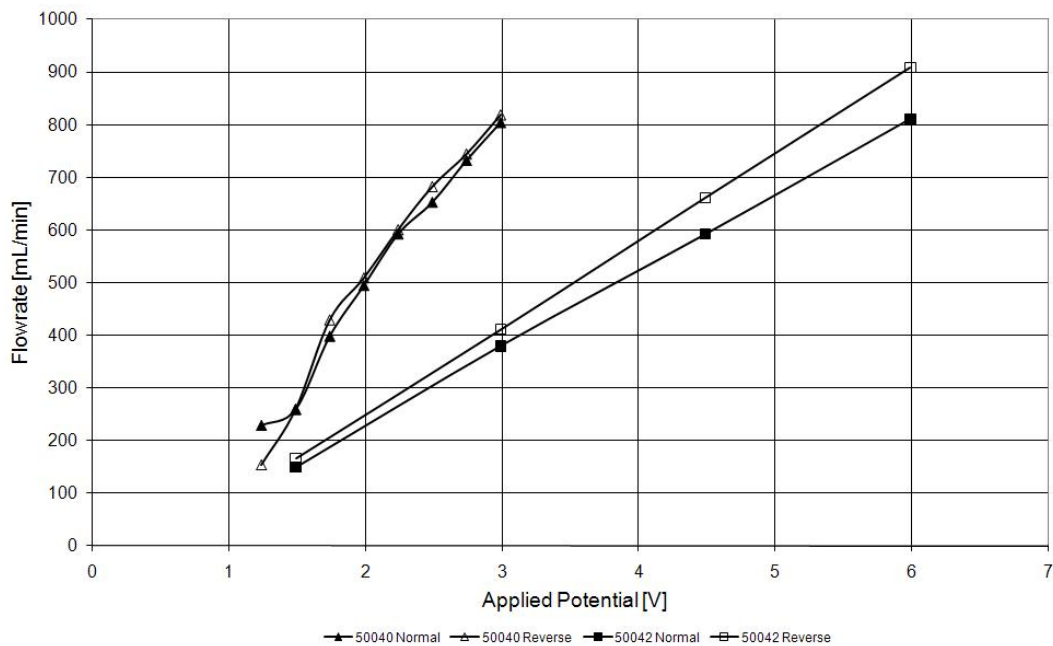


Figure 5-7 Effect of applied potential and polarity to pump throughput

Fuel cell operation was monitored whilst fuel was added continuously by means of the carrier gas picking up vapour from the fuel reservoir. The pick-up of fuel vapour was later switched on and off by monitoring fuel cell potential in a simple arrangement: when potential dropped below a preset level, the valve would switch to allow carrier gas to pass through the bubbler to entrain fuel vapour. Once a higher voltage was reached, the valve would switch back to its original state. The

effect of the valve switching, at steady-state operation approximately 2.5 hours into this thermal cycle, can be seen as fluctuations in current and voltage output (Figure 5-8). The potentials and drawn currents are synchronized with the fuel loop being switched in and out of the anode-gas-recycling loop.

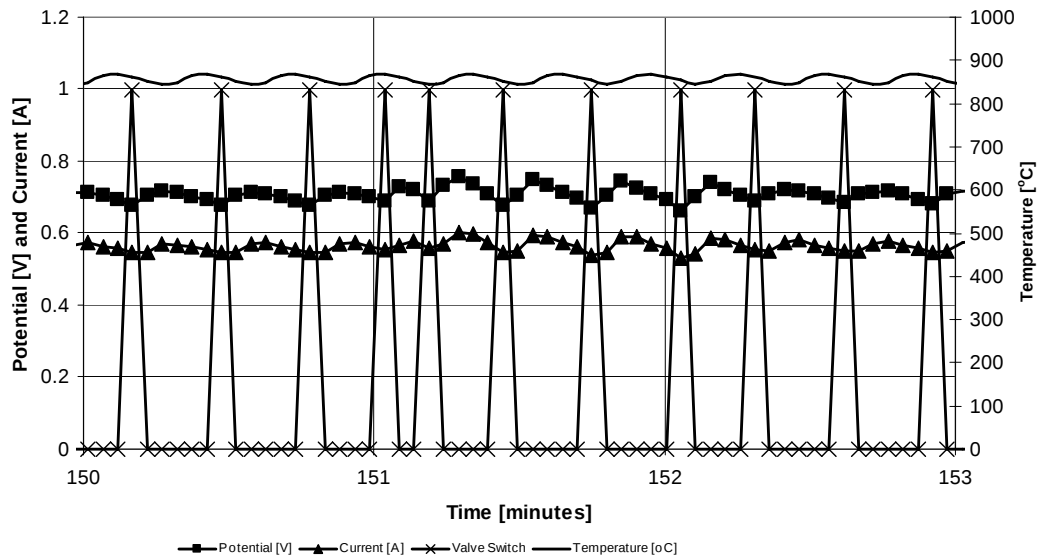


Figure 5-8 Effect of fuel addition to fuel cell performance

When fuel was constantly added to the fuel stream, the anode was exposed to hydrocarbon-rich fuel and soon became clogged with carbon deposits at the entrance to the cells. Carbon deposition occurred when correct conditions for steam or partial oxidation of the hydrocarbon fuels were not present. An alternative configuration was investigated to see if the effects of carbon deposition could be removed by blowing carbon out of the fuel cell. This configuration involved switching flow direction of carrier gas and fuel vapour using a single valve switch. The first design revision involved adding a bypass loop so gas could be recycled without constantly adding fuel. Fuel was added by switching off the fuel bypass loop when cell potential dropped below a set value. Gas flow was directed into the appropriate loop with solenoid valves. Reducing the fuel added to the recirculation flow increased fuel cell life but carbon deposits still formed at the entrances to the cells. Carbon deposition issues occurred more with iso-octane and ethanol and least with methanol.

This system design did not sufficiently control the conditions to avoid carbon deposition. As well as resolving carbon deposition, future research could also

include investigating the effect of modifying the fuel system to allow gaseous fuels such as natural gas and LPG through injection ports.

5.2.2 Summary

Anode-gas-recycling was investigated to reduce fuel consumption of the fuel cells. A basic control mechanism for fuel introduction into the loops was implemented, based on the cell potential. Recycling gases allowed liquid fuels such as methanol, ethanol and iso-octane to be used for MT-SOFCs, although carbon deposition within the anodes was evident. Further research is required to ensure non-carbon deposition conditions can be provided in an anode-gas-recycling system design. Enhancements to adding fuel to the recycle loop could be made by using a fuel injection system using gaseous and liquid fuels. Liquid fuels could be dispensed into the hot exhaust gas stream eliminating the need for a bubbler.

5.3 HEATING SYSTEM

MT-SOFCs are based on the ionic conduction of oxygen ions through the YSZ electrolyte and because this only happens at high temperature a heating system must be incorporated into the generator design which is capable of heating the MT-SOFCs to operating temperature, usually between 800°C and 900°C.

5.3.1 Electrical heating

MT-SOFC testing and some stack development was done using electrical heating systems, which provided quick consistent heating on demand so the fuel cells, manifold and stack designs could be evaluated without changing the heating method. Some literature indicates that fuel cells only need to be preheated to operating temperature; once at operating temperature, the fuel cells can maintain temperature by the electrochemical reactions [74]. Evidence of fuel cell's self-heating was not found in this research. The thermal profile of the single cell test rig was measured (Figure 5-9) and indicated 100°C temperature variation across the hot zone where the fuel cells were located for testing.

Electrical heating was also used when developing stacks with better thermal performance due to increased insulation around the stack. The thermal profile

variation for the electrically-heated stack was 50°C, although the maximum temperature achieved was only 750°C due to thermal limits of the heating element.

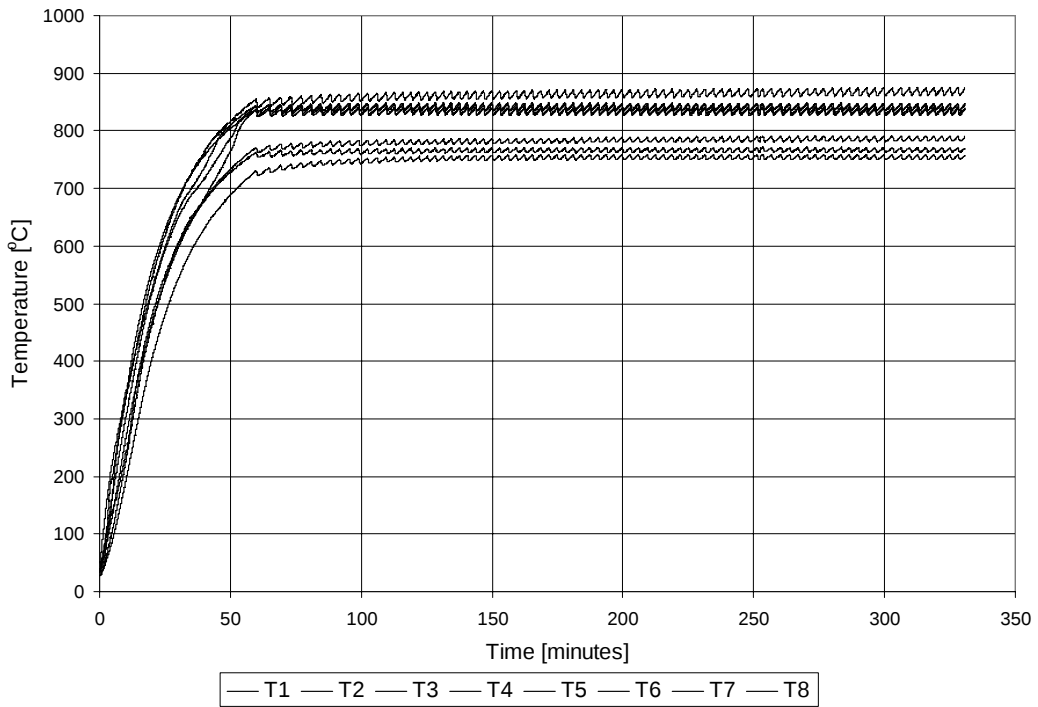


Figure 5-9 Effect of controller on furnace temperature profile

The energy consumption rate was also measured to provide a baseline for comparison with other heating systems. At steady-state conditions, the stack test rig consumed 80 W to maintaining 750°C temperature near the heating element and 700°C at the outside edges of the hot zone (Figure 5-10). Efforts were made to reduce temperature fluctuations by using the proportional–integral–derivative (PID) features of the controller. The auto-thermal controls of the controller were reset and the temperature variation range was reduced to 5°C but within 30 minutes the range had increased to 40°C. The controller’s settings were checked but no errors were found. It was thought the heating elements were affecting the control circuits, possibly due to changes in the element’s internal resistance at high temperatures near the elements’ thermal limits.

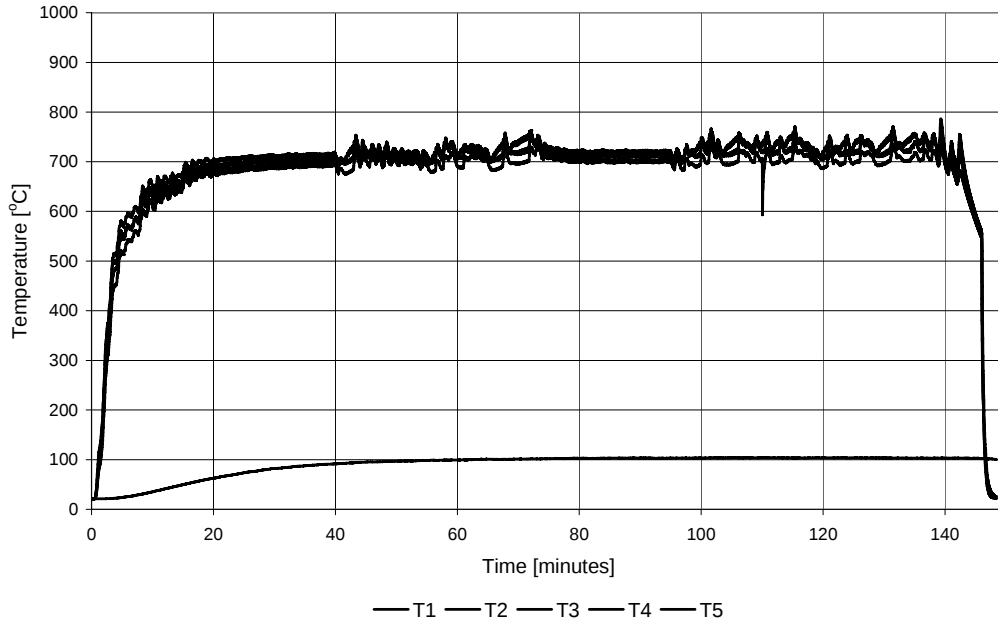


Figure 5-10 Thermal profile using electrical heating

Heating the fuel cells electrically is clearly non-productive, especially when the electrical energy used to heat the cells is greater than the amount of electrical energy generated; however, the main purpose in using electrical energy was to develop the manifolds and the system design. The effect of temperature control over fuel cell performance was also investigated but the thermal cycling peaks are not synchronized with the potential and current measurements (Figure 5-11). The potential and current peaks are consistent with fuel being added to the anode-recycling loop seen earlier.

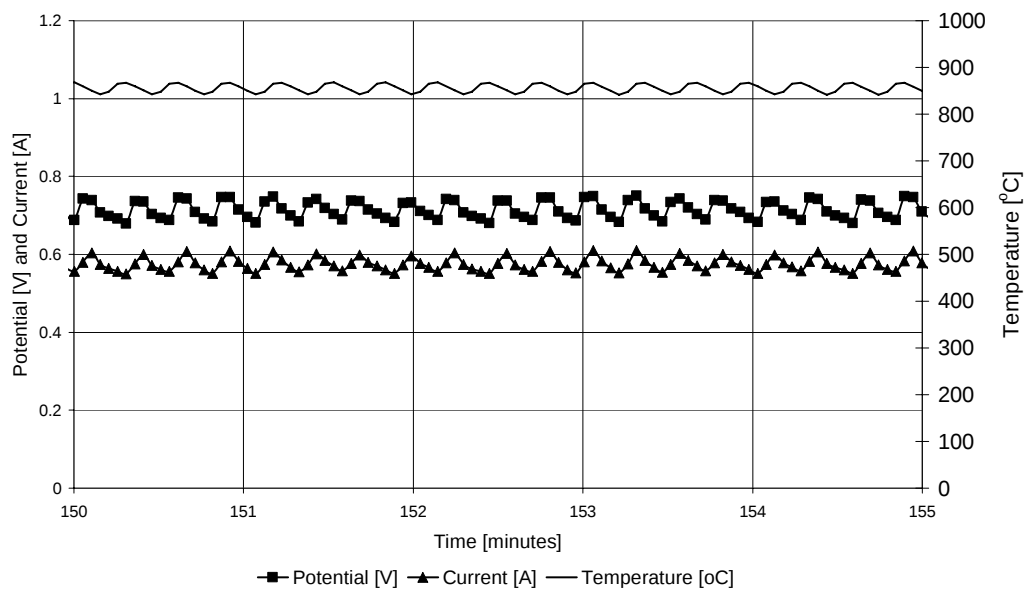


Figure 5-11 Effect of temperature fluctuations on fuel cell performance

5.3.2 Partial oxidation reactors

The first partial oxidation reactor developed consisted of a quartz tube, two small pieces of nickel mesh coiled to fit inside the quartz tube and some platinum impregnated alumina spheres. Air was blown through a liquid bubbler containing hydrocarbon fuels (iso-octane, ethanol and methanol) and into the reactor. External heat was applied to the reactor by a gas torch; once the reactor had started, the torch could be removed. The reactor was placed within insulation with approximately 10-mm spacing around it. Later, four MT-SOFCs were connected to the reactor's exhaust gas stream and placed in the hot zone next to the reactor. The fuel cells came up to OCV and enough power was drawn to power a small mechanical fan. This prototype (P6) based on the partial oxidation reactor was the first proof of concept needed to continue investigations into incorporating a partial oxidation reactor into a MT-SOFC generator design. It successfully demonstrated that a single fuel source could be used to heat the fuel cells to operating temperature and provide the fuel cells with a diluted syngas in sufficient quantity to generate useful electrical energy. (Figure 5-12).

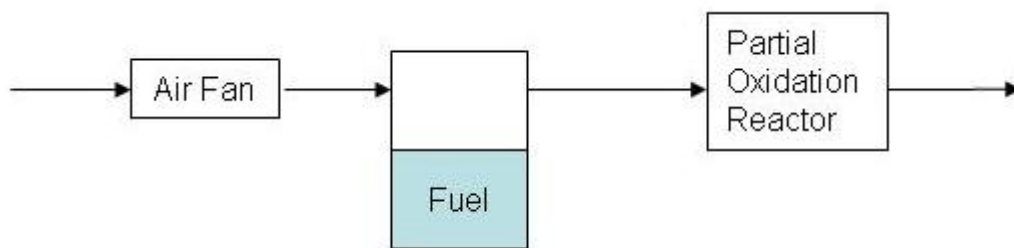


Figure 5-12 System design using partial oxidation reactor and liquid fuels

The partial oxidation reactor operated on 100% methanol, ethanol or iso-octane and also the same fuels diluted down to 20% by volume in water. The reactor's temperature could be modified by adjusting air flow rate from the air blower. The only parasitic power loss in this system was the power to the air blower (approximately 0.1 W). A rechargeable battery could be used to provide the air-blower power, which could be recharged once the fuel cells are operational. The amount of vapour released from the liquid fuels was a function of temperature. Liquid temperature decreased during the experiments as energy of the liquid was used to vaporise some of the liquid. The vapour (partial) pressure of the three fuels evaluated can be calculated as a function of its temperature (Figure 5-13).

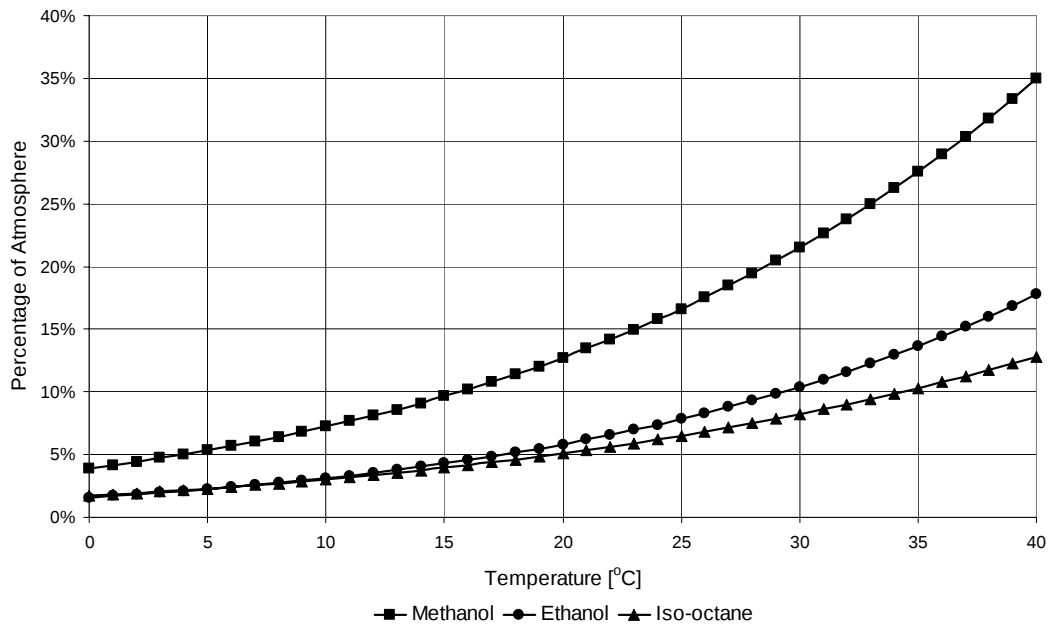


Figure 5-13 Effect of temperature on vapour pressure

A constant evaporation rate would require temperature of the liquid to be well-controlled. This could be managed by directing heat from the fuel cell exhaust gases to the fuel reservoir via a heat exchanger. Although the partial oxidation reactor was initially ignited by applying heat to the outside of the quartz tube from a portable gas torch, subsequent tests showed that the reactor could self-ignite when provided with appropriate air-fuel mixtures using liquid fuels. In later work using LPG, the self-igniting ability however could not be replicated.

While liquid fuels are convenient and offer some advantages, the need to integrate additional components such as the air blower into the generator design was considered an added complication so efforts were directed towards using gaseous fuels that could use a venturi to draw in air. A second partial oxidation reactor was fuelled by air-LPG mixtures because LPG was considered a more suitable fuel for a portable MT-SOFC generator and because air:fuel ratios could be more easily controlled than for liquid fuels (Figure 5-14).

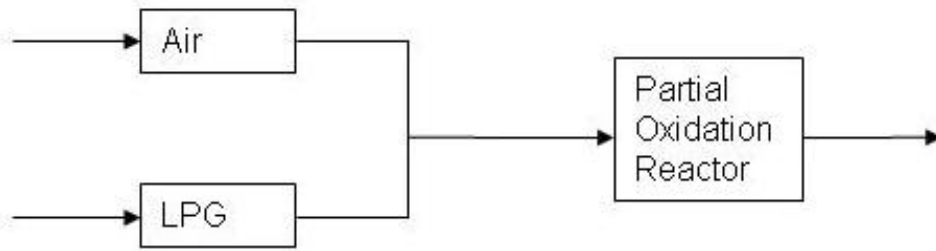


Figure 5-14 System design using partial oxidation reactor using LPG fuel

The partial oxidation reactor was inserted into the same testing rig used to measure thermal profiles of the electrically heated stack (Figure 5-15).

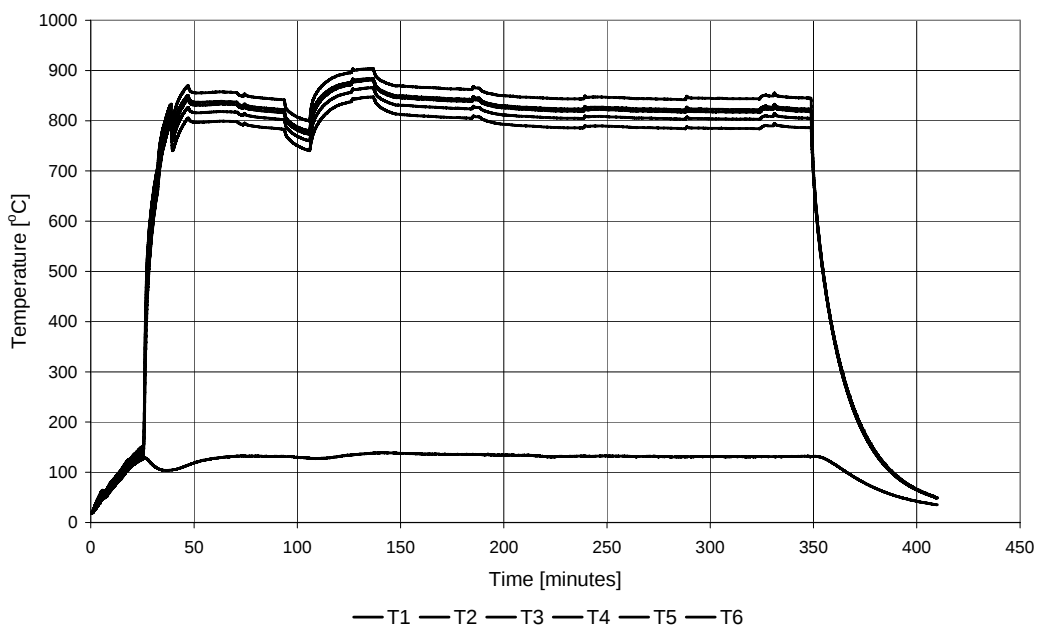


Figure 5-15 Thermal profile using partial oxidation reactor

Pre-heat was applied to the catalyst zone directly or to the incoming air:LPG mixture. When applied to the catalyst zone, the reactor started within seconds. However, when pre-heat was applied to the incoming air:LPG mixture, the reactor only started after the internal temperature had approximately 150°C, which took 25 minutes to achieve (Figure 5-16).

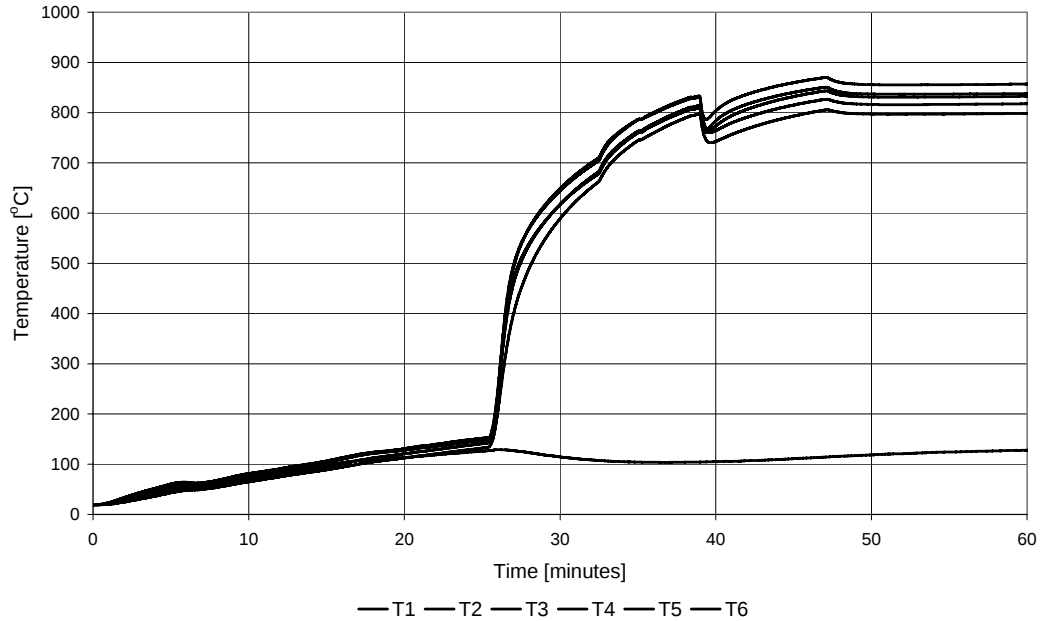


Figure 5-16 Start-up profile of partial oxidation reactor

Once the reactor had ignited, the temperature rose quickly and the MT-SOFC operational temperature of 800°C was reached in 10 minutes. The temperature drop seen at 40 minute was due to connecting additional pipe work and equipment to the reactor to collect dry exhaust gas samples for GC analysis. Condensation from the reactor occurs so any routing of exhaust gases to the MT-SOFCs must be at 100°C or higher. The thermal gradient across the hot zone was 50°C, which was approximately the same as observed in the electrically heated prototypes.

Future work could investigate integrating a partial oxidation reactor with an anode-gas-recycling design but it may be simpler and easier to design a system with a full oxidation reactor for heating the cells and a partial oxidation reactor to provide carbon monoxide and hydrogen to the fuel cells. This increases the complexity of system design but could improve efficiency. The air for the reactor experiments was sourced from a cylinder of dry air, but this could be replaced by a venturi mixing system found in currently available LPG appliances.

5.3.3 Summary

Electrically heated stacks were used to evaluate manifolds and system variations. However electrical heating is non-productive, especially when the electrical energy used to heat the cells is greater than the amount of electrical energy

generated by the fuel cells. An alternative heating system using partial oxidation of liquid and gaseous fuels was developed, which can heat the MT-SOFCs and provide suitable fuel for the MT-SOFCs. The thermal profile across the heated volume using the partial oxidation heater was comparable to that when electrical heating was used, just 50°C.

5.4 FINAL PROTOTYPE (P7)

Prototype P7 incorporated several of the design improvements developed during the research. Alumina fibre boards were used to hold the MT-SOFCs and a partial oxidation reactor was used to heat and fuel the MT-SOFCs.

5.4.1 Design

The prototype is housed within an aluminium casing with an outside diameter of 88 mm, 3.5-mm wall thickness and 100 mm long. The ends of the cylinder are capped with 3-mm aluminium end-plates. A tube of micro porous insulation block, outside diameter 81 mm, 4-mm wall thickness and 100 mm long, is inserted inside the aluminium tube. Alumina fibre board insulation with an outside diameter of 65 mm, 7.5-mm wall thickness and 60 mm long is inserted inside the micro porous block tube. Two 20-mm thick alumina fibre board discs are inserted at each end of the micro porous tube. The discs have holes appropriately sized for the partial oxidation reactor and the fuel cells (Section 5.1.3). The partial oxidation reactor was a heat source at the centre of the generator. The reactor was 14-mm diameter quartz glass tube. The immediate volume around the reactor (the hot zone) had a diameter of 50 mm and the hot zone was 60 mm long. Thus, total volume of the hot zone, including the reactor was $1.2 \times 10^{-4} \text{ m}^3$. Volume of the containment vessel and insulation but excluding the reactor was approximately $1.1 \times 10^{-4} \text{ m}^3$.

5.4.2 Performance

The energy content of the inwards mass flows (LPG and air) were readily calculated. The prototype was heated electrically and by the partial oxidation reactor. Electrically heating the stack required 80 W whereas 240 W of LPG fuel was required to heat the same volume using the partial oxidation reactor. The performance of the P7 prototype is analysed mathematically in Chapter 7.

5.5 SUMMARY

This chapter has described the importance of three key areas of the MT-SOFC generator concept: manifolds, fuel system and heating system. The development of technologies in all three areas is sufficient to design and build a generator using MT-SOFCs. Key design features of the prototypes are summarised (Table 5-1).

Table 5-1 Design features of prototypes

ID	# of cells	Fuel	Manifolds	Anode-gas recycling	Heating technique
P1	1	Methanol, Ethanol, Iso-octane	Machined metal blocks	Yes	Electrical
P2	3	Methanol, Ethanol, Iso-octane	Machined metal blocks	Yes	Electrical
P3	12	Methanol, Ethanol, Iso-octane	Machined metal blocks	Yes	Electrical
P4	3	Methanol, Ethanol, Iso-octane	Folded sheet metal	Yes	Electrical
P5	6	Methanol, Ethanol, Iso-octane	Folded sheet metal	Yes	Electrical
P6	4	Methanol, Ethanol, Iso-octane	Alumina fibre board	No	Electrical
P7	8	LPG	Alumina fibre board	No	Partial oxidation

While most trials were done with liquid fuels indicated good performance of the MT-SOFCs with such fuels, a portable generator would be easier to design and operate on gas such as LPG. The limited trials done with LPG indicated it was able to requirements of a portable generator based on MT-SOFC technology.

6 GAS ANALYSIS

Knowing gas composition at various positions helps characterise performance and efficiency of a MT-SOFC generator. Gas composition could be readily determined for the fuel source, the air-fuel mixture, and exhaust from the partial oxidation reactor. This chapter presents gas compositional data from these positions and discusses errors and variations. The composition information is used when modelling the MT-SOFC generator concept (Chapter 7). All air-fuel ratios are volumetric and in some cases this may be taken as a molar ratio providing the gas is operating within the limits of the ideal gas law.

6.1 FUEL EVALUATION

The suitability of reticulated natural gas, liquefied petroleum gas (LPG), iso-octane, and ethanol for the MT-SOFC generator concept were evaluated. Initial development of the partial oxidation reactor used liquid fuels but after re-evaluating suitable fuels and balance of plant required for liquid fuels, development was refocused on the gaseous fuels natural gas and LPG. Two sources of LPG were available: conventional barbeque gas, which was approximately 80% and 20% propane and butane respectively; and “high performance” gas for use at higher altitudes (lower pressures), which was approximately 20% and 80% propane and butane.

6.1.1 Natural gas

Composition of natural gas from the reticulated supply in the laboratory, which originated from the Rotowaro field, was supplied by Vector Limited (www.vectorgas.co.nz). The GC analysis of the gas (Table 6-1) confirmed that the major component was, as expected, methane. The main difference between the GC data and the supply specification was that carbon dioxide concentration was 13% higher than indicated in the analysis provided. (Error in GC analyses is $\pm 0.14\%$.) Vector Limited’s analysis stated that carbon dioxide concentration would be 5.4% to 6.5%, giving an unexplained difference of 0.3%. Differences can sometimes be attributed to using a standard gas that has a component concentration greater or less than 10% of the component’s actual concentration

[67] but carbon dioxide concentration in the standard gas was 5.027%. The difference was not explored further because carbon dioxide content of the fuel was not critical to operating the partial oxidation reactor.

Table 6-1 Composition [mol·%] of reticulated natural gas

Component	Waikato	Vector Limited
	University Analysis	Analysis
Methane	80.9	80.9
Ethane	7.5	7.5
Carbon dioxide	6.9	6.1
Propane	3.6	3.6
Other	1.1	1.9
Total	100.0	100.0

Natural gas was initially considered and analysed but not used in the partial oxidation reactor because it is not usually available in gas cylinders or canisters for public use and therefore is not suitable for a portable MT-SOFC generator. Although natural gas would be suitable for a stationary SOFC generator, this was outside the scope of this research.

6.1.2 Kovea gas

Four canisters (K1-K4) of Kovea KC220 butane-propane gas (Kiwi Camping Company; www.kiwicamping.co.nz) were analysed by GC (Table 6-2). Canisters K3 and K4 had the same batch number and a specified nominal composition of 70% butanes and 30% propane. There were large composition differences of up to 21 mol·% between canisters K1 and K2, especially for the primary constituents, propane and butane. The GC analysis showed K1 had 30% propane but only 67% butanes and K2 had 83% butanes but only 9% propane. Canisters K3 and K4 from two different batch numbers had a specified nominal composition of 82% butanes and 18% propane. The measured gas compositions of these two canisters and K4 were within 2% for butane and within 1% for propane. The butanes content was much lower than stated on the canister (54% and 55% versus 82%) and propane content was much higher than stated (32% versus 18%). Although Kovea gas was not used directly to develop the MT-SOFC generator, the large variation in composition between canisters highlights that any generator must be able to operate with variations in fuel quality (within limits).

Table 6-2 Composition [mol-%] of Kovea gas canisters K1-K4

	K1	K2	K3	K4
Butanes	67.4	82.6	53.9	55.1
Propane	29.5	8.9	32.4	32.1
Methane	0.1	5.8	0.4	0.5
Ethane	3.0	1.0	3.8	3.9
Nitrogen	Not found	1.4	5.7	7.1
Oxygen	Not found	0.3	3.8	1.3
Total	100.0	100.0	100.0	100.0

6.1.3 Liquid petroleum gas (LPG)

Gas analysis data of two 9-kg LPG cylinders, which had been filled consecutively by a local supplier (Gas Pro Limited, www.gaspro.co.nz), were slightly different (Table 6-3). The difference may be due to pre-existing gases in the cylinders before filling. The LPG in the cylinders is mixed phase (i.e. liquid and gaseous) and lighter components are drawn first. Hence concentration of heavier components such as butane will increase. Other researchers have demonstrated how LPG composition changes over time as the cylinder's contents reduces [82]. Periodic analysis of the LPG during this research did not show any significant changes in LPG composition.

The LPG was marketed as 80:20 propane-butanes, but GC analysis indicated it was 83:8 propane-butanes and the remaining 9 mol-% was nitrogen, oxygen and ethane. Thus, butane concentration was much lower than expected. The odorant in LPG, ethyl mercaptan, which can be between 1.5 ppm and 150 ppm [82] was not detected in the GC analysis.

Table 6-3 Composition [mol-%] of LPG cylinders LPG1 and LPG2

	LPG1	LPG2
Propane	83.3	82.6
Butanes	8.7	7.8
Ethane	4.6	5.1
Nitrogen	2.9	3.8
Oxygen	0.5	0.7
Total	100.0	100.0

6.2 AIR:FUEL RATIOS

The rotameters for controlling and measuring LPG and dry air flows had a coarse scale (10 mL/min for LPG; 500 mL/min for dry air) and needle valves that did not allow fine adjustment so air-fuel compositions were verified by gas analysis. Rotameter measurements also depended on inlet gas line pressure but were monitored and adjusted to ensure pressure remained constant. Dry air was mixed with LPG before entering the partial oxidation reactor and the ratios of dry air to LPG were controlled volumetrically using needle valves integrated into rotameter flow meters. Once flows had been set, the air:LPG ratios were confirmed by GC analyses. Air:LPG ratios from GC data were compared with ratios set using the rotameters. Oxygen:propane, oxygen:butane and oxygen:LPG ratios were also calculated.

6.2.1 Rotameter verification

Air:LPG ratios were calculated from GC analysis and compared with set air:LPG ratios. Oxygen:propane ratios were also calculated and compared with stoichiometric values (Table 6-4). The anomalous measurement, which was removed from the dataset, was a measured air:LPG ratio of 21.1:1 for the set ratio of 16.7:1. The two subsequent measurements at this setting were much closer (16.8:1 and 16.7:1). The likely causes for this anomalous data were either additional air being accidentally introduced into the sample syringe or a temporary increase in air flow or decrease in fuel flow during sampling. The mean difference between set and measured air:LPG ratios was 6%, with a maximum of 12%. These variations can be traced back to variations in air and LPG flows. Indicators on the rotameters bounced up and down regularly, especially at low flow rates. Air and LPG gas flows also varied with performance of the partial oxidation reactor; any pressure drop across the reactor would influence incoming gas flows. Gas flow rates can be kept constant using electronic mass flow controllers, which control flow by accounting for upstream and downstream gas pressures.

Table 6-4 Set and measured air:fuel ratios using rotameters and GC analysis

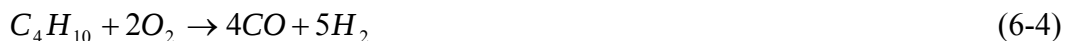
Set Ratio (Rotameters)	Measured Ratio (GC)		
11.1	10.7	11.9	12.4
16.7	21.1	16.8	16.7
22.2	20.6	20.4	20.6
27.8	25.9	24.7	24.9
33.3	31.5	30.6	30.5
38.9	35.8	36.2	35.1
44.4	41.9	41.4	41.4

6.2.2 Oxygen:propane, oxygen:butane and oxygen:LPG ratios

The stoichiometric ratio combusting propane is 5:1 (Equation 6-1) and for butane is 6.5:1 (Equation 6-2).



The LPG used was 83% propane and 8.7% butane so its combustion ratio was 4.7:1. The oxygen content of the LPG was low (approximately 0.6 mol-%). If oxygen and nitrogen levels were significantly higher, they would need to be accounted for especially because oxygen would modify the oxygen-fuel ratios. The theoretical ratio for partial oxidation of propane is 1.5:1 (Equation 6-3) and for butane is 2:1 (Equation 6-4).



Therefore, for stoichiometric combustion, the ratio of oxygen to LPG is 1.4:1. The actual oxygen:LPG ratios of the mixed gases fed to the partial oxidation reactor were calculated from the oxygen:propane and oxygen:butane ratios measured by GC (Table 6-5). Stoichiometric reaction equations for the full combustion and partial oxidation reactions give lower and upper bounds for the oxygen-LPG ratios of 1.4:1 and 4.7:1 respectively.

Table 6-5 Set, measured and calculated combustion ratios for full and partial oxidation of LPG samples

Oxygen:LPG (Set)	Oxygen:Propane (Measured)			Oxygen:Butane (Measured)			Oxygen:LPG (Computed)		
2.3	2.4	2.6	2.8	35.3	37.8	37.0	2.3	2.5	2.6
3.5	4.7	3.7	3.7	65.4	49.6	51.2	4.4	3.5	3.5
4.7	4.6	4.5	4.6	59.4	60.9	63.7	4.3	4.2	4.3
5.8	5.8	5.5	5.6	84.4	73.1	54.9	5.5	5.1	5.2
7.0	7.1	6.8	6.8	97.3	93.2	90.7	6.6	6.3	6.4
8.2	8.0	8.0	7.8	115.8	100.2	98.1	7.4	7.4	7.2
9.3	9.3	9.2	9.2	140.6	130.1	120.7	8.7	8.6	8.5

A typical composition of a near stoichiometric air:LPG ratio consisted mostly of air with a fuel content of 4.3 mol·% (Table 6-6).

Table 6-6 Composition [mol·%] of near stoichiometric air:LPG mixture

Component	Concentration
Nitrogen	75.7
Oxygen	20.0
Propane	3.4
Butanes	0.7
Ethane	0.2
Total	100.0

6.3 PARTIAL OXIDATION REACTOR EXHAUST GAS

The air-fuel mixtures of known composition (see previous section) were fed to the partial oxidation reactor and adjusted to achieve the required thermal output. Exhaust gas from the partial oxidation reactor was analysed by gas chromatography. Water in the reactor's exhaust gas was removed (Section 3.1.16). Gas samples were taken and analysed every 40 minutes to allow time for the higher hydrocarbons to elute from the columns. The air:LPG ratio was varied to achieve the required temperature profile within the reactor vessel. Initially the reactor was heated to 800°C, after which the objective was to induce hydrogen and carbon monoxide production by moving into partial oxidation whilst

maintaining operating temperature between 800°C and 900°C. Oxygen content of the exhaust gas was also monitored to judge the extent of the partial oxidation reaction. Hydrogen and carbon monoxide content of the exhaust gas were of prime interest, as they are the ideal fuel gases for SOFC.

6.3.1 Reactor A

Before starting the reactor, the air:LPG ratio was analysed for stoichiometry. The reactor was started by applying heat from a blowtorch through the quartz glass to the catalyst. Once the catalyst was glowing red, the top insulation layers were assembled and thermocouples positioned. Gas composition of the exhaust gas during start-up was not measured as each GC analysis took 40 minutes and the reactor could reach operating temperature in as little as five minutes. Thus, gas analysis could only be done after the reactor had reached steady-state.

Stoichiometric ratios of air to LPG was used to start the reactor from room temperature to approximately 800°C. Initial trials showed that temperature could only be maintained if air:LPG ratios were between 15:1 and 20:1 so exhaust gases were only analysed when the reactor was operating within this range. Once one of the temperature probes within the reactor reached 800°C, fuel flow rate was increased incrementally in 10 ml/min steps from 100 mL/min to 150 mL/min whilst air flow rate was kept at 2500 mL/min (air:LPG ratios from 25 to 16.7).

In initial experiments, air flow rate was reduced while fuel flow rate was kept constant. However, it was not possible to maintain the reactor's temperature under these conditions so temperature was allowed to fluctuate between 750°C and 900°C while changing operation mode from full to partial oxidation. If the temperature moved outside this range, fuel and/or air flow rates were adjusted appropriately.

Once the operating temperature of 800°C had been reached and maintained operating using a stoichiometric air-fuel feed gas, then either air flow rate could be reduced or fuel flow rate increased to induce a partial oxidation reaction. Initially air flow rate was reduced to try and induce partial oxidation but the temperature dropped quickly. When air was reduced, operating temperature could

not be maintained because insufficient oxygen was available for the exothermic combustion reactions. In further experiments, air flow rate was held constant and fuel flow rate increased from the stoichiometric level. This gave insufficient oxygen for complete combustion but sufficient to react with excess fuel to release enough heat energy to maintain the reactor's temperature. Under steady-state partial oxidation conditions, carbon monoxide production was 5 to 14 mol·% and hydrogen production 4 to 8 mol·% (Figure 6-1). Increasing the air:LPG ratio from 15.9:1 to 17.9:1 after steady-state conditions had been maintained for over one hour decreased carbon monoxide yield from 12 to 5 mol·%. However, hydrogen yield remained constant at 4 mol·%.

Because the reactor was shut-down by switching off the gas flows, exhaust gas composition was not monitored during the shut-down phase.

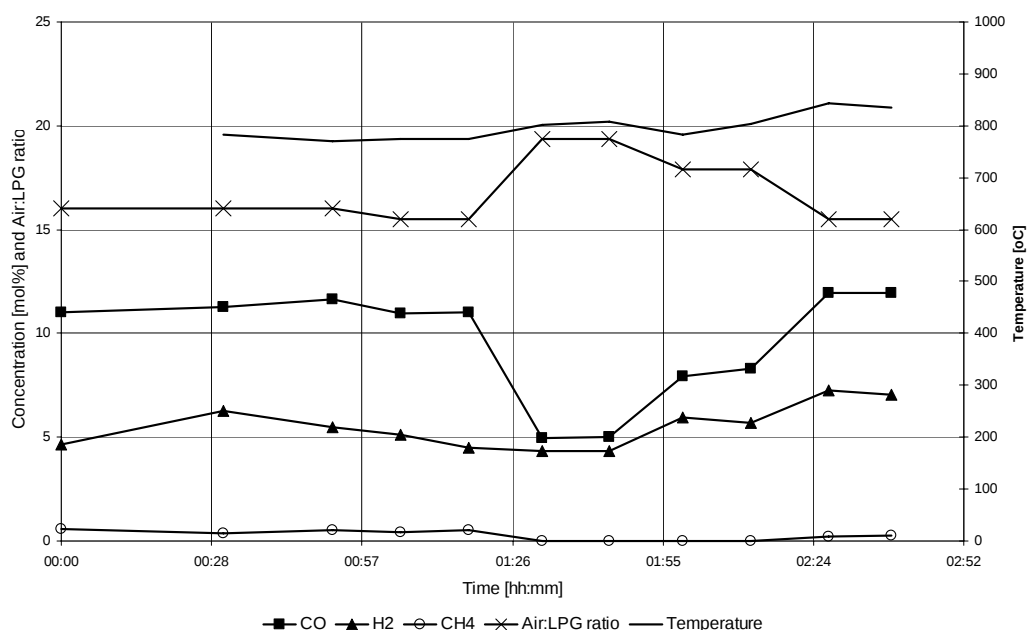


Figure 6-1 Effect of air:LPG ratio on temperature and exhaust gas composition (Reactor A)

Reactor A failed after approximately 50 hours of operation over many thermal cycles. The initial sign of impending failure was the step drop in carbon monoxide production while hydrogen production remained static. Air and fuel flow rates were adjusted and carbon monoxide production increased to the previous level briefly after which both carbon monoxide and hydrogen decreased and could not be re-established even after adjusting air and fuel flow rates. Visual

examination after the reactor had cooled to room temperature showed that the top support (stainless steel mesh) had partially disintegrated in the high temperature reducing environment and had been dislodged from its mounting position. This allowed the uppermost platinum-coated alumina spheres to move freely due to the high gas velocity.

6.3.2 Reactor B

Reactor B was made to the same specifications as reactor A, except nickel mesh was used to contain the catalyst. Air:LPG ratios were initially changed frequently to determine if the reactor responded in the same way as reactor A. Reactor B had the same operational characteristics as reactor A, especially exhaust gas composition. This enabled trials to continue. Reactor B had similar yield changes with air:LPG ratios. Thereafter, a air:LPG ratio of 15.5:1 was used and the exhaust monitored (Figure 6-2) and gases analysed every 10-12 minutes. Carbon monoxide and hydrogen yields from reactor B were similar to those from reactor A at similar air:LPG ratios (12.0 mol.% and 9.1 mol.% respectively).

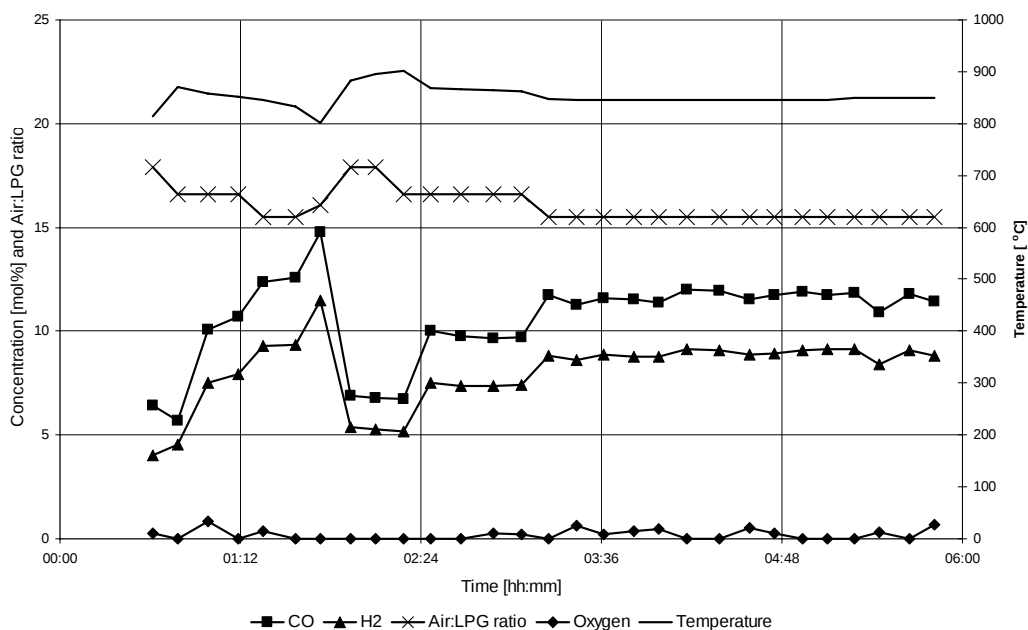


Figure 6-2 Effect of air:LPG ratio on temperature and exhaust gas composition (Reactor B)

Mean yields of carbon monoxide and hydrogen were calculated from all reactor experiments (Table 6-7). If air:LPG ratio was decreased from 20:1 to 15:1, carbon monoxide and hydrogen yields nearly doubled.

Table 6-7 Mean carbon dioxide and hydrogen concentrations in exhaust gas [mol·%] with respect to air:LPG ratios

Air:LPG ratio	CO	H ₂
15.5	11.8	8.3
16.0	11.3	5.5
16.6	9.8	6.7
17.9	7.9	5.4
19.4	6.8	5.3

Linear regression of yields with air:LPG ratios from all partial oxidation reactor experimental data (Figure 6-3) were used to calculate the gradients K_{CO} and K_{H_2} respectively (Equation 6-5 and Equation 6-6) and therefore carbon monoxide yield Y_{CO} and hydrogen yield Y_{H_2} .

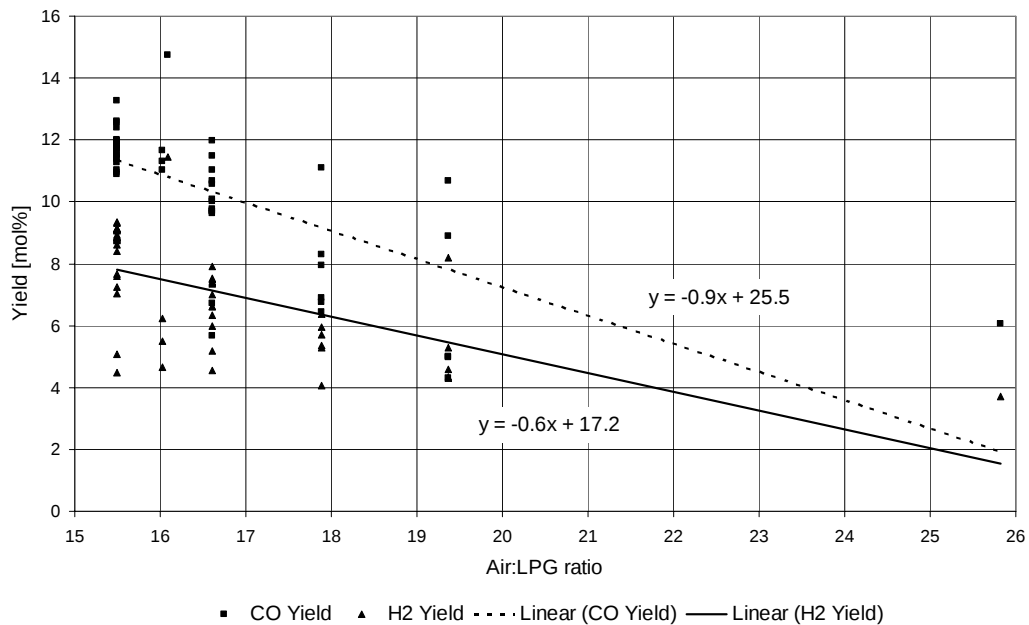


Figure 6-3 Effect of air:LPG ratio on carbon monoxide and hydrogen yield

$$Y_{CO} = -K_{CO} \cdot \left[\frac{\dot{V}_{air}}{\dot{V}_{LPG}} \right] + C_1 \quad (6-5)$$

Where $K_{CO} = 0.9$ and $C_1 = 25.5$

$$Y_{H_2} = -K_{H_2} \cdot \left[\frac{\dot{V}_{air}}{\dot{V}_{LPG}} \right] + C_2 \quad (6-6)$$

Where $K_{H_2} = 0.6$ and $C_2 = 17.2$

These equations are derived for a limited air:LPG ratio range but may be applicable beyond this range should reactor conditions be modified to maintain reactor temperature within the MT-SOFC performance requirements, typically 800°C to 900°C.

6.4 SUMMARY

The composition of natural gas, LPG, and LPG mixed with various ratios of dry air were checked by GC analysis. The partial oxidation reactor was operated on various air:LPG ratios and the reactor exhaust gases was analysed by GC. The reactor was started with a stoichiometric air-fuel ratio (approximately 100 mL/min LPG and 2500 mL/min of dry air), which allowed the reactor to quickly heat to 800°C. The reactor produced a suitable environment for operating MT-SOFCs and temperature could easily be adjusted in the range 800°C to 900°C. Higher or lower temperatures could be achieved if desired. Once the reactor had reached 800°C, LPG flow rate was increased to 150 mL/min, changing the reactor into partial-oxidation mode, which then produces hydrogen and carbon monoxide. An air:LPG ratio of 15:9:1 produced the highest amounts of hydrogen and carbon monoxide (21 mol.% of the exhaust gas). Gas composition from the partial oxidation reactor cannot be relied upon to provide 21 mol.% of hydrogen and carbon monoxide consistently so MT-SOFCs must be capable of operating on large fuel composition variations. The reactor's thermal characteristics are discussed further in Chapter 7.

7 PROTOTYPE ANALYSIS

An idealised system was devised and analysed using laws and practices of fluid mechanics and thermodynamics. The objectives were to characterise a conceptual MT-SOFC generator, to identify how generator performance can be computed, and to identify how generator performance and efficiency can be increased.

The analysis used the following assumptions:

- The generator is operating under steady-state at standard temperature and pressure.
- Air and fuel requirements for the fuel cells are based on a set electrical output, which is close to the demonstrated output.
- The fuel cells have a net zero effect on the heat balance.
- Heat losses from the system boundary affect the heating requirements and hence the fuel and air mass flow rates for the partial oxidation reactor.
- The hot zone in the generator has an ideal operating temperature of 850°C

Characterising the generator provided an analytical system; future efforts to develop and/or modify a MT-SOFC generator can target the areas that will give the most benefit. Worksheets showing the calculations are in Appendix II.

7.1 SYSTEM PROCESSES

The multiple processes taking place within a MT-SOFC generator can be quantified theoretically. Air and LPG fuel are mixed at the appropriate ratio(s) at room temperature and then fed to the partial oxidation reactor. Within the partial oxidation reactor, the oxygen in the air and the LPG react catalytically over the platinum-impregnated alumina spheres. The partial oxidation reactor (POR) heats the hot zone of the generator to 850°C. At the same time, hydrogen is fed through the middle of the MT-SOFCs and air is passed over the outside of the MT-SOFCs. Some oxygen molecules disassociate at the cathode and are conducted through the electrolyte to the anode to react with the fuel. Water is produced at the anode and is removed from the anode active sites by the fuel gas stream. These reactions only occur if an electrical load is applied to the fuel cells. Excess fuel is required

to prevent oxidation of the anode and to remove fuel cell reaction products. Excess air is also required to ensure oxygen is presented to the cathode. Incoming masses are at room temperature; heating them to the operating temperature increases the heating load on the partial oxidation reactor.

7.2 SYSTEM BOUNDARY

The system boundary for this analysis is drawn around the physical boundaries of the conceptual MT-SOFC generator (Figure 7-1). Four gas streams enter the system and three other streams exit. The “POR-fuel-in” and “POR-air-in” are mixed and leave the system boundary as a single entity, “POR-Exhaust”, which continues to supply the fuel cells with fuel (“FC-Fuel-in”). Oxygen ions from the “FC-air-in” mass conduct through the fuel cell and join the “FC-fuel-out” mass, combined with unspent fuel. Heat is transferred from the partial oxidation reactor to the surroundings and electrical energy generated by the fuel cells (FC) is presented as energy leaving the system boundary.

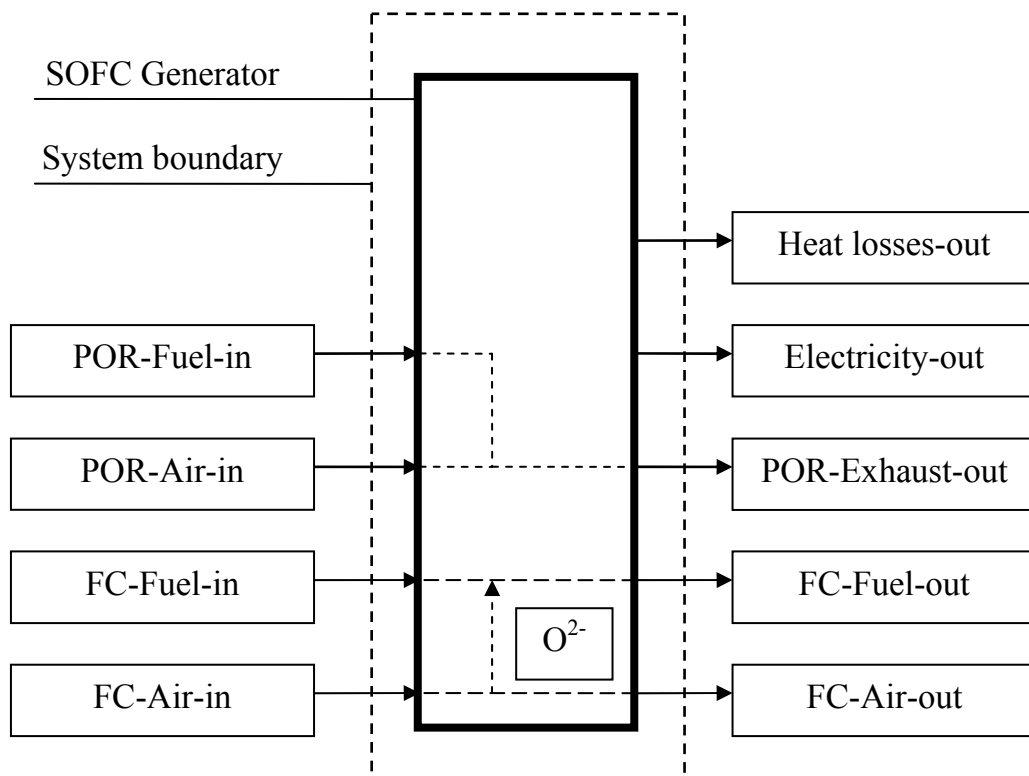


Figure 7-1 Conceptual MT-SOFC generator showing system boundary

7.3 ANALYSIS LOGIC

The following logic was used to analyse the MT-SOFC generator:

- The hot zone is uniformly at 850°C.
- Heat losses from the system can be calculated using the temperature difference between the hot zone and the surroundings, thermal resistances of the materials, and energy content of the estimated exiting mass.
- Fuel mass flow for the partial oxidation reactor can be calculated from the total heat loss.
- Air mass flow for the partial oxidation reactor can be calculated from the fuel mass flow.
- Total energy available can be calculated from inwards fuel mass flow.
- Product gases and mass flow from the partial oxidation reactor can be calculated from the reaction chemistry.
- Electrical output can be calculated from the hydrogen and carbon monoxide yields, assuming the fuel utilisation ratio is 10%. (Fuel utilisation ratio is the inward fuel molar flow less the outward molar flow divided by the inward molar flow.)
- Air mass flow for the MT-SOFCs can be calculated from performance of the MT-SOFCs, assuming an oxygen utilisation ratio of 10%.

7.4 HEAT LOSS TO THE SURROUNDINGS

Heat loss from the system boundary is calculated assuming there are no mass flows across the system boundary. Total heat loss from the system boundary is initially calculated as the sum of heat transfer in the radial and axial directions, assuming generator length is much greater than its radius. The following assumptions were made:

- One-dimensional radial conduction and convective heat transfer.
- Constant material thermal properties.

The prototype is housed within a 100-mm long aluminium casing with an outside diameter of 88 mm and with 3.5-mm thick walls. The ends of the cylinder are capped with 3-mm aluminium end-plates. A 100-mm tube of micro-porous insulation block with an outer diameter of 81 mm and 4-mm thick walls is

inserted into the aluminium tube. Alumina fibre board insulation with an outer diameter of 65 mm, 7.5-mm thick walls and 60 mm long is inserted inside the micro porous block tube. Two 20-mm thick alumina fibre board discs with holes appropriately sized for the partial oxidation reactor and fuel cells are inserted at each end of the micro porous tube (Section 6.1.3). The partial oxidation reactor made from 14-mm diameter quartz glass tube is the heat source at the centre of the generator. The immediate volume around the reactor (the hot zone) is 50 mm in diameter and has a 60-mm long hot zone. Thus, total volume of the hot zone, including the reactor is $1.2 \times 10^{-4} \text{ m}^3$. The volume of the containment vessel and insulation, excluding the reactor, is approximately $1.1 \times 10^{-4} \text{ m}^3$.

7.4.1 Radial heat loss

Temperature distribution through the composite wall was modelled by a thermal circuit made up of conduction terms for the aluminium, micro porous block, and alumina fibre board components and convection terms between the aluminium and ambient air and between the alumina fibre board and air in the heated zone. Radial heat losses can be calculated by dividing the temperature difference by the thermal resistance (Equation 7-1) [83].

$$\dot{Q}_{cc} = \left[\frac{T_1 - T_4}{\frac{1}{2\pi r_1 L h_1} + \frac{\ln(r_2 / r_1)}{2\pi k_A L} + \frac{\ln(r_3 / r_2)}{2\pi k_B L} + \frac{\ln(r_4 / r_3)}{2\pi k_C L} + \frac{1}{2\pi r_4 L h_4}} \right] \quad (7-1)$$

where \dot{Q}_{cc} is the heat transfer due to conduction and convection

$k_A = 0.17 \text{ W/m}\cdot\text{K}$ (thermal conductivity of alumina fibre board)

$k_B = 0.04 \text{ W/m}\cdot\text{K}$ (thermal conductivity of micro porous block)

$k_C = 237 \text{ W/m}\cdot\text{K}$ (thermal conductivity of aluminium)

Using the known parameters for the prototype, radial heat loss due to conduction and convection can be calculated to be 46 W.

Radiation from the surface of the aluminium cylinder is calculated using

$$\dot{Q}_{radiation} = \varepsilon \cdot \sigma \cdot A \cdot T_4^4 \quad (7-2)$$

where $\dot{Q}_{radiation}$ is the heat transfer due to radiation

$$\sigma = 5.67 \times 10^{-8} \text{ W/m}^2 \cdot \text{K}^4 \text{ (Stefan-Boltzmann constant)}$$

Therefore, radiation loss from the prototype is 50 W and total conduction, convective and radiation loss from the generator in the radial direction is 96 W.

7.4.2 Axial heat loss

The insulation is a 30-mm (x) alumina fibre board disc supported by a 3-mm (y) aluminium plate. Conduction, convection and radiation losses can be evaluated using a one-dimensional approach, similar to the radial analysis (Equation 7-3).

$$\dot{Q}_{axial} = \left[\frac{T_1 - T_4}{\frac{1}{h_1 \cdot \pi \cdot r_2^2} + \frac{x}{k_A \cdot \pi \cdot r_2^2} + \frac{y}{k_C \cdot \pi \cdot r_2^2} + \frac{1}{h_4 \cdot \pi \cdot r_2^2}} \right] + \varepsilon \cdot \sigma \cdot A \cdot T_4^4 \quad (7-3)$$

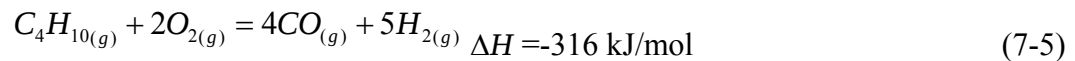
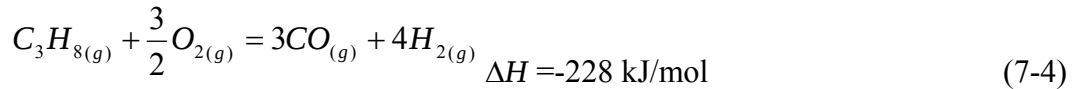
Substituting appropriate values gives a theoretical axial heat loss of approximately 14 W so total heat loss from both ends of the generator is approximately 28 W.

7.4.3 Total heat loss

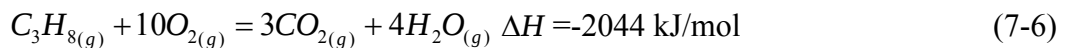
Total heat loss from the system boundary is 124 W, but this does not allow for mass flows entering and exiting the system boundary.

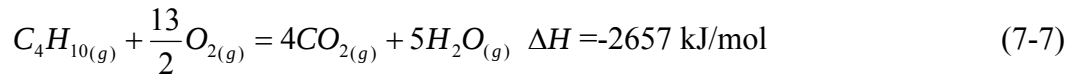
7.5 FUEL FOR PARTIAL OXIDATION REACTOR

The LPG mass flow ($\dot{m}_{POR-LPG-IN}$) can be determined from heat loss and the fuel energy content. The fuel source was commonly-available LPG, consisting of 83% propane and 8.7% butane gas (Chapter 5) from a 9-kg cylinder through a pressure regulator set at 100 kPa. The LPG was stored at ambient temperature. Heat of reaction for partial oxidation of LPG is -217 kJ/mol (Equations 7-4 & 7-5).



Heat of reaction for full oxidation of LPG is -1928 kJ/mol (Equations 7-6 & 7-7).





The calculations assume 50% of the LPG reacted via the partial oxidation reactions and 50% reacted via the full oxidation reactions. The energy available from the LPG is calculated by multiplying this proportion by the respective heats of reaction to give a combined heat of reaction of 1073 kJ/mol.

The LPG mass flow is calculated by assessing heat losses from the generator and then calculating the fuel required to meet the heat loss. The mass flow of LPG ($\dot{m}_{POR-LPG-IN}$) required to meet the loss (124 W), assuming 50:50 partial:full oxidation is 4.6×10^{-6} kg/s or an LPG volumetric flow rate of 139 mL/min.

If 4.6×10^{-6} kg/s LPG rate was reacted by full oxidation, then the maximum energy available would be 223 W.

7.6 AIR FOR PARTIAL OXIDATION REACTOR

Oxygen flow and hence air flow ($\dot{m}_{POR-AIR-IN}$) required by the partial oxidation reactor depends on the stoichiometric ratio as well as the ratio of partial to full oxidation. The reaction chemistry shows 3.5×10^{-4} mol/s oxygen is required for the partial oxidation reactor. This equates to an air mass flow ($\dot{m}_{POR-AIR-IN}$) of 4.9×10^{-5} kg/s, which is equivalent to an air volumetric flow of approximately 2.4 L/min.

7.7 PARTIAL OXIDATION REACTOR EXHAUST

Mass flow of the partial oxidation reactor ($\dot{m}_{POR-EXHAUST}$) may be determined in two ways; by conservation of mass, and by the reaction chemistry. The second approach is advantageous because theoretical species concentration in the exhaust gas can also be calculated. By conservation of mass, partial oxidation exhaust mass flow will equal the sum of incoming LPG and air mass flow, which had been determined as 4.6×10^{-6} and 4.9×10^{-5} kg/s respectively. Therefore, mass flow rate of the partial oxidation reactor exhaust gas ($\dot{m}_{POR-EXHAUST}$) is 5.3×10^{-5} kg/s.

The reaction chemistry gives the exhaust gas molar flow for each product species, which can be converted to mass flow using the species molar masses (Table 7-1).

Table 7-1 Flow rates of product gases

Species	Molar flow mol/s	Molar mass g/mol	Mass flow kg/s
Carbon monoxide	1.6×10^{-4}	28	4.5×10^{-6}
Hydrogen	2.2×10^{-4}	2	4.4×10^{-7}
Carbon dioxide	1.6×10^{-4}	48	7.7×10^{-6}
Water	2.2×10^{-4}	18	4.0×10^{-6}
Nitrogen	1.3×10^{-3}	28	3.6×10^{-5}

The total mass flow is 5.3×10^{-5} kg/s, which compares well with the previous calculation. Product gas component concentrations are calculated on a dry basis (Table 7-2).

Table 7-2 Theoretical concentration [mol·%] of product gas, dry basis

Species	Concentration
Carbon monoxide	8.7
Hydrogen	11.6
Carbon dioxide	8.7
Nitrogen	71.0

7.8 FUEL FOR FUEL CELLS

Fuel mass flow for the fuel cells ($\dot{m}_{FC-FUEL-IN}$) equals exhaust flow from the partial oxidation reactor (Equation 7-8) and represents total fuel available to the generator.

$$\dot{m}_{FC-FUEL-IN} = \dot{m}_{POR-EXHAUST} \quad (7-8)$$

Therefore, total mass flow available to the fuel cells ($\dot{m}_{FC-FUEL-IN}$) is 5.2×10^{-5} kg/s. Molar flow of carbon monoxide and hydrogen available in this gas stream, calculated from reaction chemistry, is 1.6×10^{-4} and 2.2×10^{-4} mol/s respectively.

7.9 ELECTRICAL ENERGY GENERATED

Fuel molar flow can be used to calculate the maximum electrical energy that could be generated. These calculations are independent of the number of fuel cells and the fuel cell's material properties.

7.9.1 Predicted potential

The predicted reversible potential (EMF) is derived from the first and second laws of thermodynamics (Equation 2-6).

$$V_{rev} = \frac{-\Delta^r G^\circ}{n^{el} \cdot F} \quad (7-9)$$

where $\Delta^r G^\circ$ -237.2 kJ/mol for hydrogen and -215.9 kJ/mol for carbon monoxide
 $F = 96485$ C/mol (Faraday's constant)

$n^{el} = 2$ for the ionisation of hydrogen gas

$n^{el} = 2$ for the ionisation of carbon monoxide

Thus, the reversible EMF using hydrogen at 25°C is 1.23 V and the reversible EMF using carbon monoxide is 1.12 V. Using the proportion of each fuel in the fuel gas indicates there are 1.6×10^{-3} mol/s carbon monoxide and 2.2×10^{-3} mol/s hydrogen and therefore the predicted reversible EMF for the combined flow is 1.18 V.

7.9.2 Predicted current

The current produced by the fuel cells is directly related to fuel consumption and therefore on the fuel utilisation ratio. Electric current is directly proportional to molar flow rate of spent fuel multiplied by fuel utilisation ratio (Equation 7-10).

$$I = -2\dot{n}_{FI} \cdot F \cdot U_f \quad (7-10)$$

Fuel utilisation ratio is the inward fuel molar flow less the outward molar flow divided by the inward molar flow (Equation 7-11).

$$U_f = \frac{\dot{n}_{FI} - \dot{n}_{FO}}{\dot{n}_{FI}} \cdot 100\% \quad (7-11)$$

For the calculated molar flow of 1.6×10^{-3} mol/s carbon monoxide and 2.2×10^{-3} mol/s hydrogen and assuming 10% fuel utilisation, the theoretical current generated is 7.4 A.

7.9.3 Power output

Power output is the product of current and reversible EMF:

$$P = I \cdot V_{rev} \quad (7-12)$$

Therefore, when current is 7.4 A and reversible voltage is 1.18 V, then the maximum theoretical power output would be 8.7 W.

7.10 AIR FOR FUEL CELLS

Air mass flow required by the fuel cells ($\dot{m}_{FC-AIR-IN}$) is determined by the predicted current generated and the oxygen utilisation ratio. The predicted current of 7.4 A is equivalent to an electron flow rate of 7.6×10^{-5} which equates to an oxygen molar flow of 3.8×10^{-5} mol/s or an oxygen mass flow of 1.2×10^{-6} kg/s. The volumetric air flow providing the oxygen is 290 mL/min but the fuel cells will use all the oxygen in the air. Excess oxygen and therefore excess air is required so an oxygen utilisation ratio is developed (Equation 7-13).

$$U_{oxygen} = \frac{\dot{n}_{OI} - \dot{n}_{OO}}{\dot{n}_{OI}} * 100\% \quad (7-13)$$

If oxygen utilisation ratio is assumed to be the same as fuel utilisation ratio (10%), then volumetric flow of air required by the fuel cells is 2.9 L/min. Therefore, air mass flow for the fuel cells ($\dot{m}_{FC-AIR-IN}$) is 5.8×10^{-5} kg/s.

7.11 FUEL EXHAUST FROM FUEL CELLS

Fuel cell fuel exhaust mass flow ($\dot{m}_{FC-FUEL-OUT}$) will be slightly greater than incoming mass flow due to the additional oxygen ions entering the gas stream through the fuel cell electrolyte. Fuel cell exhaust gas composition will also change due to fuel cell performance. Molar flow rates of carbon monoxide and hydrogen are 1.6×10^{-4} and 2.2×10^{-4} mol/s respectively. These flow rates are reduced by the amount of fuel used by the fuel cells, given by the fuel utilisation ratio. If fuel utilisation ratio is assumed to be 10%, then the remaining carbon monoxide and hydrogen molar flows are 1.5×10^{-4} mol/s and 2.0×10^{-4} mol/s respectively and molar flows of carbon dioxide and water are increased by 1.6×10^{-5} and 2.2×10^{-5} mol/s to 1.8×10^{-4} and 2.4×10^{-4} mol/s respectively. The

nitrogen molar flow remains at 1.3×10^{-3} mol/s. The theoretical concentration of the fuel cell exhaust gas changes slightly to reflect the further oxidation of the fuel species (Table 7-3).

Table 7-3 Species concentration [mol·%] of fuel cell exhaust gas

Species	Concentration
Carbon monoxide	7.9
Hydrogen	10.5
Carbon dioxide	9.7
Nitrogen	71.8

7.12 AIR EXHAUST FROM FUEL CELLS

Fuel cell air exhaust mass flow ($\dot{m}_{FC-AIR-OUT}$) will be slightly less than incoming air mass flow due to the oxygen loss through the electrolyte. Incoming air mass flow rate is 5.8×10^{-5} kg/s and the amount of oxygen lost through the electrolyte was calculated to be 1.2×10^{-6} kg/s (Section 7.10). Therefore, air mass flow leaving the system boundary is 5.7×10^{-5} kg/s. Oxygen concentration in the air leaving the system boundary is approximately 20 mol·%, or 1 mol·% less than the standard oxygen concentration in air.

7.13 EFFICIENCY

Generator efficiency is defined as electrical energy generated divided by energy content of the fuel (Equation 7-14).

$$\eta_{thermal} = \frac{W_{out}}{Q_{in}} \quad (7-14)$$

Energy content (Q_{in}) of the incoming LPG is 223 W (Section 7.5).

Predicted electrical output (W_{out}) is 8.7 W (Section 7.9.3).

Therefore, efficiency ($\eta_{thermal}$) is 3.9%.

7.14 STRATEGIES TO IMPROVE EFFICIENCY

Attempts to improve efficiency can be directed towards three interrelated areas of the generator: the fuel cells, thermal management, and system design. In general, efficiency can be improved by either increasing net electrical output or reducing fuel usage. If there is no need to improve electrical output (because the standard output is sufficient), then the main focus is to reduce the amount of fuel consumed to produce electrical output. To do this, one must know how much fuel is being used in the current system, understand the heat and mass flows within the system, and understand the physical and chemical constraints of the system. Changes to the system design can then be proposed, evaluated and tested.

7.14.1 Fuel cells

A theoretical fuel cell performance can be easily calculated. If sufficient fuel and oxygen supplied to the fuel cells, then the theoretical electrical output of the fuel cells depends only on the fuel and oxygen utilisation ratios. This infers that electrical energy generated is controlled by fuel and oxygen utilisation ratios, which is untrue and is only a partial explanation of what happens. Fuel cells generate electrical energy, which uses up fuel and oxygen. This decreases fuel and oxygen concentrations in their respective gas streams and thus increases fuel and oxygen utilisation ratios.

It is suspected that what actually governs electrical output from the fuel cells is a complex relationship between the materials used, their ionic and electronic conduction abilities, and diffusion characteristics of the fuel and oxidant gas flows on each side of the fuel cell. This lies outside the scope of this research, which intended to highlight the practical aspects of developing a MT-SOFC generator and provide a way to measure generator performance, theoretically and practically.

However, if fuel and oxygen utilisation ratios were both 100% due to extremely good fuel cells and generator design, efficiency would be 39%. Achieving 100% fuel and oxygen utilisation is unlikely because fuel and oxygen pass through the fuel cells only once and there is no possibility of recycling unused fuel and oxygen.

If a reactor could operate solely in a partial oxidation mode (i.e. without any full oxidation), and fuel and oxygen utilisation ratios were both 100%, then the maximum efficiency would be 78%. In this case, heating the generator and incoming mass flows would have to come solely from the partial oxidation reaction (217 kJ/mol) and all the hydrogen and carbon monoxide produced would have to react to produce electrical energy. This is an upper limit and is highly unlikely to be reached in practise in part due to thermal losses which are inherent in any system with large temperature differences.

7.14.2 Thermal management

Electrical efficiency of any generator is given by electrical output divided by fuel input. Efficiency of the MT-SOFC generator is not predominantly affected by fuel cell performance but by providing the appropriate environment for fuel cells to operate in.

One method to improve efficiency is to use a heat exchanger to preheat the air and fuel using the hot exhaust gases. Fuel cell exhaust gases (fuel and air sides) leave the system boundary at high temperature. These mass flows could preheat incoming flows through a heat exchanger. If pre-heating is not used, then energy in these streams is wasted to the surroundings. Another option is to use the oxygen-depleted air leaving the cathode side of the fuel cells in the partial oxidation reactor. This air is currently exhausted to the surroundings at high temperature. To reuse this air, the cathode air flow rate would have to be balanced between providing the partial oxidation reactor with sufficient oxygen, ensuring the fuel cells have sufficient oxygen, and minimising the heating demand.

A further option uses heat in the exhaust mass flows for another process that requires heat such as heating water. This would not be a practical extension to this design but could be integrated into future designs.

7.14.3 System design

The system design could be changed to incorporate two oxidation reactors, one being a full oxidation reactor to provide the heat to maintain the fuel cells and the other is a partial oxidation reactor to provide hydrogen and carbon monoxide for

the fuel cells. The LPG used to heat the system would be fully combusted so there would not be any hydrocarbons in the exhaust gas. The partial oxidation reactor could be reduced in size and output to provide sufficient hydrogen and carbon monoxide to the fuel cells without also being required to heat the fuel cells. This would compromise the system design and may not be suitable for small portable generators. However, this principle could be used in small stationary generators suitable for houses and small office blocks. Small portable generators have a disadvantage compared with larger systems because they cannot support the complexity and expense of integrated technologies such as heat exchangers.

7.15 ANALYSIS LIMITATIONS

The calculation of electrical energy generated did not account for the number of MT-SOFCs that could fit inside the hot zone of the generator so electrical output may be beyond that capable of the present MT-SOFC designs. If cross-sectional area of a MT-SOFC, including current collection, is 20 mm^2 and total area available through the generator is approximately 1800 mm^2 , then the maximum number of MT-SOFCs is 90. If each MT-SOFC requires at least a 5-mm radius for good air flow, then only ten MT-SOFCs could fit into the volume.

The analysis used basic accepted fluids mechanics and thermodynamics equations to demonstrate that mathematical understanding of how a MT-SOFC generator works can be achieved relatively simply. The analysis assumed steady-state operation at all times but this probably is an invalid assumption for the intended short-duration operation of a small portable MT-SOFC generator. Modelling the generator under transient conditions, i.e. start-up and shut-down phases, is best left to computer software packages. Modern computer software packages could be used to develop more accurate solutions, but this was outside the scope of this research project.

7.16 SUMMARY

Performance of a portable fuel cell can be modelled using basic thermodynamic and fluid mechanics relationships. The important factors are heat transfer to the surroundings, heat content of exhaust mass flows, assumed fuel and oxygen utilisation ratios, and assumed ratio of partial to full oxidation within the partial oxidation reactor. A theoretical model of a MT-SOFC generator was developed to describe heat and mass flows in and out of the generator, and the electrical energy generated. Heat loss from the generator was calculated to be approximately 124 W. Input energy was supplied from a LPG cylinder at a rate of 223 W. The analysis assumed that 50% of the fuel was partially oxidised to produce hydrogen and carbon monoxide and the rest was fully oxidised into carbon dioxide and water. Maximum theoretical power output was calculated to be 9.2 W, assuming the fuel cells used 10% of the available hydrogen and carbon monoxide. The potential efficiency of the MT-SOFC generator was calculated to be 4%. Strategies to improve the efficiency towards the theoretical maximum were discussed.

8 CONCLUSIONS AND RECOMMENDATIONS

This chapter summarises the key results from the electrochemical, prototype development, gas analysis and prototype analysis chapters and demonstrates how the research findings support the original objectives.

8.1 MT-SOFC PERFORMANCE

Electrochemical performance of many MT-SOFCs was evaluated under various operating conditions. Novel current collection techniques were developed to understand power production and to identify factors that limit fuel cell performance.

- Performance of MT-SOFCs produced in one production batch varied from 60 mW/cm² to just 3 mW/cm². Further work is required to identify manufacturing conditions that will reduce variability and produce MT-SOFCs with a consistent high power output.
- Electrolyte-supported MT-SOFCs in this research could produce up to a maximum of 140 mW/cm² of electrical power. If sufficient number of cells were combined, useful power could be produced.
- Electrochemical data showed that inlet fuel flow rate is not critical for MT-SOFC power output. A power output of 110 mW/cm² was maintained at fuel flow rates between 20 and 90 mL/min per MT-SOFC.
- Electrochemical performance characteristics of MT-SOFCs fuelled with methane and propane gases mixed with air or with pure hydrogen were similar. Operating MT-SOFCs on a hydrocarbon fuel and air mix or on exhaust gases from a partial oxidation reactor allows greater flexibility in generator operation; letting them run on commonly-available fuels such as natural gas and LPG.
- Operating temperature influenced electrochemical performance. Raising the operating temperature from 800° to 900°C increased power output by 33%. Therefore, heating system design is a critical factor in developing a portable MT-SOFC generator.

- The active length of the MT-SOFC was reduced to 30 mm without affecting power output. Further research could investigate if the active length could be reduced further.
- Segmenting the cathode increased electrochemical performance by 144%. Winding additional silver wires around the cathode, painting conductive silver ink, and applying silver nitrate to the cathode enhanced electronic connections and conduction at the cathode and therefore increased electrochemical performance of the MT-SOFCs.
- Inserting metal coils inside electrolyte-supported MT-SOFCs was an unreliable method for collecting current from the anodes, mainly because good physical contact between the wire and anode could not be maintained. Further research is required to identify a reliable method to collect the current from the anode.

8.2 PROTOTYPE

Manifolds, a fuel system and heating systems were developed for a MT-SOFC generator.

- Metallic manifolds imposed excessive stresses on the MT-SOFCs and complicated the scale-up of stack voltage. Sealing the MT-SOFCs into the metallic manifolds was difficult and leaks usually developed after several thermal cycles.
- Alumina fibre board did not impose excessive stresses on the MT-SOFCs. The effect of leaks from the fuel side to the air side was minimised by applying a platinum combustion catalyst to the alumina fibre board manifolds.
- Alumina fibre boards and micro-porous block insulation reduce heat loss from the hot zone and hold the MT-SOFCs in place. Although the alumina fibre board is not as heat resistant as a micro-porous block, it is easily manipulated using common workshop equipment. The micro-porous block is better as an outer insulation layer if only a limited amount of machining is required.
- An electrical heating system used in initial trials allowed good temperature control for testing MT-SOFCs and estimating heat losses. Heat loss from the final prototype was 124 W.

- A partial oxidation reactor (POR) was developed to heat and provide fuel for the MT-SOFCs. When run on LPG, this POR could heat the generator to the operating temperature more quickly than electrical heating but required more energy (223 W) to maintain temperature.

The proposed design for a portable generator uses a partial oxidation reactor to heat the MT-SOFCs. The MT-SOFCs are supported by alumina fibre board manifolds encased in a micro-porous insulation block to reduce heat transfer. The partial oxidation reactor produces sufficient carbon monoxide and hydrogen to fuel the MT-SOFCs. This generator will produce 9 W when powered on a common fuel such as LPG.

8.3 GAS ANALYSIS

The GC analysis of propane-butane gas mixes in common gas canisters showed large composition variances between different batches and none met the specified composition. The fuel management system of any portable generator to be fuelled by these canisters must be designed to cope with these large variances. The composition of LPG in common 9-kg cylinder also differed from specification. LPG marketed as 80% propane and 20% butane had 83% propane and 8.7% butane.

Air:LPG mixtures were determined by full and partial oxidation equations for propane and butane as well as from results in experimental trials with the partial oxidation reactor. Compositions of air:LPG mixtures, controlled using rotameters, were confirmed by GC analysis.

Analysis of the exhaust gas from the partial oxidation reactor, run under various air:LPG ratios showed that an air:LPG mol ratio of 16:1 produced 12 mol-% carbon monoxide and 9.1 mol-% hydrogen in the partial oxidation reactor which is sufficient to fuel MT-SOFCs.

8.4 PROTOTYPE ANALYSIS

A theoretical analysis indicated the energy required to operate the prototype MT-SOFC generator at steady state on LPG was 235 W LPG. This energy heated the MT-SOFCs and provided sufficient fuel to the MT-SOFCs. Generator efficiency was affected by the fuel and oxygen utilisations and the ratio of partial to full oxidation occurring in the POR. If fuel and oxygen ratios were both 10% and the partial to full oxidation ratio was 1:1, theoretical efficiency would be 4%. Efficiency can be increased by designing a system to use more of the fuel and oxygen available to the MT-SOFCs and by ensuring heat content of the exhaust gases is transferred to the incoming air and fuel.

8.5 RECOMMENDATIONS FOR FUTURE RESEARCH

Research on the following will help improve a portable generator based on MT-SOFC technology:

- Improving electrical connections between the MT-SOFCs and current-collectors
- Improving manifolds and seals
- Adapting the final prototype design to have two reactors, a partial oxidation reactor to supply carbon monoxide and hydrogen to the MT-SOFCs, and a full oxidation reactor to maintain the MT-SOFCs at the operating temperature.

9 REFERENCES

1. Du, Y. and N.M. Sammes, *Fabrication and properties of anode-supported tubular solid oxide fuel cells*. Journal of Power Sources, 2004. 136(1): p. 66-71.
2. Du, Y., N.M. Sammes, and G.A. Tompsett, *Optimisation parameters for the extrusion of thin YSZ tubes for SOFC electrolytes*. Journal of the European Ceramic Society, 2000. 20(7): p. 959-965.
3. Du, Y. and N.M. Sammes, *Fabrication of tubular electrolytes for solid oxide fuel cells using strontium- and magnesium-doped LaGaO₃ materials*. Journal of the European Ceramic Society, 2001. 21(6): p. 727-735.
4. Finnerty, C., G.A. Tompsett, K. Kendall, and R.M. Ormerod, *SOFC system with integrated catalytic fuel processing*. Journal of Power Sources, 2000. 86(1-2): p. 459-463.
5. Chachuat, B., A. Mitsos, and P.I. Barton, *Optimal design and steady-state operation of micro power generation employing fuel cells*. Chemical Engineering Science, 2005. 60(16): p. 4535-4556.
6. Kilbride, I.P., *Preparation and properties of small diameter tubular solid oxide fuel cells for rapid start-up*. Journal of Power Sources, 1996. 61(1-2): p. 167-171.
7. Finnerty, C.M. and R.M. Ormerod, *Internal reforming over nickel/zirconia anodes in SOFCs operating on methane: influence of anode formulation, pre-treatment and operating conditions*. Journal of Power Sources, 2000. 86(1-2): p. 390-394.
8. Kendall, K. and M. Palin, *A small solid oxide fuel cell demonstrator for microelectronic applications*. Journal of Power Sources, 1998. 71(1-2): p. 268-270.
9. Sammes, N.M. and R. Boersma, *Small-scale fuel cells for residential applications*. Journal of Power Sources, 2000. 86(1-2): p. 98-110.
10. Saunders, G.J. and K. Kendall, *Reactions of hydrocarbons in small tubular SOFCs*. Journal of Power Sources, 2002. 106(1-2): p. 258-263.
11. Staniforth, J. and K. Kendall, *Cannock landfill gas powering a small tubular solid oxide fuel cell -- a case study*. Journal of Power Sources, 2000. 86(1-2): p. 401-403.
12. Hayashi, K., O. Yamamoto, and H. Minoura, *Portable solid oxide fuel cells using butane gas as fuel*. Solid State Ionics, 2000. 132(3-4): p. 343-345.
13. Boersma, R.J., N.M. Sammes, and C. Fee, *Integrated fuel cell system with tubular solid oxide fuel cells*. Journal of Power Sources, 2000. 86(1-2): p. 369-375.
14. Lockett, M., M.J.H. Simmons, and K. Kendall, *CFD to predict temperature profile for scale up of micro-tubular SOFC stacks*. Journal of Power Sources, 2004. 131(1-2): p. 243-246.

15. Sammes, N.M., Y. Du, and R. Bove, *Design and fabrication of a 100 W anode supported micro-tubular SOFC stack*. Journal of Power Sources, 2005. 145(2): p. 428-434.
16. Winkler, W., *The influence of the mass transfer on the geometric design of SOFC stacks*. Journal of Power Sources, 2000. 86(1-2): p. 449-454.
17. Tantram, A.D.S., *Fuel cells: past, present and future*. Energy Policy, 1974. 2(1): p. 55-66.
18. Lindstrom, O. and W. Lavers, *Cost engineering of power plants with alkaline fuel cells*. International Journal of Hydrogen Energy, 1997. 22(8): p. 815-823.
19. Bitsche, O. and G. Gutmann, *Systems for hybrid cars*. Journal of Power Sources, 2004. 127(1-2): p. 8-15.
20. Williams, M.C. and H.C. Maru, *Distributed generation - molten carbonate fuel cells*. Journal of Power Sources, 2006. 160(2): p. 863-867.
21. Perry, R.H. and D.W. Green, *Perry's Chemical Engineers' Handbook*. Seventh Edition edn. 1998: McGraw Hill.
22. Larminie, J. and A. Dicks, *Fuel Cell Systems Explained*. 2nd edn. 2003, Chichester, West Sussex: J. Wiley. xxii, 406.
23. Singhal, S.C. and K. Kendall, *High-temperature Solid Oxide Fuel Cells : Fundamentals, Design, and Applications*. 2003, Oxford, UK: Elsevier. xvi, 405.
24. Hazlewood, P.E., *Factors affecting the corrosivity of pulping liquors*, PhD Thesis, Department of Materials Science and Engineering. 2006, Georgia Institute of Technology.
25. Anon., *NanoDynamics launches portable SOFC*. Fuel Cells Bulletin, 2005(1): p. 5-5.
26. Anon., *Alberta, Pirelli target industrial applications for micro SOFC*. Fuel Cells Bulletin, 2005(9): p. 4-4.
27. Alston, T., K. Kendall, M. Palin, M. Prica, and P. Windibank, *A 1000-cell SOFC reactor for domestic cogeneration*. Journal of Power Sources, 1998. 71(1-2): p. 271-274.
28. Ahmed, K., J. Gamman, and K. Foger, *Demonstration of LPG-fueled solid oxide fuel cell systems*. Solid State Ionics, 2002. 152-153: p. 485-492.
29. Anon., *GVM deal sees Sulzer Hexis reach 400 systems*. Fuel Cells Bulletin, 2002(10): p. 3-3.
30. Barrera, R., S. De Biase, S. Ginocchio, S. Bedogni, and L. Montelatici, *Performance and life time test on a 5 kW SOFC system for distributed cogeneration*. International Journal of Hydrogen Energy, 2008. 33(12): p. 3193-3196.
31. Riensche, E., U. Stimming, and G. Unverzagt, *Optimization of a 200 kW SOFC cogeneration power plant: Part I: Variation of process parameters*. Journal of Power Sources, 1998. 73(2): p. 251-256.

32. Peters, R., R. Dahl, U. Kluttgen, C. Palm, and D. Stolten, *Internal reforming of methane in solid oxide fuel cell systems*. Journal of Power Sources, 2002. 106(1-2): p. 238-244.
33. Asano, K., T. Hibino, and H. Iwahara, *A novel solid oxide fuel cell system using the partial oxidation of methane*. Journal of the Electrochemical Society, 1995. 142(10): p. 3241-3245.
34. Chen, F., S. Zha, J. Dong, and M. Liu, *Pre-reforming of propane for low-temperature SOFCs*. Solid State Ionics, 2004. 166(3-4): p. 269-273.
35. Ledjeff-Hey, K., T. Kalk, F. Mahlendorf, O. Niemzig, A. Trautmann, and J. Roes, *Portable PEFC generator with propane as fuel*. Journal of Power Sources, 2000. 86(1-2): p. 166-172.
36. Finnerty, C.M., N.J. Coe, R.H. Cunningham, and R.M. Ormerod, *Carbon formation on and deactivation of nickel-based/zirconia anodes in solid oxide fuel cells running on methane*. Catalysis Today, 1998. 46(2-3): p. 137-145.
37. Kendall, K., C.M. Finnerty, G. Saunders, and J.T. Chung, *Effects of dilution on methane entering an SOFC anode*. Journal of Power Sources, 2002. 106(1-2): p. 323-327.
38. Shao, Z., S.M. Haile, J. Ahn, P.D. Ronney, Z. Zhan, and S.A. Barnett, *A thermally self-sustained micro solid-oxide fuel-cell stack with high power density*. Nature, 2005. 435(7043): p. 795.
39. Zhan, Z. and S.A. Barnett, *Solid oxide fuel cells operated by internal partial oxidation reforming of iso-octane*. Journal of Power Sources, 2006. 155(2): p. 353-357.
40. Zhan, Z., J. Liu, and S.A. Barnett, *Operation of anode-supported solid oxide fuel cells on propane-air fuel mixtures*. Applied Catalysis A: General, 2004. 262(2): p. 255.
41. National Energy Technology Laboratory (U.S.) and United States. Dept. of Energy., *Fuel Cell Handbook*. 2005, Honolulu, Hawaii: University Press of the Pacific. 1 v. (various pagings).
42. Haynes, C., *Clarifying reversible efficiency misconceptions of high temperature fuel cells in relation to reversible heat engines*. Journal of Power Sources, 2001. 92(1-2): p. 199-203.
43. Hatchwell, C., N.M. Sammes, I.W.M. Brown, and K. Kendall, *Current collectors for a novel tubular design of solid oxide fuel cell*. Journal of Power Sources, 1999. 77(1): p. 64-68.
44. Kendall, K., C.M. Finnerty, G.A. Tompsett, P. Windibank, and N.J. Coe, *Rapid heating SOFC system for hybrid applications*. Electrochemistry, 2000. 68(6): p. 403-406.
45. Hernández-Pacheco, E., M.D. Mann, P.N. Hutton, D. Singh, and K.E. Martin, *A cell-level model for a solid oxide fuel cell operated with syngas from a gasification process*. International Journal of Hydrogen Energy, 2005. 30(11): p. 1221-1233.

46. Yashiro, K., N. Yamada, T. Kawada, J.O. Hong, A. Kaimai, Y. Nigara, and J. Mizusaki, *Demonstration and stack concept of quick startup/shutdown SOFC (qSOFC)*. *Electrochemistry*, 2002. 70(12): p. 958-960.
47. Tompsett, G.A., C. Finnerty, K. Kendall, T. Alston, and N.M. Sammes, *Novel applications for micro-SOFCs*. *Journal of Power Sources*, 2000. 86(1-2): p. 376-382.
48. Tompsett, G.A., C. Finnerty, K. Kendall, and N. Sammes, *Integrated catalytic burner/micro-SOFC design and applications*. *Electrochemistry*, 2000. 68: p. 519-521.
49. Yang, H., D.R. Cahela, and B.J. Tatarchuk, *A study of kinetic effects due to using microfibrinous entrapped zinc oxide sorbents for hydrogen sulfide removal*. *Chemical Engineering Science*, 2008. 63(10): p. 2707-2716.
50. Gao, W. and N. Sammes, *An Introduction to Electronic and Ionic Materials*. 1999, River Edge, N.J.: World Scientific. 357.
51. Trunec, M., *Fabrication of zirconia- and ceria-based thin-wall tubes by thermoplastic extrusion*. *Journal of the European Ceramic Society*, 2004. 24(4): p. 645-651.
52. George, R.A. and N. F. Bessette, *Reducing the manufacturing cost of tubular solid oxide fuel cell technology*. *Journal of Power Sources*, 1998. 71(1-2): p. 131-137.
53. Boersma, R.J., N.M. Sammes, and C.J. Fee, *Losses resulting from in-plane electricity conduction in tubular solid oxide fuel cells*. *Solid State Ionics*, 2000. 135(1-4): p. 493.
54. Song, R.-H., K.-S. Song, Y.-E. Ihm, and H. Yokokawa, *Fabrication and performance characteristics of anode-supported tubular solid oxide fuel cell*. *Electrochemical Society Proceedings*, 2001. 16: p. 1073-1079.
55. Song, R.-H., E.-Y. Kim, D.-R. Shin, and H. Yokokawa, *Fabrication and characteristics of anode-supported tube for solid oxide fuel cell*. *Electrochemical Society Proceedings*, 1999. 19: p. 845-849.
56. Van herle, J., R. Ihringer, N.M. Sammes, G. Tompsett, K. Kendall, K. Yamada, C. Wen, T. Kawada, M. Ihara, and J. Mizusaki, *Concept and technology of SOFC for electric vehicles*. *Solid State Ionics*, 2000. 132(3-4): p. 333-342.
57. Hatchwell, C.E., N.M. Sammes, and K. Kendall, *Cathode current-collectors for a novel tubular SOFC design*. *Journal of Power Sources*, 1998. 70(1): p. 85-90.
58. Simner, S.P. and J.W. Stevenson, *Compressive mica seals for SOFC applications*. *Journal of Power Sources*, 2001. 102(1-2): p. 310-316.
59. Taniguchi, S., M. Kadowaki, T. Yasuo, Y. Akiyama, Y. Miyake, and K. Nishio, *Improvement of thermal cycle characteristics of a planar-type solid oxide fuel cell by using ceramic fiber as sealing material*. *Journal of Power Sources*, 2000. 90(2): p. 163-169.

60. Staniforth, J. and K. Kendall, *Biogas powering a small tubular solid oxide fuel cell*. Journal of Power Sources, 1998. 71(1-2): p. 275-277.
61. Sammes, N.M., R.J. Boersma, and G.A. Tompsett, *Micro-SOFC system using butane fuel*. Solid State Ionics, 2000. 135(1-4): p. 487.
62. George, R.A., *Status of tubular SOFC field unit demonstrations*. Journal of Power Sources, 2000. 86(1-2): p. 134-139.
63. Peters, R., E. Riensche, and P. Cremer, *Pre-reforming of natural gas in solid oxide fuel-cell systems*. Journal of Power Sources, 2000. 86(1-2): p. 432-441.
64. Ioannides, T., *Thermodynamic analysis of ethanol processors for fuel cell applications*. Journal of Power Sources, 2001. 92(1-2): p. 17-25.
65. Lee, S.H.D., D.V. Applegate, S. Ahmed, S.G. Calderone, and T.L. Harvey, *Hydrogen from natural gas: part I--autothermal reforming in an integrated fuel processor*. International Journal of Hydrogen Energy, 2005. 30(8): p. 829-842.
66. Lide, D.R., *CRC Handbook of Chemistry and Physics, 2006-2007*. 87th edn. 2006, Boca Raton: CRC Press.
67. Cowper, C.J. and A.J. DeRose, *The Analysis of Gases by Chromatography*. 1983, Oxford; New York: Pergamon Press.
68. Hatchwell, C.E., N. Sammes, and K. Kendall. *Ag current collectors for an extruded tubular SOFC system*. in IPENZ Annual Conference, Wellington, NZ. 1997.
69. Hatchwell, C., N.M. Sammes, and I.W.M. Brown, *Fabrication and properties of $Ce_{0.8}Gd_{0.2}O_{1.9}$ electrolyte-based tubular solid oxide fuel cells*. Solid State Ionics, 1999. 126(3-4): p. 201.
70. Lockett, M.D., *A study of micro-tubular solid oxide fuel cell stacks*, PhD Thesis, Department of Chemical Engineering. 2006, University of Birmingham.
71. Saunders, G.J., *Reactions of hydrocarbons in zirconia fuel cells*, PhD Thesis, Department of Chemical Engineering. 2003, University of Birmingham.
72. Brown, M.S., *Fabrication and characterisation of nickel/yttria stabilised zirconia cermet anodes for solid oxide fuel cells*, PhD Thesis, Department of Engineering. 1998, University of Waikato.
73. Risna, K.S., *Construction and performance of a modified Adelan® micro-tubular solid oxide fuel cell*, Masters Thesis, Department of Engineering. 2002, University of Waikato.
74. Sonntag, R.E., C. Borgnakke, and G.J. Van Wylen, *Fundamentals of Thermodynamics*. 6th edn. 2003, New York: Wiley. xvii, 794.
75. Cooper, R.J., J. Billingham, and A.C. King, *Flow and reaction in solid oxide fuel cells*. Journal of Fluid Mechanics, 2000. 411(-1): p. 233-262.

76. Karakoussis, V., N.P. Brandon, M. Leach, and R. van der Vorst, *The environmental impact of manufacturing planar and tubular solid oxide fuel cells*. Journal of Power Sources, 2001. 101(1): p. 10-26.
77. Hayashi, H., T. Saitou, N. Maruyama, H. Inaba, K. Kawamura, and M. Mori, *Thermal expansion coefficient of yttria stabilized zirconia for various yttria contents*. Solid State Ionics, 2005. 176(5-6): p. 613-619.
78. Jiang, S.P., P.J. Callus, and S.P.S. Badwal, *Fabrication and performance of Ni/3 mol% Y₂O₃-ZrO₂ cermet anodes for solid oxide fuel cells*. Solid State Ionics, 2000. 132(1-2): p. 1-14.
79. Koide, H., Y. Someya, T. Yoshida, and T. Maruyama, *Properties of Ni/YSZ cermet as anode for SOFC*. Solid State Ionics, 2000. 132(3-4): p. 253-260.
80. Sammes, N.M. and Z. Cai, *Ionic conductivity of ceria/yttria stabilized zirconia electrolyte materials*. Solid State Ionics, 1997. 100(1-2): p. 39-44.
81. Shigley, J.E., *Mechanical Engineering Design*. 1st metric edn. McGraw-Hill Series in Mechanical Engineering. 1986, Singapore: McGraw-Hill. xvii, 699.
82. Wang, W., S.Q. Turn, V. Keffer, and A. Douette, *Study of process data in autothermal reforming of LPG using multivariate data analysis*. Chemical Engineering Journal, 2007. 129(1-3): p. 11-19.
83. Baukal, C.E., R. Schwartz, and J.Z. Company, *The John Zink Combustion Handbook*. Industrial combustion series. 2001, Boca Raton, FL: CRC Press. xlvi, 750.

APPENDIX I – CERTIFICATES OF ANALYSIS

SG1 – Standard gas #19792

MATHESON TRI-GAS INC
1650 Enterprise Pkwy
Twinsburg, OH 44087
1-215-648-4000

STANDARD GAS SPECIFICATION

CERTIFICATE OF ANALYSIS

Alltech Associates
2051 Waukegan Road
Deerfield, IL 60015

Ref Po# 4500835426

14 LITER DISPOSABLE

LOT NUMBER: 109-56-44242

COMPONENT	CONCENTRATION
Carbon Dioxide	5.023 %
Carbon Monoxide	5.000 %
Nitrogen	5.015 %
Oxygen	4.850 %
Methane	4.058 %
Hydrogen	4.137 %
Helium	Balance

ITEM NUMBER: GMT10404TC
CGA: 160
PSIG: 240
FILL DATE: August 2005
EXPIRATION DATE: August 2007

Above are the results of the analysis you requested, as reported by our laboratory. Results are in mole percent, unless otherwise indicated. Mixture accuracy is $\pm 2\%$. NIST traceable by weights or gaseous standards.

Thomas J Purdon 8/8/2005
Thomas Purdon, Plant Manager DATE

SG2 – Standard gas #M7014

MATHESON TRI-GAS INC
1650 Enterprise Pkwy
Twinsburg, OH 44087
1-215-648-4000

CERTIFICATE OF ANALYSIS

Alltech Associates
2051 Waukegan Road
Deerfield, IL 60015

Ref Po# 4500956578

14 LITER DISPOSABLE

LOT NUMBER: 102-61-02606-A1


COMPONENT	CONCENTRATION
Propane	99 % MIN

ITEM NUMBER: GMT10367TC
CGA: 160
PSIG: 240
FILL DATE: June 2006
EXPIRATION DATE: May 2008

Above are the results of the analysis you requested, as reported by our laboratory. Results are in mole percent, unless otherwise indicated. Mixture accuracy is $\pm 2\%$. NIST traceable by weights or gaseous standards.

Thomas J Purdon 6/6/2006
Thomas Purdon, Plant Manager DATE

SG3 – Standard gas #MA84047

 **BOC**

Laboratory Report

BOC Limited
BOC Production unit
Private Bag 93300
Otahuhu
Auckland

Issue date: **06-May-2008** Specially prepared for:
Expiry Date: **06-May-2013** 24 - 1066033
Revision: **1** **University of Waikato -
Technology Dept**
Certificate No.: **65878 - 1 - 1** Large Scale Lab Bld LSL
Order No.: **162350-replacement** Gate 9, Hillcrest Rd
Hamilton

Recipe number: **MA 84047**

α Alpha Standard

This calibration mixture has been gravimetrically prepared and the composition calculated to ISO-6142. The mixture composition is as follows:


Methane	2.02 ± 0.01 %
Ethane	2.03 ± 0.01 %
Butane (n-)	9.97 ± 0.05 %
Isobutane in Propane	10.30 ± 0.05 %


Receipt

All results are expressed on a mole/mole basis, unless otherwise specified. The reported uncertainty is based on a standard uncertainty multiplied by a coverage factor k=2, providing a level of confidence of approx 95%
Capillary GC with FID (based on ISO 6143)

Cylinder No.:	Size:	Contents:
QA 6078	GAL	0.2 m3

This report may not be reproduced except in full.

 This laboratory is accredited by International Accreditation New Zealand to ISO guide 17025 Laboratory registration number 581. The tests reported herein have been performed in accordance with its terms of accreditation.



David Granger
Laboratory Manager

APPENDIX II – ANALYSIS WORKSHEETS

HEAT BALANCE FROM TOTAL SYSTEM

	A	B	C	D	E	F	G	H
1	Calculate the heat lost from the generator							
2	RADIAL Losses for cylinder where length is much greater than diameter							
24	Dimensions	Units	Air-AFB	AFB	MCB	AI	AI-Air	
25	Length	m		0.1	0.1	0.1		
26	Inner Diameter	m		0.05	0.065	0.081		
27	Inner Radius	m		0.025	0.0325	0.0405		
28	Outer Diameter	m		0.065	0.081	0.088		
29	Outer Radius	m		0.0325	0.0405	0.044		
30	Thickness	m		0.0075	0.008	0.0035		
31	Cylinder Surface Area (based on outer diameter)	m ²	0.016	0.020	0.025	0.028	0.028	
32	Conduction							
33	Thermal Conductivity	W/mK		0.17	0.04	237		
36	Convection							
37	Convective Heat Transfer Coefficient	W/m ² K	Forced 26				Free 8	
38	Radiation							
39	Stefan-Boltzmann Constant	W/m ² K ⁴						5.67E-08
40	Absolute Temperature	K						423
41	Emissivity							1.0
42	Rate of thermal radiation	W						
43	Thermal Resistance							
44			Convection	Conduction	Conduction	Conduction	Convection	Radiation
45	Heat Transfer	W	2.4562688	2.456	8.756	0.000557	4.39217678	
46	AXIAL Losses through circular ends							
47			Convection	Conduction	MCB	AI	Convection	Radiation
48	Diameter	m		0.065				
49	Area	m ²		0.003				
50	Thickness of Insulation	m		0.03	0	0.003		
51	Thermal Conductivity	W/mK		0.17	0.04	237		
52	Thermal Resistance		11.6273079	53.181	0.000	0.004	36.5928101	
53	Axial Heat Transfer	W	28					6
54	POR-LPG-IN							
55	Mass flow rate	kg/s	4.6E-06					
56	Heat Capacity of Propane	kJ/kgK	2.400					
57	Heat Capacity of Butane	kJ/kgK	2.300					
58	Combined Heat Capacity	kJ/kgK	2.192					
59	Temperature change	K	825					
60	Heat energy required	W	8					
61	POR-AIR-IN							
62	Mass flow rate	kg/s	4.9E-05					
63	Heat capacity of air	kJ/kgK	1.004					
64	Temperature change	K	825					
65	Heat energy required	W	40					
66	FC-AIR-IN							
67	Mass flow rate	kg/s	5.8E-05					
68	Heat capacity of air	kJ/kgK	1.004					
69	Temperature change	K	825					
70	Heat energy required	W	48					
71	SUMMARY							
72	RADIAL	W	96					
73	AXIAL	W	28					
74	POR-LPG-IN	W	8					
75	POR-AIR-IN	W	40					
76	FC-AIR-IN	W	48					
77	TOTAL	W	124	221	124			

REACTION CHEMISTRY

J31 =SUM(J26:J29)												
	A	B	C	D	E	F	G	H	I	J	K	L
1	Calculate amount of oxygen and product gases as a proportion of incoming LPG flow rate and extent of partial oxidation reaction											
2												
3	Incoming LPG mass flow rate		kg/s	4.6E-06		From POR-LPG-IN worksheet						
4												
5	Molar mass of LPG		g/mol	40.1								
6												
7	Incoming LPG molar flow rate		mol/s	1.2E-04								
8												
9	Partial:Full oxidation ratio		%	50								
10												
11	Amount of propane in LPG		%	83								
12												
13	Propane molar flow rate		mol/s	9.6E-05								
14												
15	Amount of butane in LPG		%	8.7								
16												
17	Butane molar flow rate		mol/s	1.0E-05								
18												
19	Reaction matrix	C3H8	C4H10	O2	CO	H2	CO2	H2O		Energy [kJ/mol]	Air	N2
20		1		1.5	3	4	0	0	Partial oxidation	228	7.1	5.6
21			1	2	4	5	0	0	Partial oxidation	316	9.5	7.5
22		1		5	0	0	3	4	Full oxidation	2044	23.8	18.8
23			1	6.5	0	0	4	5	Full oxidation	2657	31.0	24.5
24												
25										Energy [W]		
26	Actual molar flow rates	4.8E-05		7.2E-05	1.4E-04	1.9E-04	0.0E+00	0.0E+00	Partial oxidation	11	3.4E-04	2.7E-04
27			5.0E-06	1.0E-05	2.0E-05	2.5E-05	0.0E+00	0.0E+00	Partial oxidation	2	4.8E-05	3.8E-05
28		4.8E-05		2.4E-04	0.0E+00	0.0E+00	1.4E-04	1.9E-04	Full oxidation	98	1.1E-03	9.0E-04
29			5.0E-06	3.3E-05	0.0E+00	0.0E+00	2.0E-05	2.5E-05	Full oxidation	13	1.6E-04	1.2E-04
30												
31	Total molar flow rates per species	9.6E-05	1.0E-05	3.5E-04	1.6E-04	2.2E-04	1.6E-04	2.2E-04		124	1.7E-03	1.3E-03

MASS BALANCE ON LPG TO POR

C13 =(C3/1000/C11)*C5/1000				
	A	B	C	D
1	Calculate the mass flow rate of LPG required to provide the heat losses from the generator			
2				
3	Heat energy	W	124	Required energy to heat generator calculated from heat losses
4				
5	Molar mass of LPG	g/mol	40.1	0.83% propane + 0.087% butane
6	Energy content of LPG	kJ/mol	1928	Full oxidation of LPG
7	Energy content of LPG	kJ/mol	217	Partial oxidation LPG
8				
9	Ratio of partial to full oxidation	%	50	
10				
11	Energy content by extent	kJ/mol	1073	
12				
13	Mass flow rate of LPG required	kg/s	4.6E-06	Mass flow of LPG required if partial oxidation was to heat generator
14				
15	Density of LPG	kg/m3	2	
16				
17	Volumetric flow rate of LPG	mL/min	139	

MASS BALANCE ON AIR IN TO POR

C12		=C7+C10		
	A	B	C	D
1	Calculate the amount of air required to operate the partial oxidation reactor			
2				
3	Oxygen required by POR	mol/s	3.5E-04	From CHEMISTRY worksheet
4	Nitrogen	mol/s	1.3E-03	From CHEMISTRY worksheet
5				
6	Molar mass of oxygen	g/mol	32	
7	Mass flow rate of oxygen	kg/s	1.1E-05	
8				
9	Molar mass of nitrogen	g/mol	28	
10	Mass flow rate of nitrogen	kg/s	3.7E-05	
11				
12	Mass flow rate of air	kg/s	4.9E-05	
13				
14	Density of air	g/L	1.2	
15				
16	Volumetric flow rate of air	L/min	2.4	
17				

MASS BALANCE ON FUEL REQUIRED FOR FUEL CELLS

C11		=C9*C10/1000		
	A	B	C	D
1	Calculate amount of fuel available for fuel cells			
2				
3	Use fuel in POR exhaust gas flow. Carbon monoxide and hydrogen are diluted with nitrogen carbon dioxide and water.			
4				
5	Carbon monoxide produced by POR	mol/s	1.6E-04	From CHEMISTRY worksheet
6	Molar mass of carbon monoxide	g/mol	28	
7	Mass flow rate of carbon monoxide	kg/s	4.6E-06	
8				
9	Hydrogen produced by POR	mol/s	2.2E-04	From CHEMISTRY worksheet
10	Molar mass of hydrogen	g/mol	2	
11	Mass flow rate of hydrogen	kg/s	4.3E-07	
12				

FC-AIR-IN

C24		=C22*C16/60000		
	A	B	C	D
1	Calculate the mass flow rate of air required for the MT-SOFCs			
2				
3	Current generated	A	7.4	From ELECTRICAL ENERGY worksheet
4	Faraday's constant	C/mol	96485	
5	Electron flow rate		7.6E-05	
6	Molar flow rate of oxygen molecules	mol/s	3.8E-05	
7	Molar mass of oxygen	g/mol	32	
8	Mass flow rate of oxygen	kg/s	1.2E-06	
9				
10				
11				
12	Oxygen content in air	%	21	
13				
14	Mass flow rate of air	kg/s	5.8E-06	
15				
16	Density of air	kg/m ³	1.2	
17				
18	Volumetric flow rate of air	mL/min	290	Uses up all oxygen in air
19				
20	Assume oxygen utilization rate	%	10	
21				
22	Required air flow rate	L/min	2.9	
23				
24	Mass flow rate of air supplied to fuel cells	kg/s	5.8E-05	

MASS BALANCE ON EXHAUST FROM POR

C37		=C19+C23+C27+C31+C35		
	A	B	C	D
4				
5	By conservation of mass, the exhaust mass flow rate will equal the sum of the incoming LPG and air mass flow rates			
6				
7	Incoming LPG mass flow rate	kg/s	4.6E-06	From POR-LPG-IN worksheet
8				
9	Incoming air mass flow rate	kg/s	4.9E-05	From POR-AIR-IN worksheet
10				
11	Total incoming mass flow rate	kg/s	5.3E-05	
12				
13	Therefore, POR exhaust mass flow rate is	kg/s	5.3E-05	
14				
15	Method 2			
16				
17	Carbon monoxide molar flow rate	mol/s	1.6E-04	From CHEMISTRY worksheet
18	Molar mass of carbon monoxide	g/mol	28	
19	Mass flow rate of carbon monoxide	kg/s	4.6E-06	
20				
21	Hydrogen molar flow rate	mol/s	2.2E-04	From CHEMISTRY worksheet
22	Molar mass of hydrogen	g/mol	2	
23	Mass flow rate of hydrogen	kg/s	4.4E-07	
24				
25	Carbon dioxide molar flow rate	mol/s	1.6E-04	From CHEMISTRY worksheet
26	Molar mass of carbon dioxide	g/mol	44	
27	Mass flow rate of carbon dioxide	kg/s	7.2E-06	
28				
29	Water molar flow rate	mol/s	2.2E-04	From CHEMISTRY worksheet
30	Molar mass of water	g/mol	18	
31	Mass flow rate of water	kg/s	3.9E-06	
32				
33	Nitrogen molar flow rate	mol/s	1.3E-03	From CHEMISTRY worksheet
34	Molar mass of nitrogen	g/mol	28	
35	Mass flow rate of nitrogen	kg/s	3.7E-05	
36				
37	TOTAL mass flow rate out	kg/s	5.4E-05	
38	TOTAL molar flow rate out (dry)	mol/s	1.9E-03	
39				
40	Concentrations (dry)			
41	Carbon monoxide	%	8.7	
42	Hydrogen	%	11.6	
43	Carbon dioxide	%	8.7	
44	Nitrogen	%	71.0	
45			100.0	

MASS BALANCE ON UNREACTED FROM FUEL CELLS

C22		=SUM(C9:C10,C14,C18,C20)		
	A	B	C	D
1	Calculate the characteristics of the exhaust gas from the MT-SOFCs			
2				
3	Carbon monoxide produced by POR	mol/s	1.6E-04	From CHEMISTRY worksheet
4	Hydrogen produced by POR	mol/s	2.2E-04	From CHEMISTRY worksheet
5				
6	Fuel utilization of MT-SOFCs	%	10	
7				
8	Remaining fuel			
9	Carbon monoxide	mol/s	1.5E-04	
10	Hydrogen	mol/s	2.0E-04	
11				
12	Existing carbon dioxide	mol/s	1.6E-04	From CHEMISTRY worksheet
13	Number or moles of CO ₂ produced = number of moles of CO consumed	mol/s	1.6E-05	
14	Total carbon dioxide	mol/s	1.8E-04	
15				
16	Existing water	mol/s	2.2E-04	From CHEMISTRY worksheet
17	Number or moles of H ₂ O produced = number of moles of H ₂ consumed	mol/s	2.2E-05	
18	Total water	mol/s	2.4E-04	
19				
20	Existing nitrogen	mol/s	1.3E-03	From CHEMISTRY worksheet
21				
22	Total molar flow rate	mol/s	2.1E-03	
23	Total molar flow rate (dry)	mol/s	1.9E-03	
24				
25	Concentrations (dry)			
26	Carbon monoxide	mol%	7.9	
27	Hydrogen	mol%	10.5	
28	Carbon dioxide	mol%	9.7	
29	Nitrogen	mol%	71.8	

MASS BALANCE ON AIR LEAVING FUEL CELLS

C8		=C3-C6		
	A	B	C	D
1	Calculate the characteristics of the air leaving the generator			
2				
3	Mass flow rate of air supplied to fuel cells	kg/s	5.8E-05	From FC-AIR-IN worksheet
4	Volumetric flow rate of air supplied to fuel cells	L/min	2.9	From FC-AIR-IN worksheet
5				
6	Mass flow rate of oxygen lost through electrolyte	kg/s	1.2E-06	From FC-AIR-IN worksheet
7				
8	Mass flow rate of air leaving control volume	kg/s	5.7E-05	
9				
10	Molar flow rate of oxygen supplied to fuel cells	mol/s	3.8E-04	
11	Molar flow rate of oxygen lost through electrolyte	mol/s	3.8E-05	
12	Molar flow rate of oxygen leaving control volume	mol/s	3.4E-04	
13	Molar flow rate of nitrogen entering and leaving control volume	mol/s	1.4E-03	
14	Concentration of oxygen in air leaving control volume	mol%	20	
15				

ELECTRICITY PRODUCED

C26		fx =C13*C24		
	A	B	C	D
1	Calculate the electrical energy produced based on fuel flow rate to MT-SOFCs and utilization factor			
2				
3	Potential			
4	n-el (carbon monoxide)		2	
5	n-el (hydrogen)		2	
6	Faraday's constant	C/mol	96485	
7	Gibbs free energy (carbon monoxide)	kJ/mol	215.9	
8	Gibbs free energy (hydrogen)	kJ/mol	237.2	
9				
10	Reversible voltage (carbon monoxide)	V	1.12	
11	Reversible voltage (hydrogen)	V	1.23	
12				
13	Reversible voltage (proportional)	V	1.18	
14				
15				
16	Current			
17	Carbon monoxide produced by POR	mol/s	1.6E-04	From CHEMISTRY worksheet
18	Hydrogen produced by POR	mol/s	2.2E-04	From CHEMISTRY worksheet
19	Fuel utilization	%	10	
20				
21	Current (carbon monoxide)	A	3.2	
22	Current (hydrogen)	A	4.2	
23				
24	Total current	A	7.4	
25				
26	Power	W	8.7	

EFFICIENCY OF GENERATOR

C17		fx =C13/C7*100	
	A	B	C
1	Calculate the efficiency of the generator		
2			
3	Energy in		
4	Mass flow rate of LPG	kg/s	4.6E-06
5	Molar mass of LPG	g/mol	40.1
6	Heat of reaction of LPG	kJ/mol	1928
7	Total energy in	W	223
8			
9			
10	Electrical energy produced		
11	Potential	V	1.2
12	Current	A	7.4
13	Power	W	8.7
14			
15			
16	Efficiency		
17	Electrical energy divided by fuel energy input	%	3.9